ROAD IMPACT ON EROSION DEVELOPMENT DURING OVERTOPPING FLOOD EVENTS

MASTER THESIS IN CIVIL ENGINEERING AND MANAGEMENT

ANOUK BOMERS

JUNE, 2015

Cover picture: Kuiken, 2012

ROAD IMPACT ON EROSION DEVELOPMENT DURING OVERTOPPING FLOOD EVENTS

MASTER THESIS IN CIVIL ENGINEERING AND MANAGEMENT
FACULTY OF ENGINEERING AND TECHNOLOGY
UNIVERSITY OF TWENTE

Author: A. Bomers Bsc.
E-mail: a.bomers@student.utwente.nl
Phone: 06 58 93 68 01

Location and date: Enschede, June 11, 2015
Thesis defence date: June 18, 2015

Graduation Committee:

Prof. Dr. S.J.M.H. Hulscher (Suzanne)
University of Twente
E-mail: s.j.m.h.hulscher@utwente.nl
Telephone: 053 489 3546
Direct line: 053 489 4256

Dr. J.J. Warmink (Jord)
University of Twente
E-mail: j.j.warmink@utwente.nl
Telephone: 053 489 3546
Direct line: 053 489 2831

J.P. Aguilar-Lopez Msc. (Juan Pablo)
University of Twente
E-mail: j.p.aguilarlopez@utwente.nl
Telephone: 053 489 3546
Direct line: 053 489 4038

UNIVERSITY OF TWENTE.

PREFACE

This thesis is the final part of my master Civil Engineering and Management at the University of Twente. The thesis investigates the influences of a road structure at the crest of a dike on the erosion development during wave overtopping flood events. I worked with great pleasure on the research and learned a lot about computational fluid dynamics and modelling with the use of the finite element method. I worked with COMSOL Multiphysics, which was a new modelling environment for me. I went to two workshops in order to improve my modelling skills and I really enjoyed working with this software.

I would like to thank my supervisors. First I would like to thank Juan Pablo for his enthusiasm about the topic and my progress during the project. I would also like to thank him for his ideas and discussions. Furthermore I would like to thank Jord for his feedback and suggestions for improvements. Finally, I would like to thank Suzanne for her critical view and questions during our meetings.

In addition, I would like to thank Ruud Börger and Frank van Gool from the COMSOL support. Especially in the beginning of the project they have helped a lot by answering questions about the working of the software. During the workshops Ruud was very interested in my topic and gave multiple suggestions for improvements of my model. This was really useful.

Furthermore, I would like to thank Jentsje van der Meer from Van der Meer Consulting B.V. and Léon Schouten from INFRAM for providing the data and information that I needed in order to do this research.

Finally, I would like to thank my family, friends and fellow students for their support the last couple of months.

Anouk Bomers

Enschede, 11 June, 2015

ABSTRACT

In the Netherlands, a large number of riverine flood defences are combined with roads located at the crest. However, the influence of this road on erosion development during wave overtopping is not yet known. The objective of the research is therefore to quantify the influence of a road located on top of a flood defence on the erosion development during wave overtopping.

Experiments were performed with the wave overtopping simulator, which is a device to perform destructive tests on inner slopes of dikes in order to establish the erosion resistance against overtopping waves. In Millingen aan de Rijn an experiment was performed on a dike with a road on top. Measurements of this experiment were used as boundary conditions and validation data.

A coupled hydrodynamic-bed model was developed. With the use of COMSOL Multiphysics a CFD simulation was performed, which models the water released by the wave overtopping simulator and the hydrodynamics along the dike profile. Tests with a discharge of 50 and 100 l/s per meter were simulated. With the computed bed shear stresses, the amount of scour was determined.

The simulated eroded dike profiles show some discrepancies compared to the measured data. These discrepancies can be explained by the heterogeneities in soil properties. Local variations of the grass strength were neglected during the simulation, while the berms were damaged due to traffic. In addition, the soil underneath the grass sod also includes debris, roots with different strengths and sand. The model assumes a homogenous clay layer, which is a cohesive sediment and has a higher erosion resistance.

Erosion at the crest of the dike increases significant due to a road located on top of the dike. This increase is caused by a combination of the smoother asphalt section and the damaged berms at the transitions. The model is highly sensitive to irregularities in the dike profile. An upward slope with an angle larger than 25˚ leads to a substantial increase of the maximum bed shear stresses. In addition, the overtopping tongue loses less energy due to the lower friction of the road section compared to a grass cover. Moreover, the turbulence of the flow increases due to a sudden increase of the bed roughness at the transition of the road section with the grass sod. The erosion along the slope and toe of the dike decreases slightly. However, this decrease is small compared to the increase of the amount of scour at the crest. It can therefore be concluded that a road located at the crest has a negative influence on the erosion development during wave overtopping and must be included during the safety assessment.

It is recommended to use the hydrodynamics at the outlet of the simulator as boundary conditions of the model and to exclude the wave overtopping simulator from the geometry. The hydrodynamics inside this simulator are very complex and dependent on several factors, leading to uncertainty in the model. This can be captured by excluding the simulator.

Furthermore, it is recommended to investigate if the maximum bed shear stress can be expressed as a function of bed roughness, slope and wave volume. With this expression it is possible to compute the erosion without doing the CFD simulation, which has a relatively large computation time.

This research only investigates the influence of a road on erosion development. To get a complete picture of the influences of a road on the safety level of a dike also failure mechanism such as macro stability must be considered.

LIST OF CONTENTS

1. Introduction 1
   1.1. Problem definition 2
   1.2. Research objective 4
   1.3. Methodology 4
   1.4. Reading guide 5
2. Data 6
   2.1. Wave Overtopping Simulator 6
   2.2. Experiment Millingen aan de Rijn 6
      2.2.1. Experiment 1: Erosion measurements 8
      2.2.2. Experiment 2: Hydraulic measurements 8
   2.3. Translation data 9
      2.3.1. Steering lists 9
      2.3.2. Dike profiles 12
   3.1. CFD Simulation 13
      3.1.1. Theoretical background 13
      3.1.2. Geometry 14
      3.1.3. Two-phase flow 15
      3.1.4. Initial and Boundary conditions 16
      3.1.5. Mesh 17
      3.1.6. Parameters 18
      3.1.7. Validation CFD simulation 20
   3.2. Bed Model 23
      3.2.1. Theoretical background 23
      3.2.2. Erosion model 25
      3.2.3. Parameters 26
      3.2.4. Overview bed model 28
      3.2.5 Validation bed model 29
4. Results 31
   4.1. Experiment Millingen aan de Rijn 31
      4.1.1. Results CFD simulation 32
      4.1.2. Results erosion development 34
   4.2. Direct impact of a road 42
   4.3. Indirect impact of a road 43

4.3.1. Change in overtopping volume 44
4.3.2. Change in erosion 45
4.4. Effects of a road along the dike profile 48
5. Sensitivity Analysis 50
5.1. Sensitivity CFD simulation 50
5.1.1. Volume fraction coefficient (Vf) 50
5.1.2. Initial interface thickness (ϵ_{pf}) 51
5.1.3. Mobility tuning parameter (χ) 51
5.1.4. Surface tension 52
5.1.5. Nikuradse roughness height (k_{es}) 52
5.1.6. Velocity scale (U_{scale}) and length scale (L_{fact}) 52
5.1.7. Time step (t) 53
5.2. Sensitivity bed model 53
6. Discussion 55
7. Conclusions 57
8. Recommendations 59
9. References 60
List of symbols 64
Appendixes 66

1. INTRODUCTION

Due to the population growth in coastal and river areas, cities will expand. Most likely 140 million people and 30.000 billion euro of assets depend on flood protection in large port cities around the world by 2070 (Kok & Vrijling, 2013). Most of those flood defences are aging or will not meet the safety standards in the future due to the expected change in climate conditions. The sea level will rise and the peak discharges of the rivers in the Netherlands will increase. This leads to the necessity of more robust flood defences (Kok & Vrijling, 2013). In addition, competing land claims for urban development and other functions such as recreation and flood protection urge for multi-functional and efficient use of land (Kok & Vrijling, 2013).

Figure 1.1. Dike with a road at the crest (Cormont, 1995)

An example of multi-functional land use is a dike with a road located at the crest (Figure 1.1). In the Netherlands, a large number of riverine flood defences are combined with roads located at the crest. For this reason it is interesting to investigate the influences of this road on the stability of the dike.

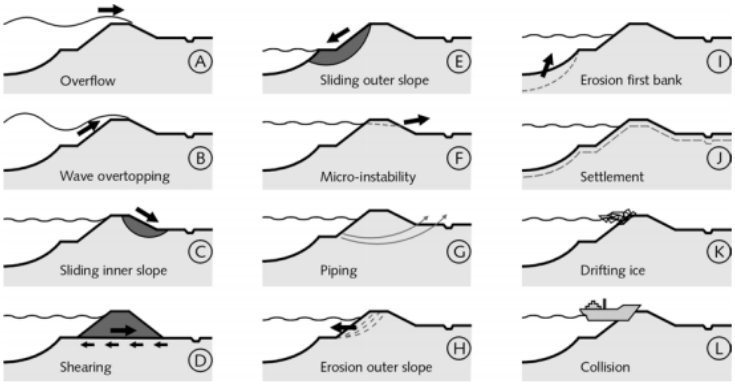

Figure 1.2. Failure mechanisms for a dike (Technische Adviescommissie voor de Waterkeringen, 1998)

In the assessment of the safety of the dikes, 12 failure mechanisms are considered to be important. These mechanisms have their own causes and consequences (Figure 1.2). Wave overtopping refers to the intermittent water flow over the dike crest, including wave action (Ciria, 2013). Wave overtopping discharge occurs because of waves running up the dike slope. If wave run-up levels are high enough water will reach and pass over the crest of the flood defence, which is defined as the 'green water' overtopping case where a continuous sheet of water passes over the crest (EurOtop, 2007). A second form of overtopping occurs when waves break on the slope of the dike and produce significant volumes of splash. These droplets may be carried over the dike either under their own momentum or as a consequence of wind forces (EurOtop, 2007). Note that overflow is not the same as wave overtopping. The velocities in an overtopping wave are much larger than velocities during overflow, even for the same discharge (Van der Meer, Hardeman, Steendam, Schüttrumpf, & Verheij, 2010).

Another classification of these failure mechanisms can be done based on external erosion, internal erosion, stability failure and subsoil failure. 70.2% of the dike breaches are formed by external erosion (Ciria, 2013). Therefore external erosion is the main failure cause of breaches, which is mainly caused by wave overtopping. The flow velocities of an overtopping wave can create scour at the crest or the inner side of the dike when the water passes.

Progressive damage caused by wave overtopping has frequently occurred in the past. Erosion and sliding down of parts of the inner slope has often been the leading failure mechanism to dike breach, which occurred during the severe floods in 1953 in The Netherlands and United Kingdom, in 1962 in the north of Germany and in 2005 with hurricane Katrina in the United States (Van der Meer, Bernardini, Snijders, & Regeling, 2007). In addition, it can be expected that a road structure mainly influences failure mechanism wave overtopping. The road structure is located at the crest of the dike, which affects the hydrodynamics of the overtopping waves. For these reasons wave overtopping is investigated.

Nowadays the dike safety assessment is done based on the overload approach per dike ring. The failure probabilities are based on a standard dike, with no constructions inside or on top. The possible influences of a road are not included during the assessment. For this reason it is important to know to what extend the erosion changes during wave overtopping when a road is located at the crest of the dike.

The erosion development depends strongly on the hydrodynamics. During wave overtopping, three flow stages are identified. At the outer slope of the dike the flow is subcritical and at the crest of the dike the flow is critical. At the inner slope the flow velocities increase significantly due to the steep slope, leading to supercritical flow (Chinnarasri, Tingsanchali, Weesakul, & Wongwises, 2003). Figure 1.3 gives the three flow stages. The flow during overtopping is highly turbulent, which is an important factor for erosion and may be responsible for dike breaches (Yuan, Li, Amini, & Tang, 2014).

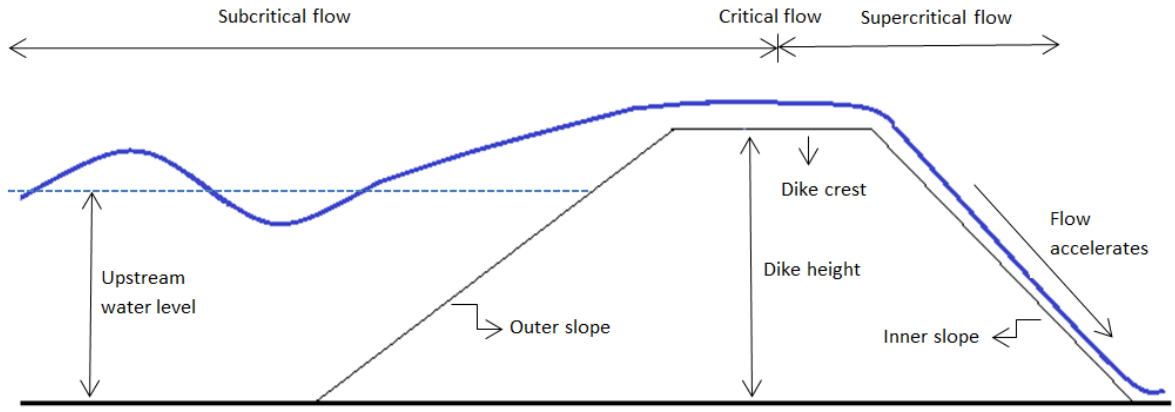

Figure 1.3. Flow stages during wave overtopping

1.1. PROBLEM DEFINITION

The safety levels of the dikes are computed based on a standard grass covered dike; a dike with no construction on top or inside like a road, tree or pipe. However, when these constructions lead to earlier failure of the dikes, the safety levels are overestimated. This is not desirable, because failure of a flood defence can have large economic and environmental consequences for the land which was protected by this certain flood defence. It may even lead to loss of people or animals. It is therefore important to have a better understanding of the impact of a road located at the crest of a dike for the erosion development of the dike profile.

Chinnarasri et al. (2003) mention in their paper that measured data of dike damage during overtopping is still lacking. To fill the gap of lacking data, experiments were conducted with the

wave overtopping simulator. The wave overtopping simulator is a device to perform destructive tests on inner slopes of dikes in order to establish the erosion resistance against overtopping waves (Van der Meer et al., 2009). Figure 1.4 shows an image of the simulator.

Figure 1.4. Wave overtopping simulator (Bakker, Melis, & Mom, 2013)

With the use of the wave overtopping experiments the cumulative overload model was developed. This model gives insight in the number of overtopping waves, in which the velocity is higher than the critical flow velocity, may overtop before the dike fails (Steendam, Van Hoven, Van der Meer, & Hoffmans, 2013). The model indicates when initial damage, damage at various locations and dike failure evolves. Figure 1.5 shows these three damages.

Figure 1.5. Initial damage, damage at various locations and dike failure (Van Hoven et al., 2013)

With the wave overtopping simulator and the cumulative overload model it is possible to estimate after how many waves the dike will collapse. However, it does not provide information about how much scour develops due to a single particular wave volume.

During wave overtopping erosion of the dike profile is most significant at the inner toe of the dike (Van der Meer et al., 2009). However, this finding is based on experiments performed at dikes with no road on top. In case of a road on top of the dike, erosion occurs at the transitions of the road and the crest of the dike. This erosion may develop due to local flow turbulence caused by the geometry and/or roughness variations (Morris, 2012).

Up till now it is not known what the exact influences of a road are on the amount of scour during an overtopping wave of a certain volume. Studies exist that describe the changes in erosion due to a construction on top of a dike in a qualitative sense, such as Morris (2012). However, no literature is found which investigates the exact change in erosion. This leads to the following problem definition:

What is the influence of a road located at the crest of a flood defence on the erosion process during wave overtopping flood events?

1.2. RESEARCH OBJECTIVE

The objective of this thesis is to quantify the influence of a road located at the crest of a flood defence on the erosion development during wave overtopping. The objective is reached by answering the following three research questions:

1. **How can erosion of the dike profile be modelled for a dike with a road on top?**
2. **How does a road structure at the crest of a dike influence the erosion process of the dike profile during wave overtopping?**
3. **What is the sensitivity of the parameters with respect to the model output?**

1.3. METHODOLOGY

To study the research objective two models are combined, which leads to a coupled hydrodynamic-bed model. First, the input data is processed in such a manner that it can be used as boundary conditions of the computational fluid dynamics (CFD) simulation. The routed overtopping volumes are based on a steering list which is used during the overtopping experiment in Millingen aan de Rijn. This list consists of a large amount of different overtopping volumes and is simplified to just a few wave volumes for the CFD simulation. The erosion development during the experiment was measured with a 3D laser scan. The laser scan data consists of millions of points and from this set a dike profile is constructed. This is done with the use of MATLAB, in which a set of points is chosen and with interpolation the dike profile is constructed.

After the input data is translated into boundary conditions, the CFD simulation is performed with the software COMSOL Multiphysics. The hydrodynamics are simulated with the use of the RANS-equations and a k-ε model is used to incorporate the turbulent character of the flow. At the boundary of the model domain wall functions are applied. The set of equations are solved using the finite element method. When the model is set up, the different overtopping volumes are routed. The results are validated with the use of field measurements obtained during experiments with the wave overtopping simulator to get confidence in the results of the CFD simulations.

The results of the CFD simulations of the different routed volumes are used as input data of the bed model. The erosion model of Valk (2009) is applied and all the parameters in the model are set to values which correspond with the experiment performed in Millingen aan de Rijn. The outcomes are validated with the use of the 3D laser scans made during the wave overtopping experiment.

Different simulations are performed in order to investigate the influence of a road structure on the erosion development. Finally, the model parameters are adapted to study the sensitivity of the parameters with respect to the model output.

1.4. READING GUIDE

In this thesis the following structure is used:

Chapter 2 – Data: a description of the wave overtopping experiment performed in Millingen aan de Rijn and translation of the input data to boundary conditions.

Chapter 3 – The model: development of the coupled hydrodynamic-bed model.

Chapter 4 – Results: results of the erosion development of the test performed in Millingen aan de Rijn and differences between a dike profile with and without a road located at the crest.

Chapter 5 – Sensitivity Analysis: determination of the sensitivity of the parameters with respect to the model output.

Chapter 6 – Discussion: discussion of the assumptions made in the coupled hydrodynamic-bed model.

Chapter 7 – Conclusions: answers to the research questions.

Chapter 8 – Recommendations: recommendations for further research.

2. DATA

Several experiments were performed with the use of the wave overtopping simulator to test the amount of scour of the dike profile. In this research data is used of the experiment conducted in Millingen aan de Rijn, where a road was located at the crest. In section 2.1 a description of the wave overtopping simulator is given, where after in section 2.2 the experiment in Millingen aan de Rijn is described. Section 2.3 explains the translation of the input data into boundary conditions.

2.1. WAVE OVERTOPPING SIMULATOR

Experiments of wave overtopping cannot be performed on small scale, because it is not possible to scale down clay and grass properly. Some tests were performed in large wave flumes. However, these tests are costly and the dike can only partly be modelled (Van der Meer et al., 2009). For these reasons the wave overtopping simulator was developed.

The objective of the wave overtopping simulator is to simulate overtopping waves at the dike crest, as forecasted for a particular storm, and to study the behaviour of the stability of the crest and inner side of the dike (Van der Meer et al., 2007). The simulator consists of a mobile box to store water. The water is released at specific times through a butter-fly valve and a guidance to the crest. The released discharge is such that for each overtopping volume the flow velocity and thickness of the water tongue at the crest corresponds with the characteristics (speed, turbulence and thickness of the stream) that can be expected (Van der Meer et al., 2009). Figure 2.1 gives the principle of the wave overtopping simulator. Various overtopping volumes are released randomly in time in order to simulate the real world as good as possible. The flow is highly turbulent, with a lot of air inclusion, and the surface is not smooth (Van der Meer et al., 2009).

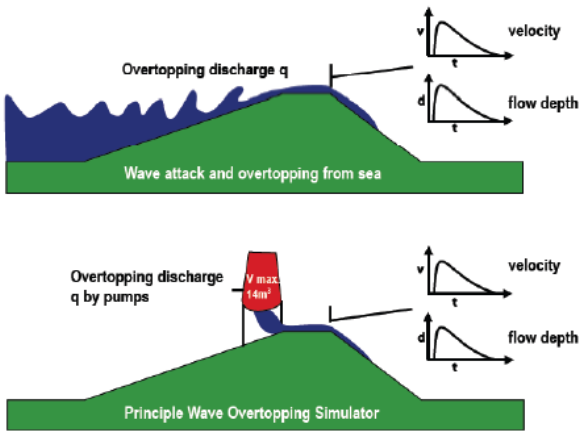

Figure 2.1. Principle of the wave overtopping simulator (Van der Meer et al., 2009)

2.2. EXPERIMENT MILLINGEN AAN DE RIJN

To investigate the influences of a road located at the crest of a dike, experiments were performed in Millingen aan de Rijn. At the crest of the dike the C.R. Waaiboerweg is situated. Figure 2.2 shows the exact location. The experiment was performed in January and February of 2013. It was conducted in the winter period because the conditions of the grass are relatively

bad in the winter compared to the other periods of the year. Grass does not grow below a temperature of 7 degrees, an overview is given by Steendam et al. (2009). In addition, most storms in the Netherlands occur in the winter period.

It can be expected that a road structure will lead to external erosion caused by water run off being focused at the transition of the road and the dike, and by local flow turbulence due to structure geometry or roughness variations (Morris, 2012).

Figure 2.2. Test location wave overtopping experiment in Millingen aan de Rijn (Bakker et al., 2013)

The experiment in Millingen aan de Rijn had four main goals (Bakker et al., 2013):

- Determination of the erosion resistance of the grass cover layer during overtopping.
- Determination of the influence of a discontinuity on the mentioned erosion resistance.
- Determination of the critical flow velocity for the grass cover.
- Determination of the (front) flow velocity and the layer thickness of the overtopping wave by measurements.

The wave simulator was located at the crest of the dike. The test section was four meters wide and bounded by 0.5 meters high guidance walls in order to keep the overtopping water in the test section.

The water was released approximately 1.5 meters from the edge of the asphalt pavement. The road has a width of 3.1 meters. Both berms are damaged due to traffic and therefore some bare spots are present on both sides of the road over a distance of 0.5 meters. The berms are 5 till 10 centimetres lower than the road.

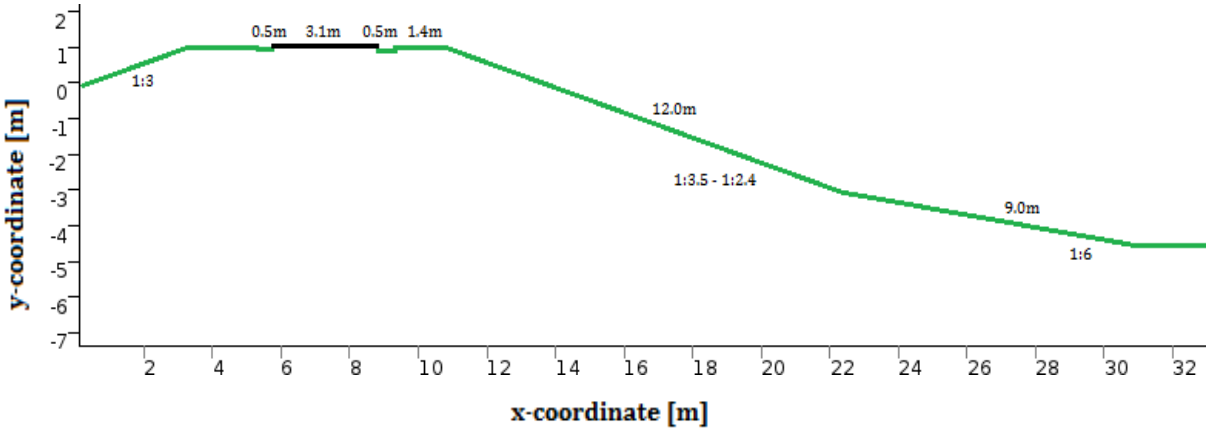

Figure 2.3. Overview dike profile Millingen aan de Rijn

The inner crest of the dike is located 1.4 meters from the edge of the asphalt pavement. From the inner crest up till circa 1 meter, the slope changes gradually up till a slope of 1:3. Over a length of 11 meters the slope varies between 1:3.5 and 1:2.4. After this, the slope becomes less steep with a gradient of 1:6. The toe of the dike is situated 25 meters from the edge of the wave overtopping simulator. Figure 2.3 presents an overview of the dike profile.

To reach the goals of the experiment, the experiment was divided into two parts. In the first part erosion of the dike profile was measured with the use of a 3D laser scan. During the second part hydraulic measurements were conducted. A description of both experiments is provided.

2.2.1. *Experiment 1: Erosion measurements*

During the first experiment different overtopping discharges were simulated. This has led to five tests which all had a duration of six hours. Depending on the inflow of the wave overtopping simulator, the tests were executed accelerated or decelerated. Table 2.1 provides the simulated discharges and corresponding information.

Table 2.1. Overview of the tests performed in Millingen aan de Rijn

Discharge [l/s per meter]	Duration experiment [h]	Accelerated [+]/ Decelerated [-]	Accelerated/ Decelerated test duration	Interval of laser scan measurement [h]
1	6	+ 5x	72 min	-
10	6	-	-	2
50	6	-	-	1
100	6	- 1.25x	7.5 h	1
200	6	- 2x	12 h	4

To be able to see the amount of erosion caused by the overtopping waves, the initial profile of the dike was recorded with a 3D laser scan. After a couple of hours, depending on the discharge released, the dike profile was scanned (Bakker et al., 2013). Figure 2.4 presents the location of the 3D laser scan and the laser scan itself.

Figure 2.4. 3D laser scan used during the experiment (Bakker et al., 2013)

2.2.2. *Experiment 2: Hydraulic measurements*

The second experiment starts after completion of the first experiment. During the second experiment the flow velocities and the layer thicknesses of the overtopping waves were measured. For the measurements of the layer thicknesses a 'surf board' device was used (Figure 2.5). Due to the form and his relatively low weight, the board will float. In the surf board a hinge was mounted. The water depth could be computed by measuring the angular rotation of this hinge (Bakker et al., 2013).

In addition, the surf boards are equipped with paddle wheels to measure the flow velocities at the surface of the overtopping waves. By counting the amount of rotations the paddle wheel makes, the flow velocity is determined (Bakker et al., 2013).

Figure 2.5. Surf boards used during the experiment (Van Hoven et al., 2013)

The hydraulic measurements were conducted at several locations at the crest and along the slope of the dike (Figure 2.6). However, during this experiment the wave overtopping simulator was located at the road section and a heavy geotextile was placed at the transition of the road and the grass cover in order to make a smoother transition. During the experiment of the erosion measurements the wave overtopping simulator was located before the road section. The transition of the road with the grass sod has an influence on the hydrodynamics and for this reason only the measurements at location SM1 are used as indication. In addition, during the experiment the thickness of the water layer was hard to measure due to air inclusion and the turbulent character of the flow. The 400, 1000, 1500 and 2500 litres per meter volumes were measured two times and the results are provided in Table 2.2.

Table 2.2. Hydraulic measurements Millingen aan de Rijn

Volume [l/m]	u_{sm1} [m/s]	h_{sm1} [m]
400	3.55	0.10
400	3.63	0.09
1000	4.09	0.16
1000	4.20	0.15
1500	4.54	0.21
1500	4.66	0.23
2500	5.08	0.26
2500	5.04	0.26

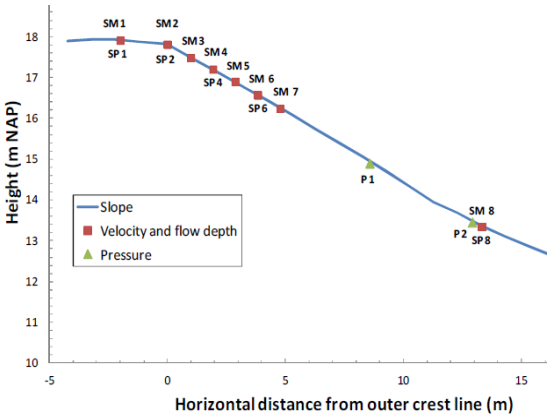

Figure 2.6. Locations of the surfboards and paddle wheels (Van Hoven et al., 2013)

2.3. TRANSLATION DATA

2.3.1. STEERING LISTS

The overtopping volumes which must be generated by the wave overtopping simulator are provided in steering lists. The lists give the exact times when the gates of the wave overtopping simulator must be opened and which volume should be released. The amount of overtopping waves and volumes are dependent on the representative wave conditions and the geometry of the outer side of the dike. The test in Millingen aan de Rijn was performed for the following conditions (Bakker et al., 2013):

- Significant wave height: 1.0 meters
- Peak period: 4.0 seconds
- Outer slope: 1:3

First, it is described how the steering lists are constructed, where after a method is provided how this data can be used as boundary condition.

2.3.1.1. Construction of the steering lists

Wave overtopping is often described by an average overtopping discharge. It represents the total volume of water which overtopped the dike in certain duration, divided by this duration. Wave overtopping can be given with (Van der Meer, 2002):

$$\frac{q}{\sqrt{gH_{m0}^3}} = \frac{0.067}{\sqrt{\tan \propto}} \gamma_b \xi_0 \exp(-4.3 \frac{R_c}{H_{m0}} \frac{1}{\xi_0 \gamma_b \gamma_t \gamma_\beta \gamma_v}) \quad (1)$$

Where:

q	= average wave overtopping discharge	[m³/s per m]
g	= gravitational acceleration	[m/s²]
H_{m0}	= significant wave height at toe of dike	[m]
ξ_0	= breaker parameter	[-]
$\tan \propto$	= slope	[-]
R_c	= free crest height above still water line	[m]
γ	= influence factors of berm, roughness elements, angle of wave attack, and vertical wall on slope	[-]

The average discharge given in Equation (1) does not provide information about the amount of water that flows over the crest for a single overtopping wave. Overtopping events are very dynamic and for this reason the average discharge does not describe the actual behaviour of these events accurately. The wave overtopping volumes differ substantially from the average wave overtopping discharge.

However, with the use of the average overtopping discharge it is possible to calculate the probability distribution function for the overtopping volume per wave. This probability distribution function follows a Weibull distribution with a shape factor of 0.75 and a scale factor a. This scale factor depends on the average overtopping discharge and the probability of overtopping waves. The probability distribution function is given with (Van der Meer, 2002):

$$P_V = P(\underline{V} \leq V) = 1 - \exp[-(\frac{V}{a})^{0.75}] \qquad \text{With:} \qquad a = 0.84 T_m \times \frac{q}{P_{ov}} \quad (2)$$

Where:

P_V	= probability that wave overtopping volume per wave V is greater than or same as $\underline{V}$	[-]
V	= wave overtopping volume per wave	[m³ per m]
T_m	= average wave period	[s]
P_{ov}	= probability of overtopping per wave	[-]

The overtopping volume follows the distribution described by Equation (2). Figure 2.7 presents the volumes corresponding to the different discharges that were generated during the experiment in Millingen aan de Rijn, in which the red lines indicate the average volumes for each overtopping discharge.

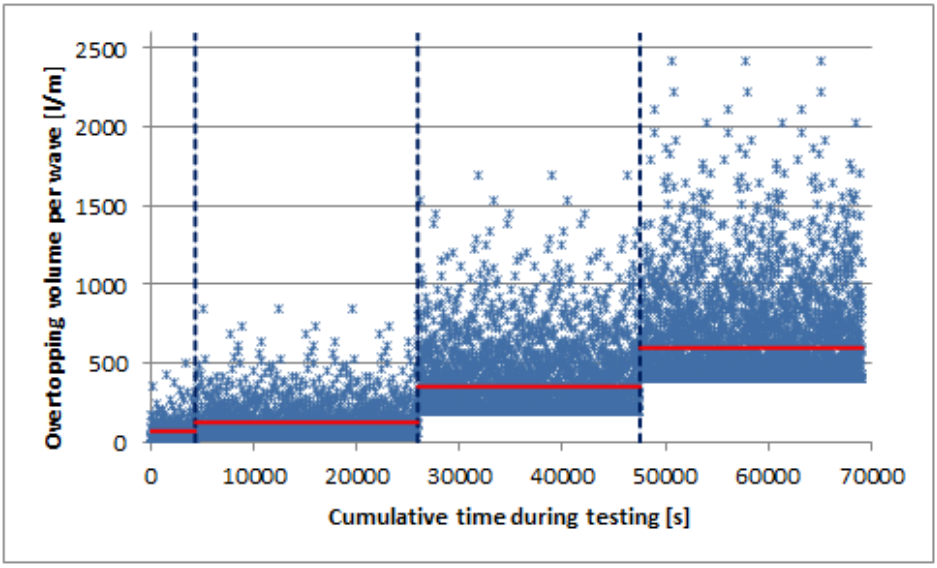

Figure 2.7. Wave volumes released by the wave overtopping simulator

2.3.1.2. Boundary condition definition

The steering list consists of a large amount of volumes for different mean overtopping discharges that are released by the wave overtopping simulator at certain times. However, it is difficult and not required to generate exactly each volume individually (Van der Meer et al., 2007). For this reason the volumes given in the steering list are schematised to a fixed number of overtopping volumes, keeping the total volume that overtops approximately equal. The volumes 150, 400, 700, 1000, 1500 and 2500 l/m are simulated, because validation data of these volumes is available. Appendix A provides a part of the 50 litres per second per meter steering list. Figure 2.8 gives proposals for simulation of the overtopping volumes for the 50 and 100 l/s per meter overtopping discharges.

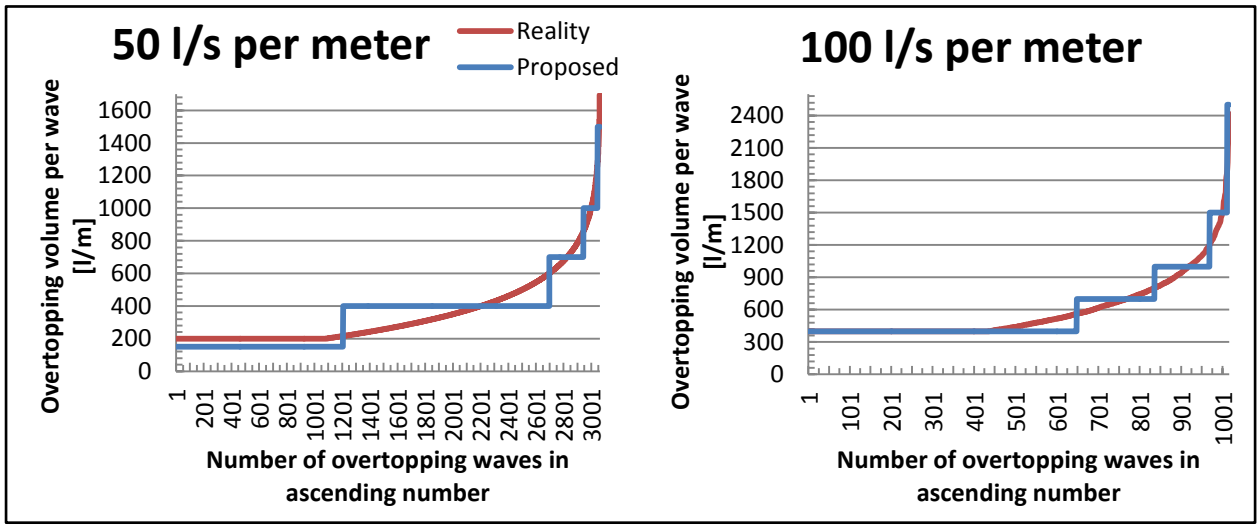

Figure 2.8. Proposed simulation for the 50 and 100 litres per second per meter tests

In this research only the 50 and 100 l/s per meter discharges are simulated. Almost no erosion developed during the tests with a lower discharge. The 100 l/s per meter test is simulated up to 100 minutes. After this, erosion became so large that the transition of the road with the grass sod was covered with a heavy geotextile.

Note that the 50 and 100 l/s per meter overtopping discharges are highly extreme situations and will most probably not evolve in reality as the maximum allowed overtopping discharge for a dike with a clayey soil and reasonably good grass cover equals 1.0 l/s per meter (Van der Meer, 2002).

2.3.2. DIKE PROFILES

Before and after every test the dike profile was scanned with a 3D laser scan. The data is stored in a matrix consisting of millions of points. Each point is given with a certain x-, y- and z-value. The data that is used in this research was already filtered by INFRAM. The data set was filtered for a certain distance criterion in z-direction, which has led to a reduction of the amount of points in the matrices.

Wave overtopping tests were performed on a dike for a width of four meters. The guidance walls, which are located on both sides of the test section, have a certain influence on the hydrodynamics. Therefore the profile located in the middle of the test section is used. Data points on this cross section are plotted. To make sure enough data points are plotted to provide an accurate profile, a width in x-direction is chosen. The profile near the road should be more precise than the slope of the dike, because the transition zones are most important for the determination of the influence of the road structure on erosion development. For this reason different widths in x-direction are used to construct the dike profile. Figure 2.9 gives the data points made by the scan and the interpolated dike profile. The figure presents the dike profile after the 10 l/s per meter test, which is used as initial situation in the CFD simulation. Appendix E.1 provides the MATLAB-script of the construction of the dike profile.

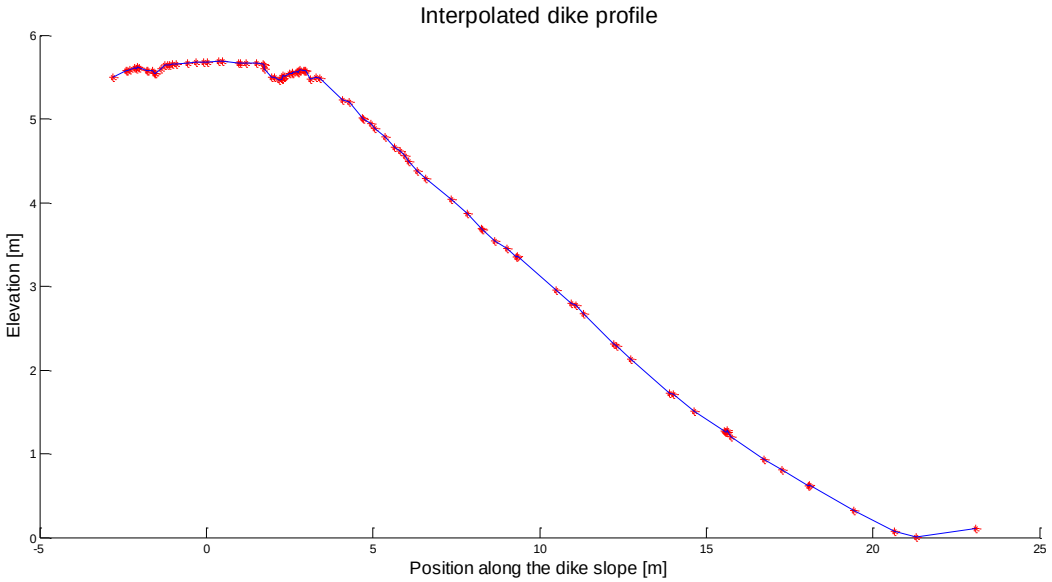

Figure 2.9. Measured data points and interpolated dike profile

3. THE MODEL

In this chapter a coupled hydrodynamic-bed model is developed. This model consists of two parts. First a CFD simulation is performed, leading to bed shear stresses for certain overtopping volumes. These stresses are used to compute the amount of scour. The eroded dike profiles are obtained by subtracting the amount of scour from the initial dike profile. This updated dike profile is loaded into the CFD simulation in order to compute the shear stresses for a new overtopping event. It is assumed that the grass sod is completely eroded when the erosion depth is larger than 0.1 meters. The roughness at these scour locations are then adapted to a value that corresponds with clay.

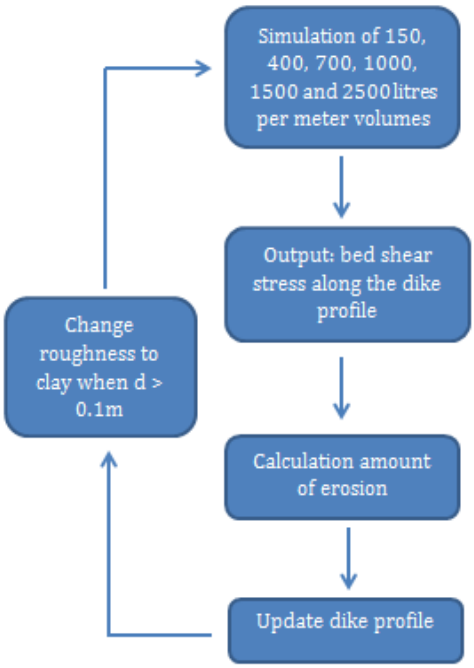

Figure 3.1. Coupled hydrodynamic-bed model

The 50 and 100 l/s per meter tests consist both of approximately 3000 waves. The erosion that evolves due to a single overtopping wave is relatively small and for this reason it is not necessary to simulate each overtopping wave with an updated dike profile. The dike profile is updated after circa 200 waves for the 50 l/s per meter test, which corresponds with one hour testing in Millingen aan de Rijn. The 100 l/s per meter test is updated after approximately 500 waves, which corresponds with 50 minutes. The erosion due to these overtopping durations is computed by accumulating the amount of scour as a result of the single overtopping wave volumes. Figure 3.1 presents the coupled hydrodynamic-bed model.

In section 3.1 the construction of the CFD simulation is presented, where after in section 3.2 an erosion model is provided which is used to compute the amount of scour.

3.1. CFD SIMULATION

The hydrodynamics during wave overtopping are simulated with the use of computational fluid dynamics (CFD). The approach of solving the hydrodynamic problem is primarily concerned with the conservation of mass and momentum (Anderson et al., 2009). These conservation principles are given in the form of partial differential equations. CFD is able to solve these partial differential equations which would cost a lot of time, or is even impossible, to solve by humans.

3.1.1. THEORETICAL BACKGROUND

The hydrodynamics during wave overtopping are simulated with an unsteady two dimensional model. A two dimensional model is needed because the flow velocities near the bed are not equal to the velocities at the surface. To investigate erosion during wave overtopping it is important to know the flow conditions near the bed of the dike profile. The model is unsteady because the turbulent character of the overtopping flow is highly unsteady. A Reynolds-Averaged Navier-Stokes (RANS) model combined with a $k \sim \varepsilon$ turbulence model is used. A turbulence model is included to solve the complex behaviour of wave overtopping. The $k \sim \varepsilon$

turbulence model is applied because of its good convergence rate and relatively low memory requirements. It is a good trade-off between accuracy and complexity. In addition, the k ~ ε turbulence model performs well around complex geometries and applicable for two-phase flow (Frei, 2013b). At the bed of the model domain wall functions are applied. Wall functions have significantly lower computational requirements than solving the entire complex behaviour of the hydrodynamics near the bed (Frei, 2013a). To solve the partial differential equations involved in the CFD simulation, the finite element method (FEM) is used. In this method the domain is subdivided into cells or elements, which forms a grid. A great advantage of FEM is the ability to deal with arbitrary geometries (Ferziger & Peric, 2002). In addition, FEM permits a rapidly change in element size. More information about the RANS equations, k ~ ε turbulence model and the finite element method is presented in Appendix B.

The CFD simulation is performed with the use of COMSOL Multiphysics, which is a platform for physics-based modelling and simulation using the finite element method. Applying changes in the geometry is simplistic due to the different features COMSOL Multiphysics has. This is convenient because the geometry needs to be updated multiple times as a result of the scour caused by wave overtopping. Appendix B provides more information about COMSOL Multiphysics.

3.1.2. GEOMETRY

The dike profile is constructed as described in section 2.3.2. The geometry of the wave overtopping simulator and dike profile are combined in order to model the test set-up in Millingen aan de Rijn. The resulting geometry is presented in Figure 3.2.

Figure 3.2. Geometry wave overtopping simulator and dike profile for the experiment in Millingen aan de Rijn

The 3D laser scan data shows that erosion on the dike slope is relatively small compared to erosion at the crest. A test simulation is performed with a wave overtopping volume of 2500 litres per meter, which is the worst case scenario in this research. Erosion was computed for 30 overtopping wave events and Figure 3.3 presents the scoured dike profile. The maximum erosion at the crest is approximately 45 centimetres, while at the slope this is only 16 centimetres. For this reason it is justified to exclude the dike slope from the analysis to decrease the computation significantly. Figure 3.2 presents by the dashed line which part of the dike slope is excluded from the geometry.

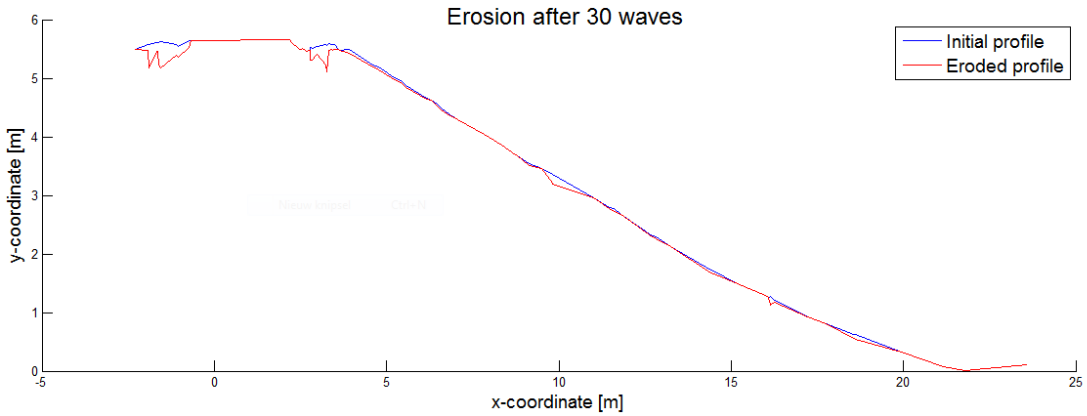

Figure 3.3. Erosion after 30 waves with a volume of 2500 l/m

Several changes in the original geometry of the wave overtopping simulator are made to avoid stability problems during the CFD simulation. The front guidance and the opening valve of the wave overtopping simulator are removed. Due to the opening valve the water had troubles leaving the wave overtopping simulator. The size of the opening is set to the required value of 0.5 meters. Furthermore, only the part of the simulator where water is present is modelled. The upper part where air is present is cut off. The complex process that evolves in the upper part of the simulator when water is flowing downward is not relevant for the model. These changes have led to the geometry as given in Figure 3.4. For this situation the simulator is filled with a volume of 1500 l/m width.

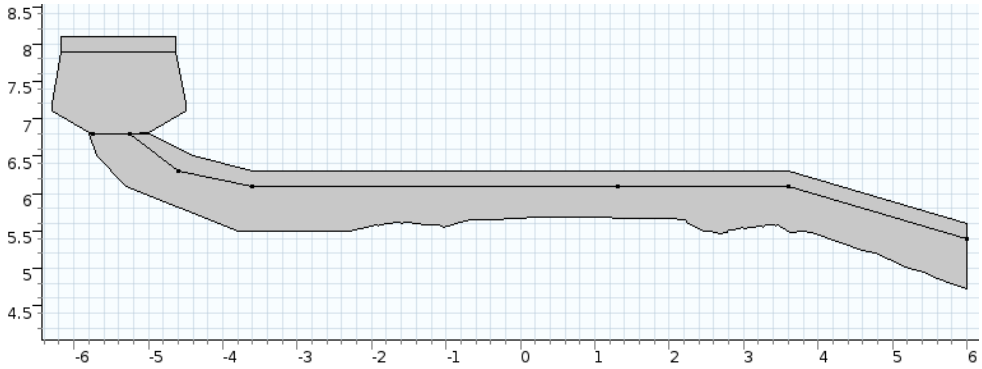

Figure 3.4. Simplified geometry whereby the simulator is filled with 1500 litres per meter

3.1.3. TWO-PHASE FLOW

The free-surface is modelled with the use of the interface capturing method. In this method the governing equations are solved for both the air and the water phases, and is therefore also referred as the two-phase method (Senocak & Iaccarino, 2005). The two-phase method is applicable for problems in which the air phase somehow get pressurized during the computations and thus for problems in which air is trapped or bubbles are formed inside the flow (Carrica, Wilson, & Stern, 2005). This method simulates the turbulence of overtopping flow accurately and is therefore used during the CFD simulation. Figure 3.5 presents the principle of the two-phase flow method.

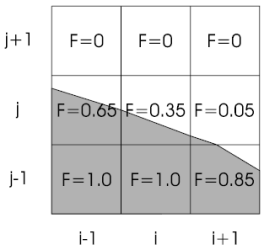

Figure 3.5. Principle of the two-phase flow method (Troch, Van Gent, Schüttrumpf, Lemos, & De Rouck, 2002)

In the two-phase method the position of the interface between the water and the air is tracked by solving two transport equations, one for the phase field variable and one for the free energy (Schlegel, 2015). The movement of the surface is determined by minimisation of free energy. A volume fraction (F) of zero indicates that no water is present in the mesh element, while a volume fraction of one indicates that only water is present. A value between the zero and one represents that both air and water are located in the mesh element.

3.1.4. INITIAL AND BOUNDARY CONDITIONS

The model has two initial conditions, namely the pressure distribution throughout the whole domain and the initial interface. Figure 3.6 gives the initial conditions and are as follow:

- At the initial situation a pressure distribution is defined as a function of the height and the fluid density. It represents the gravity in the domain and is given with:

$$P_0 = \rho \times g \times y \tag{3}$$

Where:

P_0	= pressure at t = 0	[Pa]
ρ	= density of fluid present in the domain	[kg/m^3]
g	= gravitational acceleration	[m/s^2]
y	= y-location	[m]

- Initial interface represents the interface between the air and water in the initial situation. Two initial interfaces are present, one at the water surface and one at the outlet of the wave overtopping simulator.

Three boundary conditions exist, namely inlet, outlet and a wall function. Figure 3.6 shows the boundary conditions and are as follow:

- Above the wave overtopping simulator a thin strip of air is schematized. At the top of this strip a pressure inlet is present. Backflow is suppressed, in order to prevent air or water leaving the domain through the boundary. The pressure at the inlet at t = 0 equals zero Pa.
- Two types of pressure outlets are implemented. For the horizontal outlet an initial condition of zero pressure is assumed, while for the vertical outlet a pressure distribution is defined which is dependent of the height as described by Equation (3). For both outlets the backflow is suppressed, in order to prevent water or air entering the domain through the outlet.
- The wall functions are applied to implement the effects of the roughness of the different sections (steel, geotextile, grass, asphalt, clay).

Figure 3.6 presents the initial and boundary conditions. The blue and red volumes indicate water and air is present respectively.

Figure 3.6. Boundary and initial conditions of the CFD simulation

3.1.5. MESH

The mesh discretises the geometry into small units, referred to as mesh elements (COMSOL bv, 2008). The model is discretized as triangular elements. These elements support adaptive mesh refinement and only need little user input (Frei, 2013a). During the CFD simulation it is of high importance that the overtopping volume is modelled as accurate as possible. For this reason the geometry is divided into two domains. One part is located near the bottom surface with a relatively small maximum element size. The other part is located at the top of the domain, with a larger maximum element size. The element size increases in upward direction to obtain a higher accuracy near the bottom of the geometry where the shear stresses are required to be computed with higher detail.

At the inner slope of the dike the velocities increase, resulting in a reduction of the overtopping water depths. It is important that the flow conditions at the bottom of the slope are simulated adequately and therefore a more refined mesh is needed. To provide this, quadrilateral mesh elements are used along the dike slope. The flow is parallel to the bottom of the slope and almost no changes in normal direction are expected. For this situation quadrilateral mesh elements are more capable of capturing the flow conditions. Figure 3.7. presents the mesh of the model. It has 13,391 elements and 930 boundary elements. The exact details of the meshes for the different overtopping volumes are provided in Appendix C.

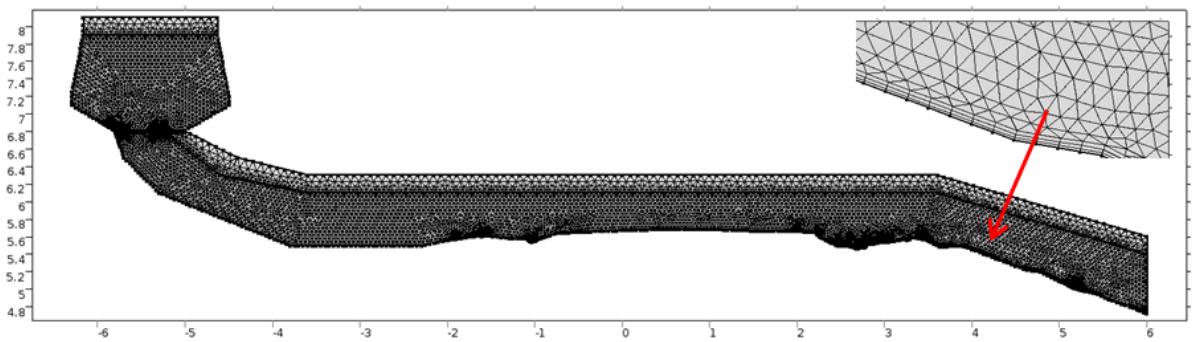

Figure 3.7. Mesh of the geometry

3.1.6. PARAMETERS

This section gives the parameters that are included in the CFD simulation.

3.1.6.1. Characteristics air and water

The CFD simulation includes two materials, namely air and water. The material of the wave overtopping simulator, steel, is represented with the use of a friction coefficient for the boundary. For solving the partial differential equations, only the dynamic viscosity and the density of water and air are necessary. Table 3.1 presents these values.

Table 3.1. Characteristics air and water

	Property	Value	Unit
Air	Dynamic viscosity	2.0×10^{-5}	Pa*s
	Density	1.2	kg/m^3
Water	Dynamic viscosity	1.0×10^{-3}	Pa*s
	Density	1.0×10^{3}	kg/m^3

3.1.6.2. Turbulence model

Launder, Morse, Rodi, & Spalding (1972) examined free turbulent flows. They have made a recommendation of the values for the dimensionless constants in the equations of the k ~ ε model. These values are used and presented in Table 3.2.

Table 3.2. Values dimensionless constants k ~ ε model

Parameter	Value [-]
C_1	1.44
C_2	1.92
C_μ	0.09
σ_ϵ	1.3
σ_k	1

3.1.6.3. Initial interface thickness and surface tension

The initial interface thickness represents the thickness of the interface between the water and the air at the beginning of the time domain. A smaller thickness leads to results with higher accuracy. However, the thickness has a large influence on the computation time. When the thickness of the initial interface is smaller than the mesh size, the interface cannot be described with the use of this mesh. Taking above two points into account has led to an interface thickness and maximum mesh size of 0.05 meters.

The surface tension may only be excluded from the model when it has a negligible effect on the hydrodynamics during overtopping. Jervis and Peregrine (1996) describe that surface tension plays an important role when the surface curvature is sufficiently high. During overtopping, thin jets are often produced which have a very high curvature at the tip. They found that surface tension can have a significant effect on the shape of this jet (Jervis & Peregrine, 1996). For this reason surface tension should be included during the CFD simulation.

3.1.6.4. Roughness coefficients

The dike consists of a grass cover with a clay layer underneath, and a road located at the crest. The wave overtopping simulator was made of steel. All these materials give another resistance and must be implemented in the model.

For turbulent rough flows the Manning's coefficient is recommended to express the roughness of the wall. The Manning's coefficient is defined as the resistance to flow and is given with the following equation (Chow, 1959):

$$v = \frac{1.49}{n} R^{2/3} S^{1/2} \quad (4)$$

Where:

v	= mean velocity	[m/s]
n	= Manning's coefficient	[-]
R	= hydraulic radius	[m]
S	= slope of energy line	[-]

The roughness coefficients of clay and steel are based on the work of Chow (1959). In his work, he defines a minimum, normal and maximum value for each material. The normal value is recommended in the case of good maintenance, and is used for the clay. The roughness of steel was determined with the use of some test runs. The normal value gave too high flow velocities compared to reality and therefore the maximum value of Chow (1959) is used. The roughness coefficients of the grass and asphalt sections are based on a report of the experiment in Millingen aan de Rijn (Van Hoven, Verheij, Hoffmans, & Van der Meer, 2013).

During the experiment in Millingen aan de Rijn a heavy geotextile was located at the transition of the wave overtopping simulator and the grass sod. The roughness of the geotextile is assumed to have a Manning's coefficient of 0.012 (Novak, Moffat, Nalluri, & Narayanan, 2007).

The Manning's coefficients needs to be adapted to values of the Nikuradse roughness height in order to be implemented in the CFD simulation. Gonzalez, Melching, & Oberg (1996) measured the flow velocity in an open channel with the use of an acoustic Doppler current profiler. With this data they were able to establish the following formula (Gonzalez et al., 1996):

$$n = 0.0391 {k_s}^{1/6} \quad (5)$$

Where:

k_s	= Nikuradse roughness height	[-]

Table 3.3 presents the Manning's coefficients and corresponding Nikuradse roughness heights for the five materials.

Table 3.3. Manning's coefficients and corresponding Nikuradse roughness heights for the different materials

Material	Manning's coefficient [-]	Nikuradse roughness height [-]	Reference
Grass	2.5×10^{-2}	6.8×10^{-2}	(Van Hoven et al., 2013)
Clay	1.4×10^{-2}	2.1×10^{-3}	(Chow, 1959)
Asphalt	1.6×10^{-2}	4.7×10^{-3}	(Van Hoven et al., 2013)
Steel	1.7×10^{-2}	6.8×10^{-3}	(Chow, 1959)
Geotextile	1.6×10^{-2}	4.7×10^{-3}	(Novak et al., 2007)

Figure 3.8 shows in which sections the different roughnesses are applied.

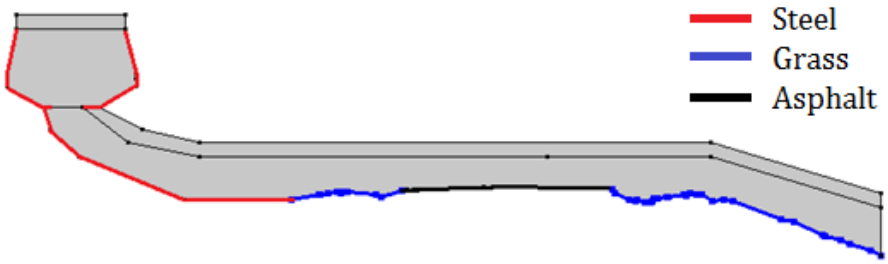

Figure 3.8. Different roughness sections in the CFD simulations

3.1.6.5. Volume fraction coefficient

The volume fraction indicates whether air, water or a mixture of both is present in a mesh element. A volume fraction must be determined till when it is assumed that the characteristics such as velocity and shear stress are due to the hydrodynamics and not as a result of the air motions. The outcomes of the different volume fractions are compared with measured data. This has led to the differences between the simulation and measured validation data. These errors are presented in Table 3.4, in which the differences of the 150, 400, 700, 1000, 1500 and 2500 l/m volumes are averaged. Appendix F provides the outcomes of the volume fractions per wave volume.

Table 3.4. Averaged differences between validation data and CFD simulation for different volume fractions

Volume fraction	0.30	0.40	0.50	0.60	0.65	0.70	0.75
u_{max}							
u_{sm1}	22.1%	20.2%	20.7%	20.0%	19.7%	21.0%	22.6%
T_{ovt}	18.0%	21.8%	25.6%	30.3%	32.1%	34.5%	36.8%

The flow velocities are the most important characteristics, as they are based on theoretical knowledge and measurements performed. The overtopping time is based on physical reasoning and is therefore a less reliable validation parameter (ComCoast, 2007). The maximum velocities are correct modelled for a volume fraction of water smaller than 0.65. For a volume fraction smaller than 0.65, a fraction of 0.60 is most accurate in simulating the velocities at location SM1. For this reason a value of 0.60 is used, even though the overtopping times are not modelled correctly.

3.1.7. VALIDATION CFD SIMULATION

In this section the outcomes of the CFD simulations are validated. This is done with the use of measured data during the experiment in Millingen aan de Rijn as well as with theory for which the wave overtopping simulator was developed. This theory gives ranges of the maximum near bed velocities and overtopping times when the wave leaves the overtopping simulator. Table 3.5 presents the validation data and the outcomes of the CFD simulations. The table shows that the maximum velocities are modelled accurately. They are in the range of theory, except for the 150 l/m wave volume. The layer thickness of the overtopping tongue for this volume is so small that no volume fraction of water larger than 0.6 meters is present. This leads to the zero flow velocities and overtopping times (Table 3.5). It is assumed that the 150 l/m volume has no effect on the erosion development, because the forces acting on the dike profile as a result of this volume is relatively small. The overtopping times are too small, except for the 2500 l/m volume.

The overtopping times were established based on physical reasoning and not on theoretical knowledge (ComCoast, 2007). The flow velocities are therefore the leading factors and it can be concluded that the hydrodynamics at the outlet of the simulator are modelled accurately. However, this does not account for the smallest volume.

Table 3.5. Validation maximum near bed flow velocity and overtopping time

Volume [l/m]	u_{max} [m/s] theory	u_{max} [m/s] simulation	T_{ovt} [s] physical reasoning	T_{ovt} [s] simulation
150	2.5 – 3.5	0.00	1.5 – 2.5	0.0
400	3.5 – 5.0	3.76	2.0 – 3.0	0.9
700	4.2 – 5.7	4.45	2.5 – 3.5	1.4
1000	5.0 – 6.5	5.06	3.0 – 4.0	2.0
1500	5.5 – 7.0	5.75	3.0 – 4.0	2.6
2500	6.0 – 8.0	6.31	3.5 – 5.0	3.6

During the experiment in Millingen aan de Rijn different overtopping volumes were released and the velocities and water layer thicknesses were measured. This data is presented in Table 3.6, as well as the outcomes of the CFD simulations. Each wave volume is measured two times during the experiment, leading to two velocities and water depths. The average is used to compute the difference between the measurements and simulation. Figure 3.9 shows the location of SM1. This figure also shows the other measurement locations. These locations are not used for validation due to high differences in the geometries. In the model a large pit was present at the transition of the road with the grass sod, which was covered by a heavy geotextile during the measurements. For this reason the CFD simulation gives significant lower flow velocities at these locations than was measured.

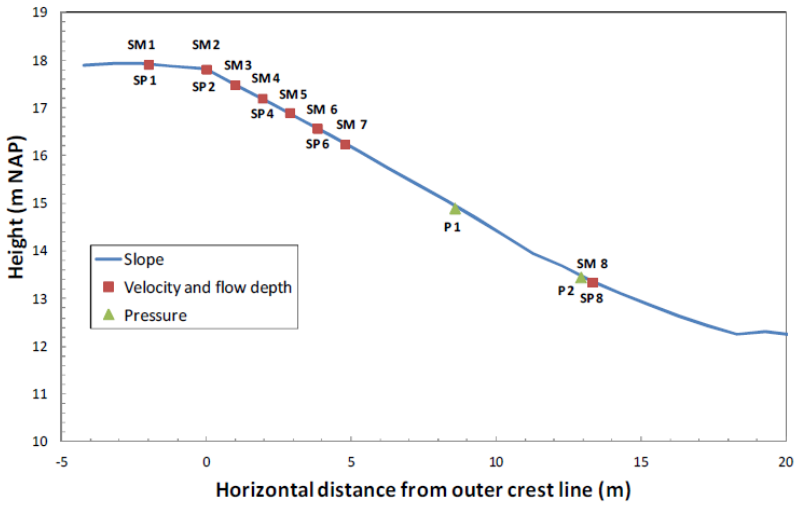

Figure 3.9. Locations of the surfboards and paddle wheels experiment in Millingen aan de Rijn (Van Hoven et al., 2013)

Table 3.6 shows that local variations of the velocities and water depths exist for the measurement and therefore the simulation may deviate slightly from the measurement values. It is assumed that the velocities and water depths are simulated accurately when the deviation is smaller than 15%. This value is chosen arbitrarily. The depths are simulated quite accurately for all overtopping volumes. However, the flow velocities at test location SM1 are only correct for

the middle volumes. The little overtopping volumes are slowed down too much, while the large overtopping volumes do not loose enough energy.

Table 3.6 Validation velocities and water depths at location SM1

Volume [l/m]	u_{SM1} [m/s] measured	u_{SM1} [m/s] simulation	Difference [%]	h_{SM1} [m] measured	h_{max} [m] simulation	Difference [%]
400	3.55 3.63	2.83	−21.2%	0.10 0.09	0.09	−5.3
1000	4.09 4.20	4.49	+8.3%	0.16 0.15	0.14	−9.7
1500	4.54 4.66	5.24	+13.9%	0.21 0.23	0.20	−9.1
2500	5.08 5.04	6.91	+36.5%	0.26 0.26	0.23	−11.5

Final validation points are the rough surface of the flow and the velocity pattern inside the flow. The surface is not smooth due to turbulence and the velocities near the bed must be lower than at the surface due to the roughness of the bed profile. Figure 3.10 shows that both points are simulated correctly.

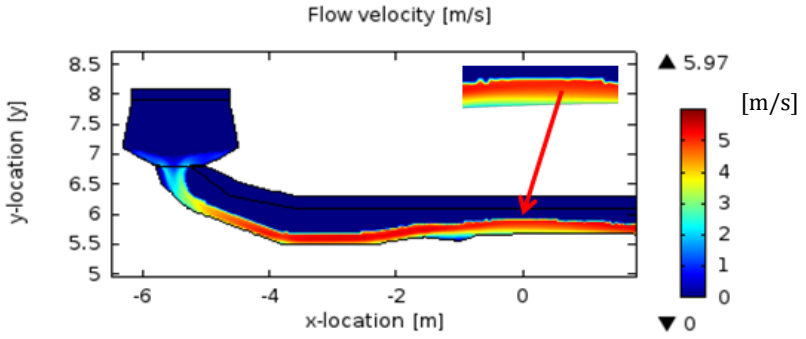

Figure 3.10. Overtopping tongue with a volume of 1500 l/m

The validation was performed with the use of the maximum flow velocities, the overtopping times and the velocities and water depths at location SM1. The overtopping times were based on physical reasoning and the measurements performed at location SM1 deviate from the CFD simulation. During the measurements the road section was covered with a heavy geotextile and the overtopping simulator was located at the road section instead of in front the road. The maximum velocities were based on theory and are therefore the most reliable validation parameters. All wave volumes, except the 150 l/m volume, are modelled correctly as they are all in the range of theory. The velocities at test location SM1 are modelled quite accurately for the 1000 and 1500 l/m waves and the water depths are simulated correctly for all wave volumes. This leads to the conclusion that the hydrodynamics of the CFD simulation are quite accurate for the 700 l/m up till the 1500 l/m volumes, while only the flow velocities of the smaller and larger volumes show some discrepancies. The positive validation results give enough confidence of the accuracy of the model. Because the simulated hydrodynamics are close to the measurements it can be expected that the friction velocities at the bed that evolve due to wave overtopping are simulated accurately as well. This friction velocity is used to compute the bed shear stress and to predict the amount of scour.

3.2. BED MODEL

In this section theoretical background of the erosion process of a grass covered dike profile with a clay layer underneath is described. There after an erosion model from literature is described and adapted to the situation in Millingen aan de Rijn, which leads to the bed model. This section ends with validation of the bed model.

3.2.1. THEORETICAL BACKGROUND

Erosion occurs when a critical threshold is exceeded. This threshold is often expressed as a function of the critical Shields number and represents the dimensionless bed shear stress. The Shields number can be given with the following formula:

$$\theta = \frac{\tau_b}{(\rho_s - \rho_w)gD} \tag{6}$$

Where:

θ	= Shields number	[-]
τ_b	= bed shear stress	[N/m^2]
ρ_s	= density of soil	[kg/m^3]
ρ_w	= density of water	[kg/m^3]
D	= average grain size	[m]

When the Shields number is larger than the critical Shields number, grains are set into motion and erosion evolves. However, the Shields parameter is applicable for uniform flow and non-cohesive sediment (Valk, 2009). The flow during overtopping is non uniform and the core of the dike consists of clay, which is a cohesive sediment. For these reasons the Shields parameter is not appropriate for the prediction of erosion in this research. Therefore an erosion model is applied which is a function of the critical bed shear stress and a turbulence coefficient.

From large-scale laboratory studies and experiments done with the wave simulator it seems that a grass cover may slow down the erosion process. A grass cover can be divided into two layers, namely the top soil and the sub soil (Figure 3.11). The porous turf, located in the top layer, has a high root density and is elastic in most conditions (Hoffmans, Akkerman, Verheij, Hoven, & Van der Meer, 2008). The characteristics of the grass are found in the structure of the root layer. The root structure holds the clay aggregates together and prevents them from being washed out. The underlying substrate is stiff and less permeable. For clay relatively large forces are necessary to break the bonding aggregates, while relatively small forces are necessary to transport the sediment (Hoffmans et al., 2008).

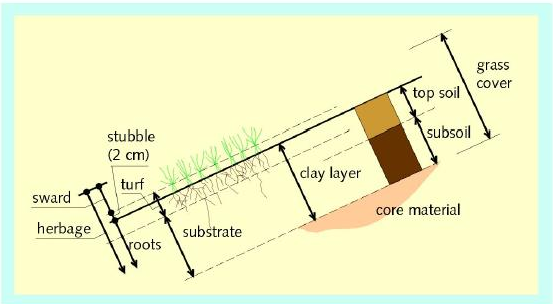

Figure 3. 11. Structure of a grass cover layer (Technische Adviescommissie voor de Waterkeringen, 1997)

The erosion mechanisms of grass can be divided into three stages (Vavrina, 2006):

- The first mechanism consists of loose sediments and particles that are scoured out of the grass cover layer. This stage leads to a rougher surface with increased drag, shear and lift

forces on the elements leading to a further increase of flow velocity due to local constriction.

- The second mechanism consists of washing out aggregates of the top layer. This leads to the situation in which the roots activate their strength. The roots of the grass cover are harder to erode than sediments due to their friction and their tensile strength.
- In the end the roots fail by being pulled out or tearing up. The grass cover layer is now completely eroded. After this stage, scour of the dike core continues.

Figure 3.12 shows the three mechanisms of erosion of a grass cover layer.

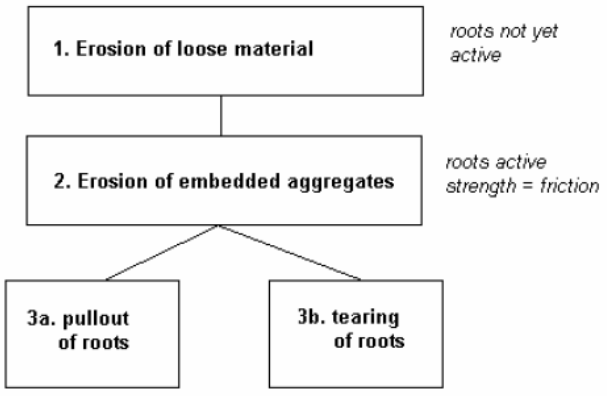

Figure 3.12. Mechanisms of erosion of a grass sod (Vavrina, 2006)

The erosion process is not only influenced by flow velocity and turbulence of the overtopping wave, but also by the strength parameters of the grass and clay layers. Near the surface, the strength is dominated by the root reinforcement. Deeper below the surface, the amount of roots decreases rapidly. In this section the cohesion and the internal friction angle of the clay itself determines the strength (Hoffmans et al., 2008). Due to the complexity of the erosion process of a grass sod with a clay layer underneath, assumptions must be made to model this complex process.

It is assumed that the grass sod in Millingen aan de Rijn has a depth of 10 centimetres. No local variation of the grass quality along the dike profile is considered. In addition, a homogenous clay layer underneath the grass sod is assumed. Erosion development under the road section is not incorporated. Figure 3.13 shows a sketch of the cross section of the dike profile.

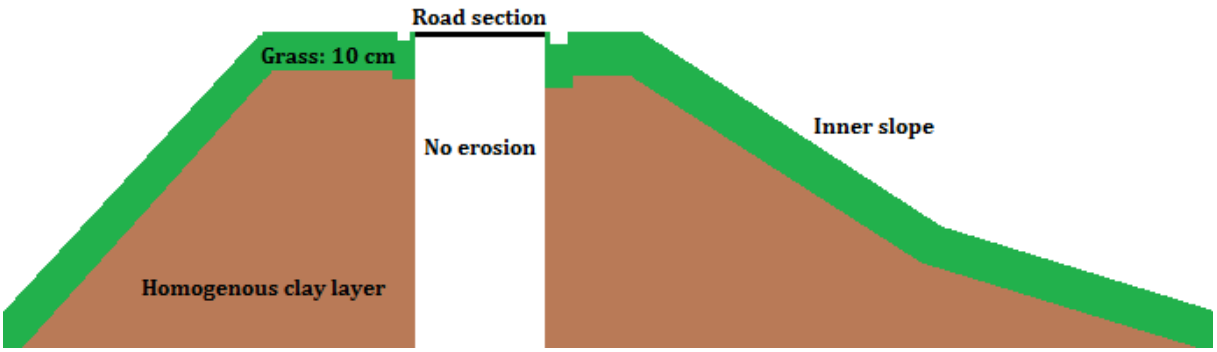

Figure 3.13. Sketch of the cross section of the dike profile

3.2.2. EROSION MODEL

Valk (2009) has developed an erosion model to investigate erosion development at the toe of the dike during wave overtopping. This model is based on the turf-element model of Hoffmans et al. (2008) and the EP method ('Erosiegevoelige Plekken Methode') of Van den Bos (2006). Both models are only applicable for an erosion depth smaller than 0.1 meters. Valk (2009) extended this for greater depths. The model is therefore not restricted to the scour of the grass sod only, but can also model the erosion of the dike core. This is done by implementing a depth-dependency factor for the strength and load terms. In addition, the erosion function is dependent on the maximum bed shear stress instead of the maximum flow velocities. This is more appropriate for this research. Pits in the geometry lead to velocities close to zero, while the bed shear stresses may be high at these locations. The formula for the scour of the erosion model is (Valk, 2009):

$$\frac{dY}{dT} = \frac{(\omega^2 \tau_{b,max} - \tau_c(d))}{E_{soil}(d)} \tag{7}$$

Where:

Y	= amount of scour	[m]
T	= overtopping time	[s]
ω	= turbulence coefficient	[-]
$\tau_{b,max}$	= maximum bed shear stress	[N/m²]
τ_c	= critical bed shear stress	[N/m²]
E_{soil}	= soil parameter	[-]
d	= erosion depth caused by earlier overtopping waves	[m]

Equation (7) computes the change in bed level in which only erosion is considered. This means that deposition is neglected from the erosion process and that an increase in bed level due to deposition is not possible to evolve. All eroded sediment is assumed to be discharged out of the model domain.

The critical bed shear stress and the soil parameter are both dependent on the cohesion of the clay and the strength of the roots. The strength obtained by the roots and the clay cohesion is not constant over depth but decreases, where after it increases again. Near the surface the strength is dominated by the root system, whereas with increasing depth cohesion and internal friction of the clay dominates (Hoffmans et al., 2008). The critical shear stress, including depth-variability, is written as (Valk, 2009):

$$\tau_c(d) = \alpha_\tau \times ((\rho_s - \rho_w) g d_a + \tau_{total}(d) \tag{8}$$

With

$$\tau_{total}(d) = f \times \left(\tau_{clay}(d)\right) + \sigma_{roots}(d) \tag{9}$$

Where:

α_τ	= pressure fluctuation coefficient (1/18)	[-]
d_a	= aggregate diameter	[m]
f	= a factor for the clay cohesion	[-]
$\tau_{clay}(d)$	= clay cohesion as a function of depth	[N/m²]
$\sigma_{roots}(d)$	= grass strength as a function of depth	[N/m²]

Valk (2009) assumes a linear increase of the clay cohesion and an exponential decrease of the root density with respect to depth:

$$\tau_{clay}(d) = \tau_{clay,0}(1 + a_{cs} \times d) \tag{10}$$

And

$$\sigma_{roots}(d) = \sigma_{roots,0} \times e^{-\beta d} \tag{11}$$

Where:

a_{cs} = coefficient of clay cohesion increase over depth [-]
β = coefficient of root decrease over depth [-]

Applying these two equations leads to an integration of the clay cohesion within a grass layer.

The soil parameter E_{soil} is given with the following equation (Hoffmans et al., 2008):

$$E_{soil} \equiv {C_E}^{-1} \quad \text{with} \quad C_E = \alpha_E \frac{g^2 d_a}{\upsilon \times {U_c}^2} \tag{12}$$

Where:

C_E = overall strength parameter [$m^{-1}s^{-1}$]
α_E = a coefficient (10^{-10}) [-]
υ = kinematic viscosity of water [m^2/s]
U_c = critical depth-averaged velocity [m/s]

The critical depth-averaged velocity represents a threshold which should be exceeded before erosion starts to develop. The critical flow velocity is presented with (Valk, 2009):

$$U_c = \frac{\alpha_0}{r_0}\sqrt{\Delta g d + \frac{\tau_{total}(d)}{\rho_w}} \tag{13}$$

Where:

α_0 = a coefficient [-]
Δ = relative density [-]
c_s = clay cohesion [N/m^2]
σ_g = normal grass tensile stress [N/m^2]

Appendix D.1 provides information of how Equation (8) and Equation (13) were developed.

3.2.3. PARAMETERS

The parameters that have to be defined in the bed model are the turbulence coefficient, the soil parameter, the bed shear stress and critical bed shear stress. These parameters are described.

3.2.3.1. Turbulence coefficient

The turbulence coefficient is given with the following equation (Valk, 2009):

$$\omega = 1.5 + 5r_0 \tag{14}$$

Where:

r_0 = depth-averaged relative turbulence intensity [-]

During the experiment in Millingen aan de Rijn hydraulic measurements were conducted at two locations; at the crest of the dike and near the toe of the dike. These measurements showed that the flow is significant turbulent at the crest. Near the toe of the dike the turbulence decreases to uniform flow conditions, where the turbulence factor has a value of approximately equal to 1. Table 3.7 presents the computed turbulence factors for the crest of the dike. Based on this information a turbulence coefficient of 0.17 is applied for the crest, while a value of 0.1 is used for the slope of the dike.

Table 3.7. Turbulence factors (Van Hoven et al., 2013)

Volume [l/m]	Turbulence coefficient [-]
1000	0.177
2500	0.169
4000	0.162

3.2.3.2. Bed shear stress

The CFD simulation defines the friction velocities near the bed of the dike profile during wave overtopping. With this data it is possible to calculate the bed shear stress as a function of time. This is done with the following equation:

$$\tau_b = {u_*}^2 \times \rho_w \tag{15}$$

Where:

u_* = friction velocity [m/s]

3.2.3.3. Critical bed shear stress

To be able to calculate the critical bed shear stress the strength of the roots and the clay cohesion at the surface must be defined, as well as the parameters that define the increase and decrease of these strengths. Figure 3.14 presents the strength of the soil over depth. The density of the soil is assumed to be 2000 kg/m^3. A value of 0.21 for the coefficient of f is implemented, as recommend by Valk (2009).

The tensile stress of the roots depends strongly on the type and quality of the grass. The tensile stress at the surface was measured at several locations along the dike profile. This has led to an average value of 7.76 kN/m^2, meaning that the quality of the grass lies between poor and averaged (Van Hoven et al., 2013). Valk (2009) recommends a value of 22.32 for the coefficient of the decrease of the tensile stress over depth (β).

It is assumed that the clay at the dike in Millingen aan de Rijn has a good quality. Hoffmans (2008) suggests a clay cohesion of 11.9 kN/m^2 at the surface (Appendix D). Valk (2009) suggests two values for the coefficient of the increase of the clay cohesion over depth (α_{cs}), namely 20 and 1.75. A value of 20 is applied for the 50 l/s

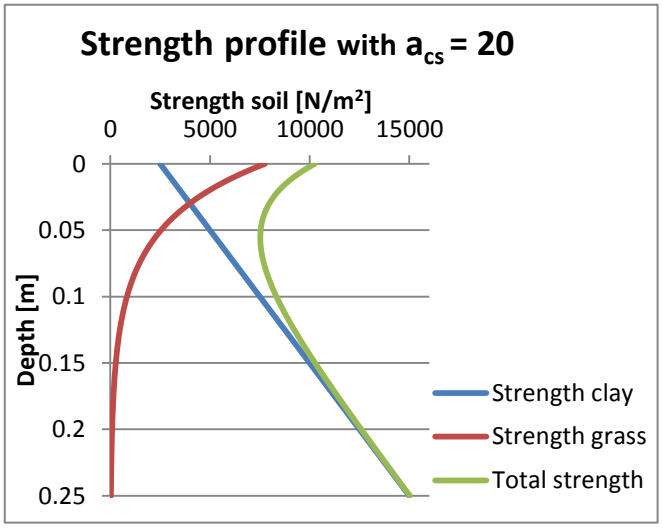

Figure 3. 14. Strength of the soil over depth

per meter test. It is assumed that the bonding forces of the clay aggregates are significant reduced during the 50 l/s per meter test and therefore a value of 1.75 is used for the 100 l/s per meter test. Appendix D.2 gives more information about the quality of the grass sod and the clay layer.

3.2.3.4. Soil erosion parameter

E_{soil} is a parameter which determines the qualities of both grass and clay. The parameters that involve this relationship are already presented in the previous section. Only the aggregate diameter (d_a) and the kinematic viscosity of water (υ) are still unkown. For the aggregate diameter a value of 0.004 meters is suggested (Valk 2009) and for the kinematic viscosity of water a value of 10^{-6} Pa*s is used.

3.2.4. OVERVIEW BED MODEL

Table 3.8 gives an overview of the bed model. Also the values that are used are given. Appendix E.2 provides a MATLAB-script of the bed model. The equation that needs to be solved to be able to compute the amount of scour due to a single wave is:

$$Y = \frac{(\omega^2 \tau_0 - \tau_c(d))}{E_{soil}(d)} \times T \tag{16}$$

This formula is the integral of equation (7) and determines the amount of scour (Y) as a consequence of a single overtopping wave.

Table 3.8. Overview equations of erosion model

Load term	Eq.	Parameters
$\boldsymbol{\omega = 1.5 + 5r_0}$	(14)	$r_0 = 0.17$ at the crest $r_0 = 0.10$ along the slope
Strength terms		
$\boldsymbol{\tau_c(d) = \alpha_\tau \times ((\rho_s - \rho_w) g d_a + \tau_{total}(d)}$	(8)	α_τ = 1/18 ρ_w = 1000 kg/m^3 ρ_s = 2000 kg/m^3 d_a = 0.004 m
$\boldsymbol{\tau_{total}(d) = f \times \tau_{clay,0}(1 + a_{cs} \times d) + \sigma_{roots,0} \times e^{-\beta d}}$	(9)	f = 0.21 $\tau_{clay,0}$ = 11.9 kN/m^2 a_{cs} = 20/1.75 $\sigma_{roots,0}$ = 7.76 kN/m^2 β = 22.32
$\boldsymbol{E_{soil} \equiv \frac{\alpha_{soil}}{C_E}}$	(12)	α_{soil} = 1
$\boldsymbol{C_E = \alpha_E \frac{g^2 d_a}{\upsilon \times U_c^{\,2}}}$	(12)	α_E = 10^{-10} υ = 10^{-6} Pa*s
$\boldsymbol{U_c = \frac{\alpha_0}{r_0} \sqrt{\Delta g d + \frac{\tau_{total}(d)}{\rho_w}}}$	(13)	α_0 = 2.0

3.2.5 VALIDATION BED MODEL

During the experiment in Millingen aan de Rijn the dike profiles were measured with the use of a 3D laser scan. The scan after three hours of testing with a discharge of 50 l/s per meter is used for validation. A heavy geotextile was located at the transition of the wave overtopping simulator and the grass sod (Figure 3.15). This geotextile is implemented in the model and therefore no erosion was able to develop at this section.

Figure 3.15. Heavy geotextile (Bakker et al., 2013)

Figure 3.16 presents the initial slope, the measured eroded profile and simulated eroded profile after three hours of testing. The dashed line indicates till where the geotextile was located and therefore no erosion could develop. Figure 3.17 provides corresponding erosion depths.

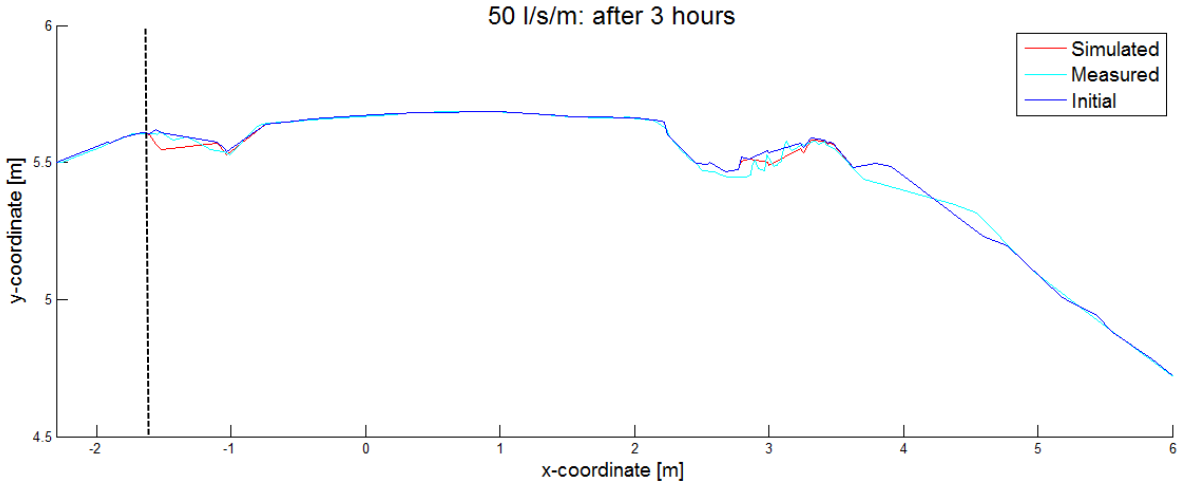

Figure 3.16. Measured and simulated dike profile after 3 hours of 50 l/s per meter test and initial profile

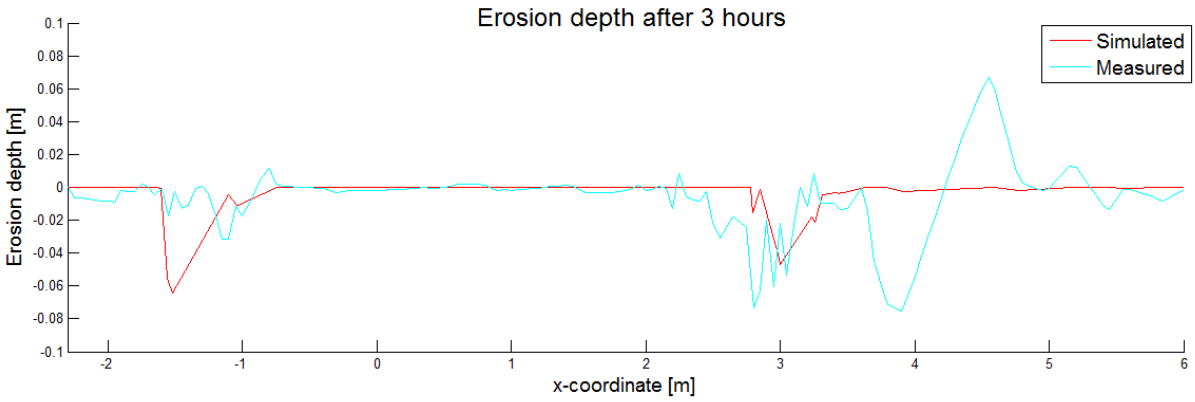

Figure 3.17. Measured and simulated erosion depths after 2 hours of 50 l/s per meter test

The erosion development at the left transition of the grass sod with the road section is more significant simulated than was measured. The flow has most energy at the outlet of the simulator, leading to higher forces acting on the bed and therefore to higher erosion development. The exact dimension and roughness of the geotextile were unknown. It may be that a too small Nikuradse roughness height is chosen, leading to too little loss of energy and as a result to too high shear stresses and amount of scour.

The simulated erosion depth at the right transition is of the same order of magnitude as was measured during the experiment. In addition, the location of this erosion development is modelled quite accurately. However, the data shows an increase of the dike profile at several locations. During overtopping the grass sod is folded before it is teared off, leading to a temporarily increase of the dike profile. This process is not considered during the simulation. In addition, it is assumed that the eroded sediment is discharged out of the model domain and that no deposition evolves. These assumptions lead to discrepancies between the measurements and simulations.

It can be concluded that the bed model is capable of predicting the scour locations correctly and it simulates erosion depths in the same order of magnitude as was measured during the experiment. These results give enough confidence of the accuracy of the model.

4. RESULTS

In this chapter the results of the coupled hydrodynamic-bed model are provided. The points for which the maximum bed shear stress and erosion are computed are provided in Figure 4.1.

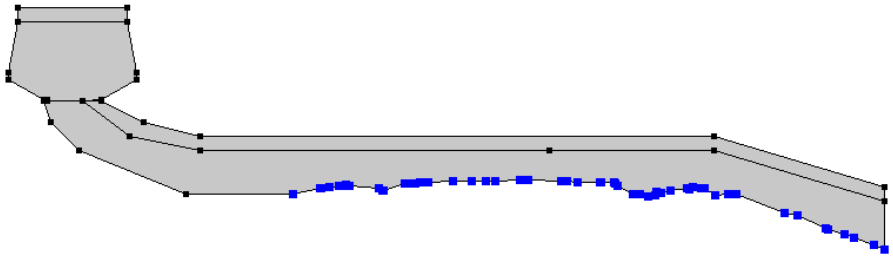

Figure 4.1. Output data points

The erosion that evolves due to a single wave can be computed by equation (16). The amount of scour after a certain overtopping duration can be computed by summating the erosions that evolve due to the waves that overtop in this duration, which leads to the following equation:

$$Y = \sum_{n=1}^{N} \frac{(\omega^2 \tau_0 - \tau_c(d))}{E_{soil}(d)} \times T \qquad (17)$$

Where:

N = number of waves [-]

First, the experiment in Millingen aan de Rijn is simulated and differences between the outcomes of the simulation and measurements performed are described. There after the influence of a road structure on erosion development is presented.

4.1. EXPERIMENT MILLINGEN AAN DE RIJN

The 50 l/s per meter test and the 100 l/s per meter test till 100 minutes are simulated. The profile is updated every hour during the 50 l/s per meter test and after 50 minutes during the 100 l/s per meter test. Table 4.1 presents the amount of waves that are simulated each time interval.

Table 4.1. Overtopping wave volumes during the CFD simulation

	50 l/s per meter						**100 l/s per meter**	
Volume	*0-60 min*	*60-120 min*	*120-180 min*	*180-240 min*	*240-300 min*	*300-360 min*	*0-50 min*	*50-100 min*
150L	200	200	200	200	200	200	0	0
400L	262	237	262	237	262	237	345	303
700L	41	41	41	41	41	41	84	104
1000L	15	19	15	19	15	19	71	62
1500L	3	3	3	3	3	3	17	25
2500L	0	0	0	0	0	0	2	3

4.1.1. RESULTS CFD SIMULATION

The maximum bed shear stresses are the main indicator of the amount of scour that will develop. Figure 4.2 presents the maximum bed shear stresses caused by the different overtopping wave volumes of the initial dike profile. The 150 l/m volume is not presented because this volume results in shear stresses equal to 0 N/m^2.

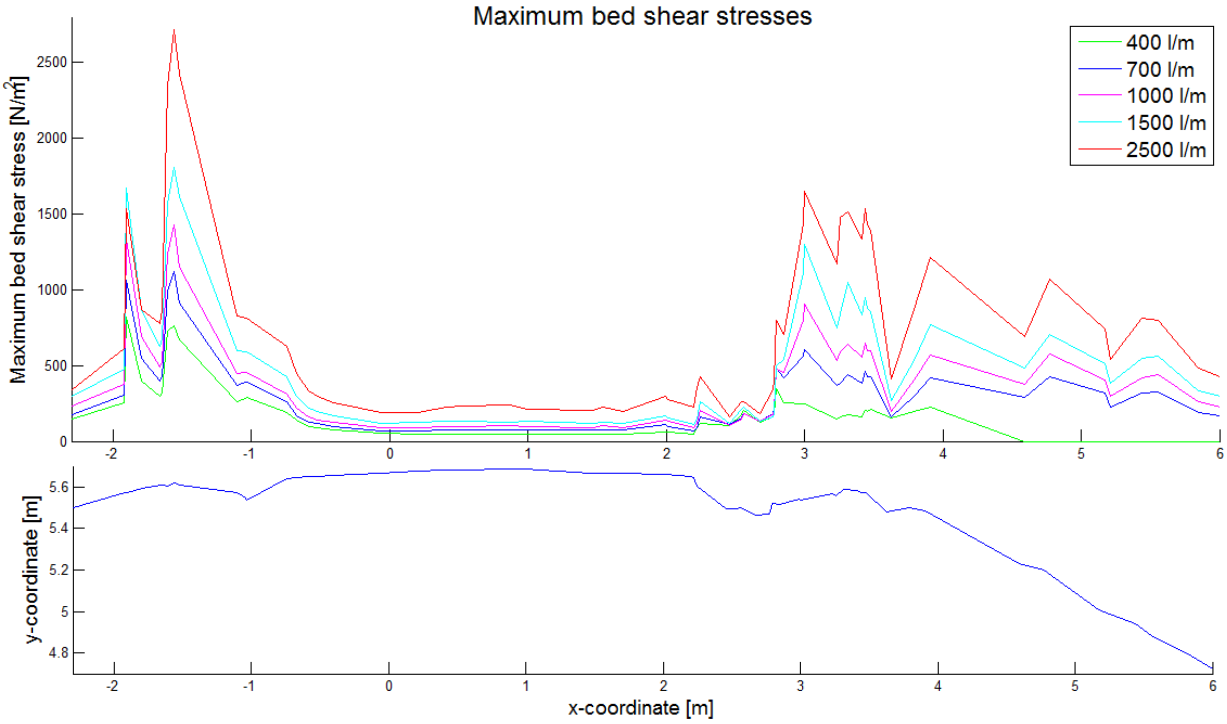

Figure 4.2. Maximum shear stresses due to overtopping wave volumes of 400, 700, 1000, 1500 and 2500 l/m

Figure 4.2 shows that the highest shear stresses evolve on the left side of the road. The flow is released by the simulator and has most energy at the outlet of the wave overtopping simulator. The two peaks are due to irregularities of the dike profile. Remarkably, the shear stresses at the peaks are relatively high while the irregularities in these locations are little. Figure 4.3 shows the upward slopes leading to the high peaks. At the road section the shear stresses decreases significantly due to the decrease of the bed roughness and the smooth profile.

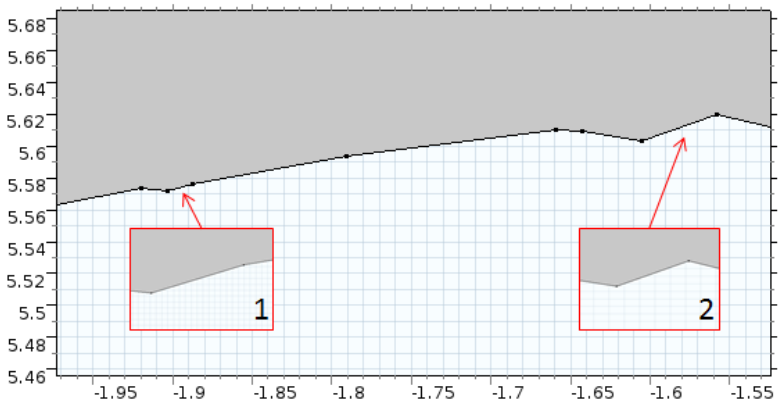

Figure 4.3. Irregularities in de the dike profile

To investigate the exact influences of an irregularity, simulations are performed with different upward slopes. The friction coefficient of the slopes corresponds with a grass cover. Figure 4.4 shows the erosion as a result of these slopes and in Table 4.2 the simulated slopes and corresponding erosion are listed. With this it is possible to state that up to an upward slope of 25˚ the increase of erosion is relatively small. However, steeper slopes result in a significant increase of the amount of scour up to an increase of 49.7% for a 45˚ slope compared to a 5˚ slope. This explains the high shear stresses caused by irregularity 1 and 2 (Figure 4.2 and 4.3).

Table 4.2. Maximum bed shear stresses for different slopes

Slope [˚]	Erosion [mm]	Change [%]
5	19	--
15	20	3.0
25	21	10.2
35	25	28.4
45	29	49.7

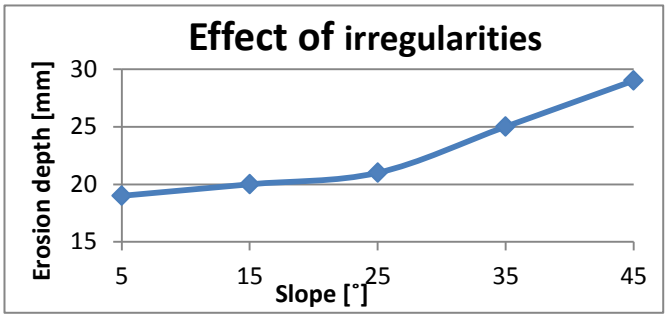

Figure 4.4. Dependency upward slopes on erosion development

During the experiment with the wave overtopping simulator the dike profile becomes smoother. Large irregularities are scoured, leading to flattening of the surface. The irregularities in the dike profile leads to high shear stresses and for this reason the maximum shear stresses along the dike profile are decreasing during the experiment due to a smoother dike profile over time. Figure 4.5 shows the maximum shear stresses as a function of overtopping wave volume for irregularity 1 (Figure 4.3). It is visible that a linear-relationship is present between the overtopping wave volume and resulting maximum shear stress. A higher overtopping volume leads to higher velocities and therefore to larger friction forces at the bed.

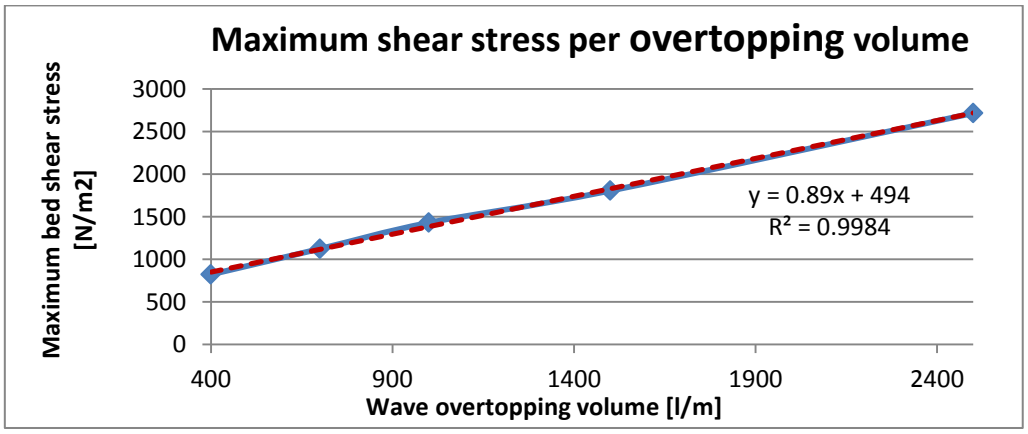

Figure 4.5. Maximum shear stresses as a function of overtopping volume for irregularity 1

4.1.2. *RESULTS EROSION DEVELOPMENT*

During the CFD simulation the maximum shear stresses are simulated caused by six different wave overtopping volumes. With these shear stresses it is possible to compute the amount of scour. Table 4.2 shows the erosion per overtopping wave volume due to irregularity 1 (Figure 4.3). Figure 4.6 gives the dependency. The erosion depth is computed for the situation that the grass sod is still intact, no earlier erosion has evolved. The amount of scour increases with increasing maximum shear stress. No linear relationship is present, as the slope up till a wave overtopping volume of 700 l/m is smaller than for larger overtopping volumes. This means that the increase in erosion development is more substantial for larger overtopping volumes.

Table 4.2. Erosion due to different overtopping volumes

Volume [l/m]	Erosion [mm]
150	0
400	0.12
700	0.25
1000	0.46
1500	0.83
2500	1.52

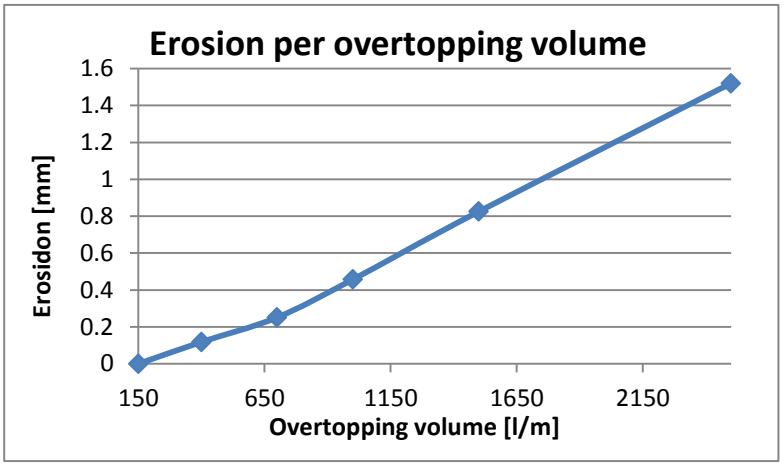

Figure 4.6. Erosion depth as a function of overtopping volumes

In the next sections the erosion after three and six hours of testing with a discharge of 50 l/s per meter and after 100 minutes with a discharge of 100 l/s per meter are presented. Appendix G provides the erosion development of the other time intervals.

4.1.2.1. Erosion after 3 hours: 50 l/s per meter test

Figure 4.7 presents the measured and simulated eroded dike profiles after 3 hours of testing with a discharge of 50 l/s per meter. Figure 4.8 shows corresponding erosion depths. According to the simulation most erosion develops in front of the road section. This corresponds with the high maximum shear stresses at these locations as was determined in previous section. The flow has most energy at this side leading to high shear forces acting on the bed. Little scour developed at the right side of the road. This amount of scour is small compared to the left side, as it is only 34 milimeters compared to 92 milimeters. The erosion on the slope is negligible. Due to the large amount of irregularities the flow has losed a lot of energy when it reaches the slope transition. In addition, the slope has a relatively smooth profile and therefore no substantial increase of the shear stresses develops.

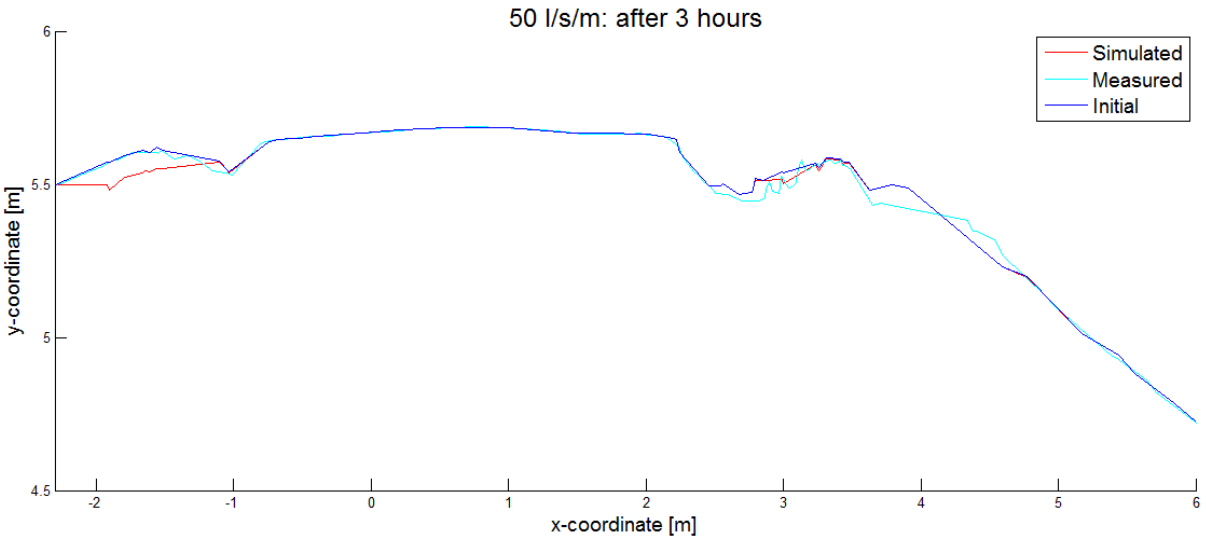

Figure 4.7. Dike profiles after 3 hours of testing with a discharge of 50 l/s per meter

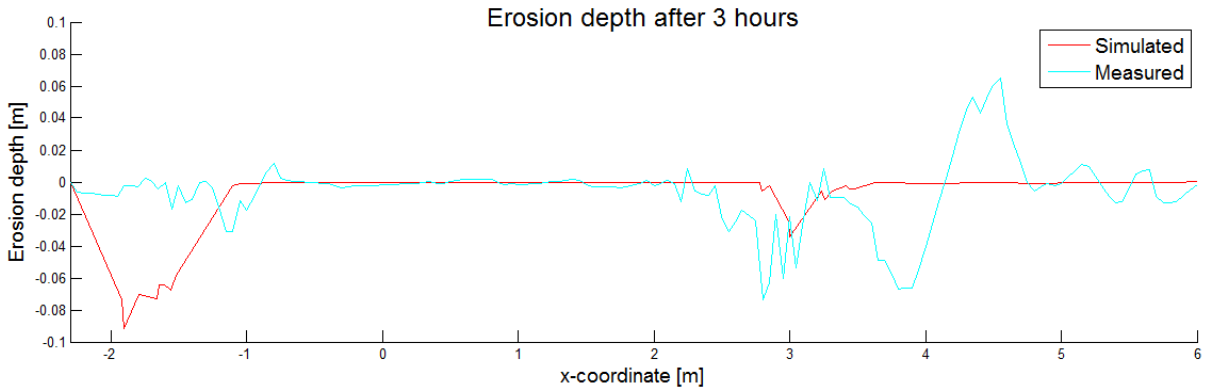

Figure 4.8. Erosion depths after 3 hours of testing with a discharge of 50 l/s per meter

It is visible that the amount of erosion on the left side of the road is larger simulated than was observed during the experiment in Millingen aan de Rijn. During the experiment a geotextile was located at the transition of the outlet of the wave overtopping simulator and the grass sod, as described during the validation of the bed model. This geotextile prevented the underlying dike profile to be eroded. In the CFD simulation this section was modelled as a grass cover, where scour is able to develop. This explains the overestimation of the amount of scour on the left side of the road. The geotextile is not implemented in the model, because no smooth transition exist during real wave overtopping events. The discrepancy of the erosion depth at the left transition is also present during later stages of the experiment and is not discussed in the next sections.

The measured erosion depth shows a substantial increase of the dike profile along the slope of the dike. Due to the overtopping waves, the grass sod is folded before it is teared off. This leads to a temporarily increase of the dike profile. This process is not considered during the simulation, leading to the discrepancy of the simulated and measured erosion depths along the dike slope.

4.1.2.2. Erosion after 6 hours: 50 l/s per meter test

Figure 4.9 presents the measured and simulated eroded dike profiles after six hours of testing. Figure 4.10 shows corresponding erosion depths. During the simulation, erosion on the left side of the road section stagnated after four hours. The irregularities in this section are flattened, leading to a smoother dike profile. As a result the flow is less disturbed and more capable of conserving his energy. Consequently, the shear stresses at the right side of the road increase and therefore the amount of scour increases. It can be concluded that in the begin phase of the experiment erosion on the left side of the road section was much more significant, while substantial erosion at the right side starts to develop when the left side is flattened.

The scour location of the right transition is simulated quite accurately and it is of the same order of magnitude as was measured during the experiment. In addition, almost no erosion developed on the dike slope for both the simulated as mearused profiles. The measured data shows an increase of the dike profile at several locations due to the processes of deposition and folding of the grass sod, what is not considered in the simulation.

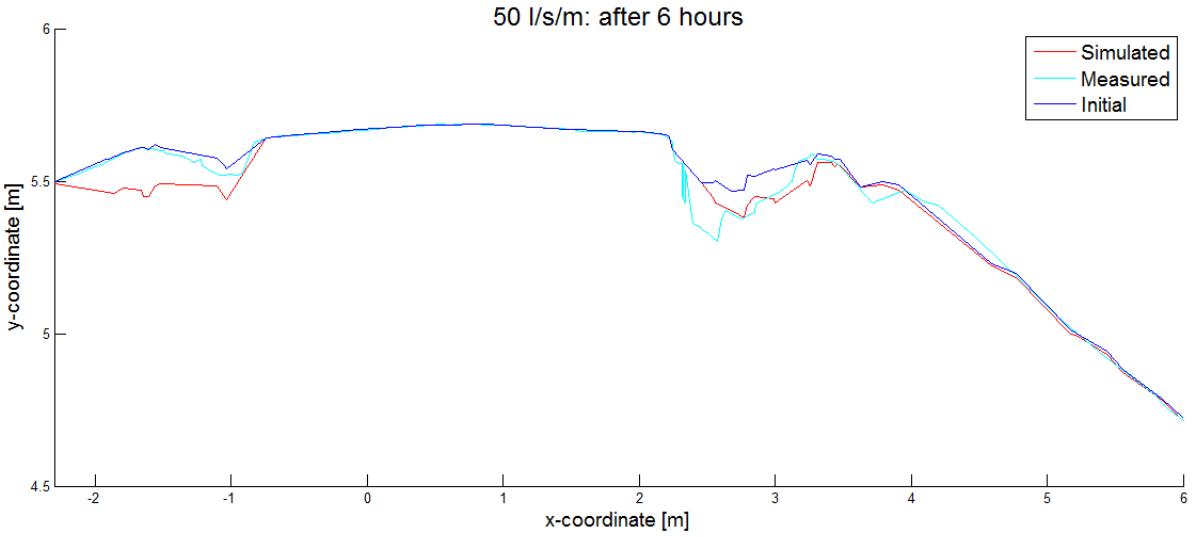

Figure 4.9. Dike profiles after 6 hours of testing with a discharge of 50 l/s per meter

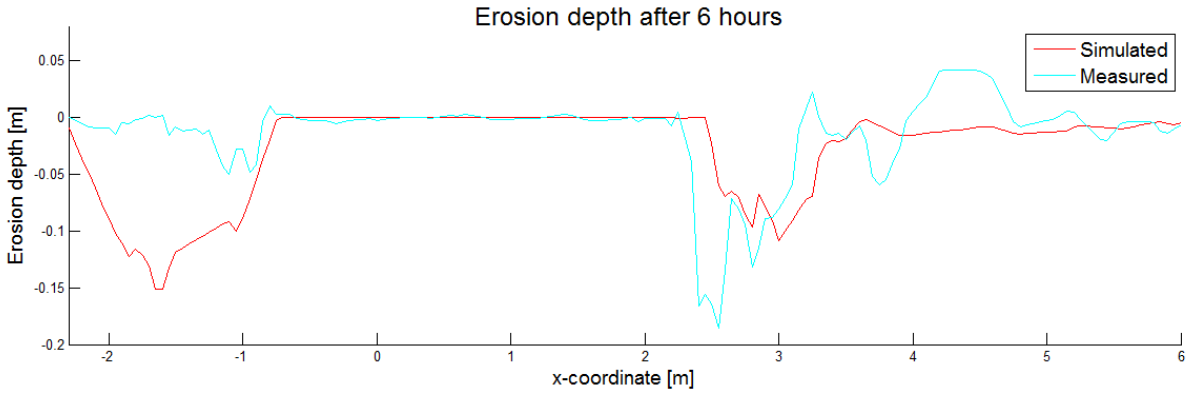

Figure 4.10. Erosion depths after 6 hours of testing with a discharge of 50 l/s per meter

After four hours of testing the simulated erosion depth at the left side became larger than 10 centimeters, meaning that the grass sod was complitely eroded. Therefore the roughness of these sections were changed to a roughness corresponding with clay. After six hours of testing a scour depth larger than 0.10 centimeters developed after the road section.

Figure 4.11 presents the locations were the grass sod is completely eroded and is replaced by a clay layer in the CFD simulation.

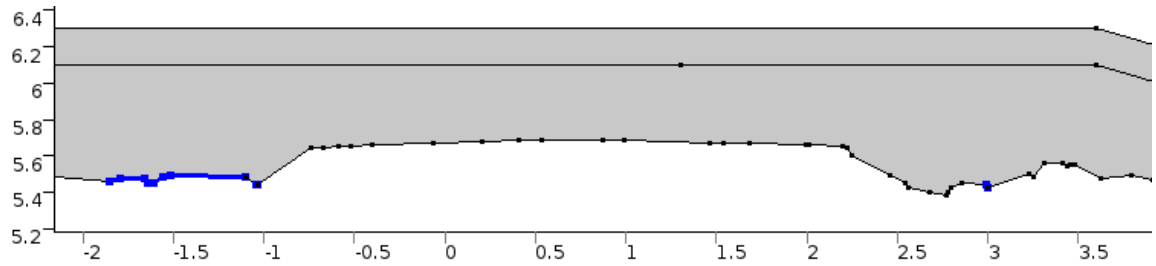

Figure 4.11. Sections where roughness is changed to a value that corresponds with clay

4.1.2.3. Erosion final stage: after 100 l/s per meter tests

After six hours the 50 l/s per meter test finished and the 100 l/s per meter test started with a duration of 100 minutes. During the simulation the dike profile is updated after 50 minutes. Figure 4.12 presents the final measured and simulated eroded profiles and Figure 4.13 gives corresponding erosion depths. The simulated erosion depths on both sides of the road are now more or less equal, while the erosion along the slope of the dike is negligible. It can be expected that for further wave overtopping the scour hole at the right side will increase more significant with respect to the left side. The left side is already flattened by overtopping waves. Therefore no high shear stresses evolve at this section. The right transition is still very irregular, leading to higher shear stresses and more erosion. The smooth measured profile in front of the road may indicate that a geotextile was present during the 100 l/s per meter test.

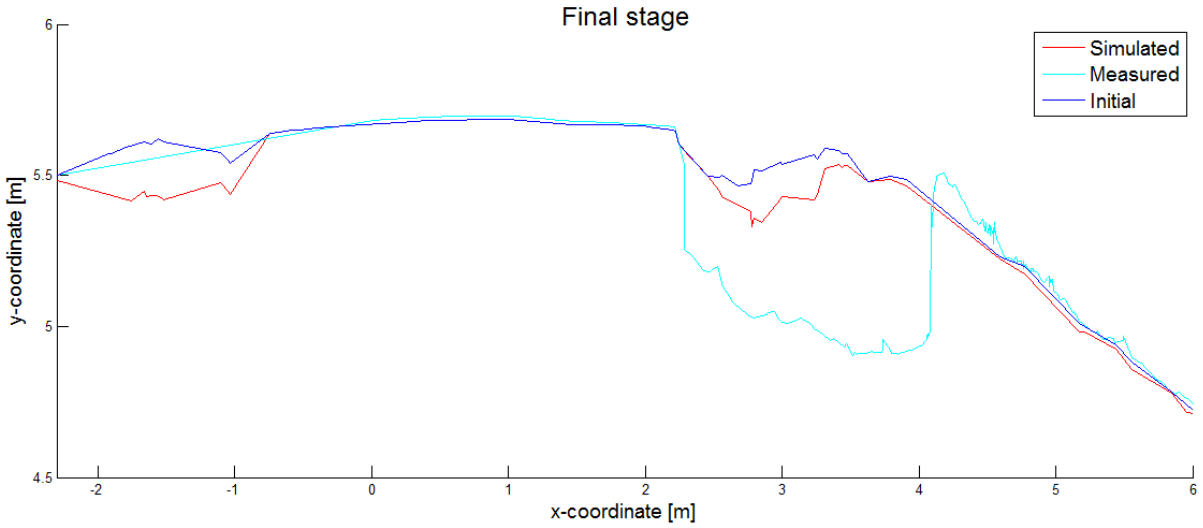

Figure 4.12. Dike profiles after the 100 l/s per meter test

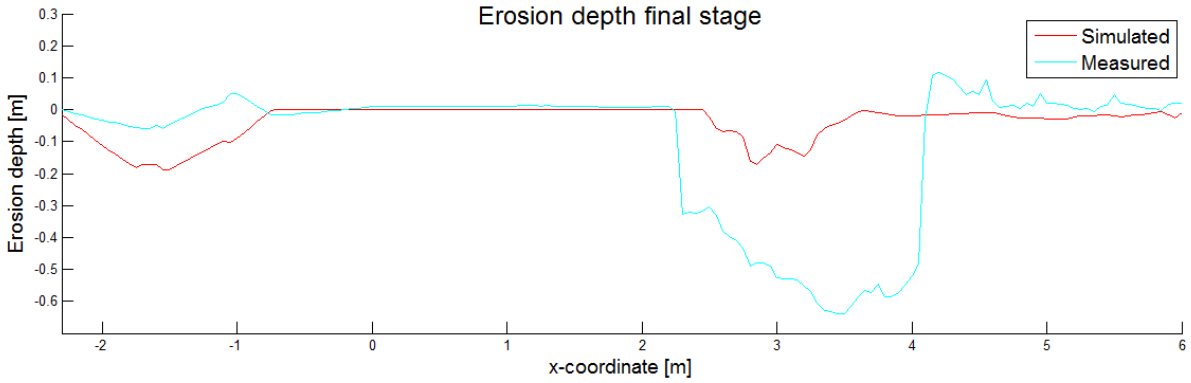

Figure 4.13. Erosion depths after the 100 l/s per meter tests

At the right transition a large difference between the measured and simulated erosion depths is present. The location of erosion is correct modelled. However, the erosion observed during the experiment is much more significant. The underestimation of the erosion at the right transition may be a consequnce of the overestimation of the soil properties. Both transitions were damaged due to traffic. However, the damage at the right transition was more extreme. During the CFD simulation local variations in grass strength were neglected. In addition, a homogeneous clay layer underneath the grass sod was assumed. However, most dikes in the Netherlands have a clay layer of 50 till 70 centimeters thick and a sand core underneath this clay layer (Van Hoven, Hardeman, Van der Meer, & Steendam, 2010). When the clay layer is eroded, erosion of the sand core starts to evolve. Sand is a noncohesive sediment and therefore much easier to erode, which may be the cause of the underestimation of the erosion development at the right pit.

Another reasonable explaination is the overestimation of the increase of the clay cohesion over depth. Figure 4.14 presents the scour of the right transition after 50 and 100 minutes. It is visible that the scour during the first 50 minutes is relatively large compared to the second 50 minutes, while more large overtopping volumes were simulated during the second 50 minutes. Overestimation of the increase of the clay cohesion over depth results in too high critical shear stresses and as a consequence the erosion development is restricted to a certain depth.

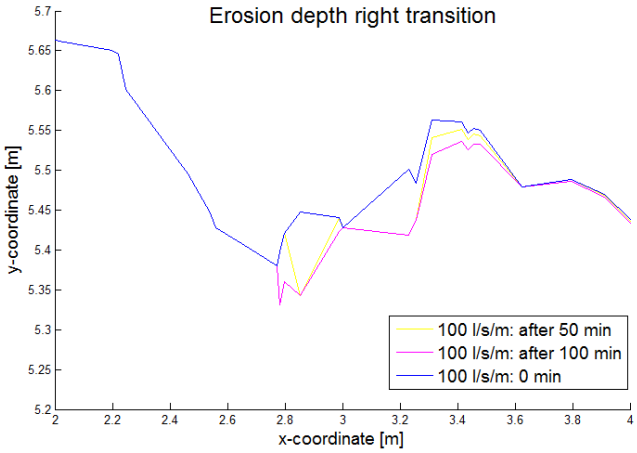

Figure 4.14. Development of the erosion depth at the right transition during the 100 l/s per meter test

The simulation shows a gradual increase of the erosion depth of the right pit, while during the experiment a pit was observed with a vertical left boundary (Figure 4.12 and 4.13). The cause of this discrepancy can be explained by the soil properties. In reality the soil underneath the road is

more compacted due to the load of the asphalt layer and the traffic that drives over this road. The compacted soil is stiffer and therefore much more difficult to erode than the more loose clay underneath the grass sod. This can lead to the vertical erosion line as was measured. The model does not take the differences in compaction into account.

Another discrepancy between the CFD simulation and the experiment is the composition of the soil underneath the grass sod. The model assumes a homogeneous clay layer, while in reality much more materials are present. Underneath the road a foundation layer is present and at the berms debris and sand is located within the clay layer. The foundation layer was relatively easy to erode, leading to scour depths of 20 centimetres at the right berm during the 50 l/s per meter test. The assumption of a homogenous clay layer with a relatively high increase of the clay cohesion over depth is most probably the main cause of the discrepancy between the measurements and the simulated erosion depths.

To investigate if the amount of erosion of the right transition becomes larger as a result of the heavy geotextile, simulations are performed in which the left side of the road is protected by a geotextile. The dashed line in Figure 4.16 indicates till where the geotextile was located and therefore no erosion could develop. Figure 4.15 shows resulting scour development of the right transition. It shows that the erosion development is more extreme for the situation with the geotextile. Due to this textile the overtopping tongue is less slowed down and the shear forces acting on the bed are therefore larger. However the erosion is still much smaller than was measured during the experiment (Figure 4.16). This difference can be explained by the discrepancies of the soil properties as mentioned above.

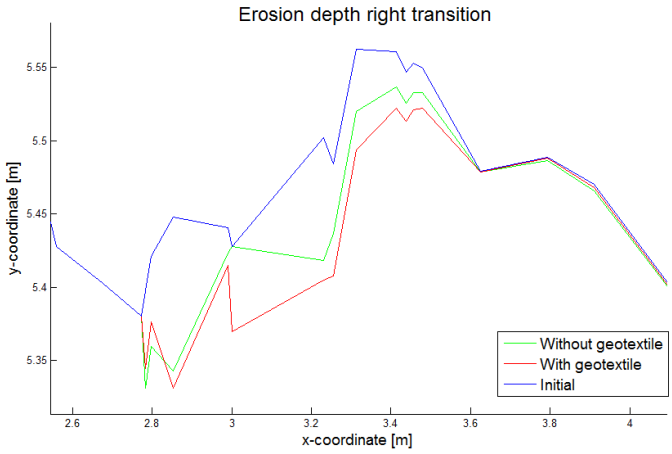

Figure 4.15. Difference in erosion depth due to a heavy geotextile

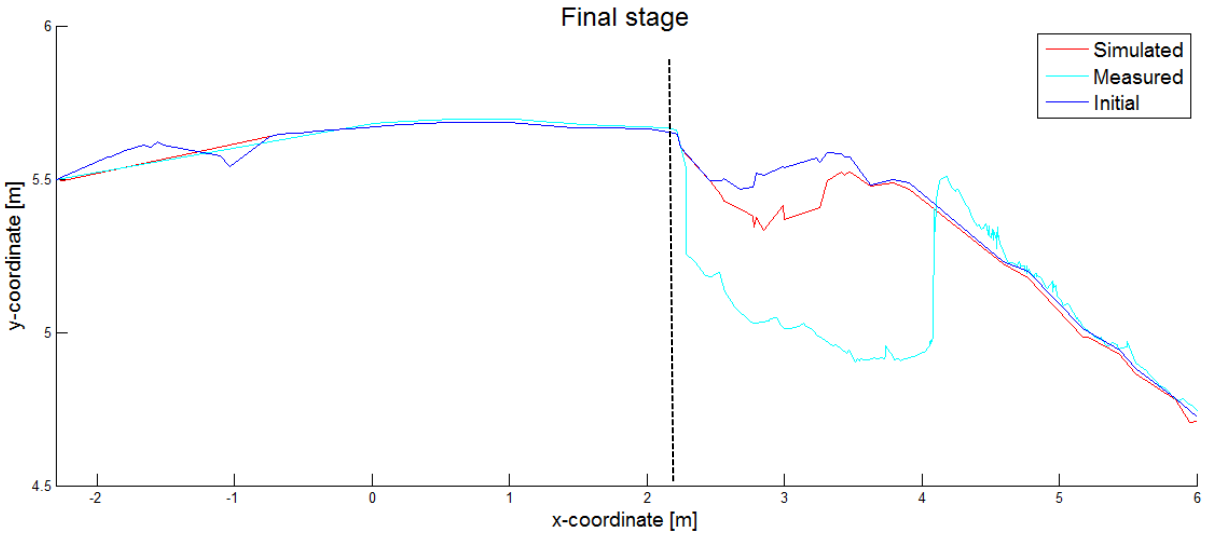

Figure 4.16. Dike profiles after the 100 l/s per meter tests including a heavy geotextile

4.1.2.4. Overview measured and simulated erosion depths

Figure 4.17 gives the simulated and measured eroded dike profiles as a result of wave overtopping. This shows that the locations of the scour development are predicted accurately and that erosion along the dike slope is negligible. Erosion on the left side of the road section was significant lower during the experiment as a result of the heavy geotextile that was located at the transition of the overtopping simulator and grass sod. During real storms no smooth transition is present and therefore this geotextile is not included during the simulations. The simulated amount of erosion at the right transition is much smaller compared to the measurements, which is a consequence of the overestimation of the soil properties. A foundation layer was located underneath the road, which was relatively easy to erode. The model assumes a homogenous clay layer. In addition, most dikes in the Netherlands have a clay layer of 50 till 70 centimetres with a sand core underneath. The model assumes a homogeneous clay core, leading to overestimation of the erosion resistance.

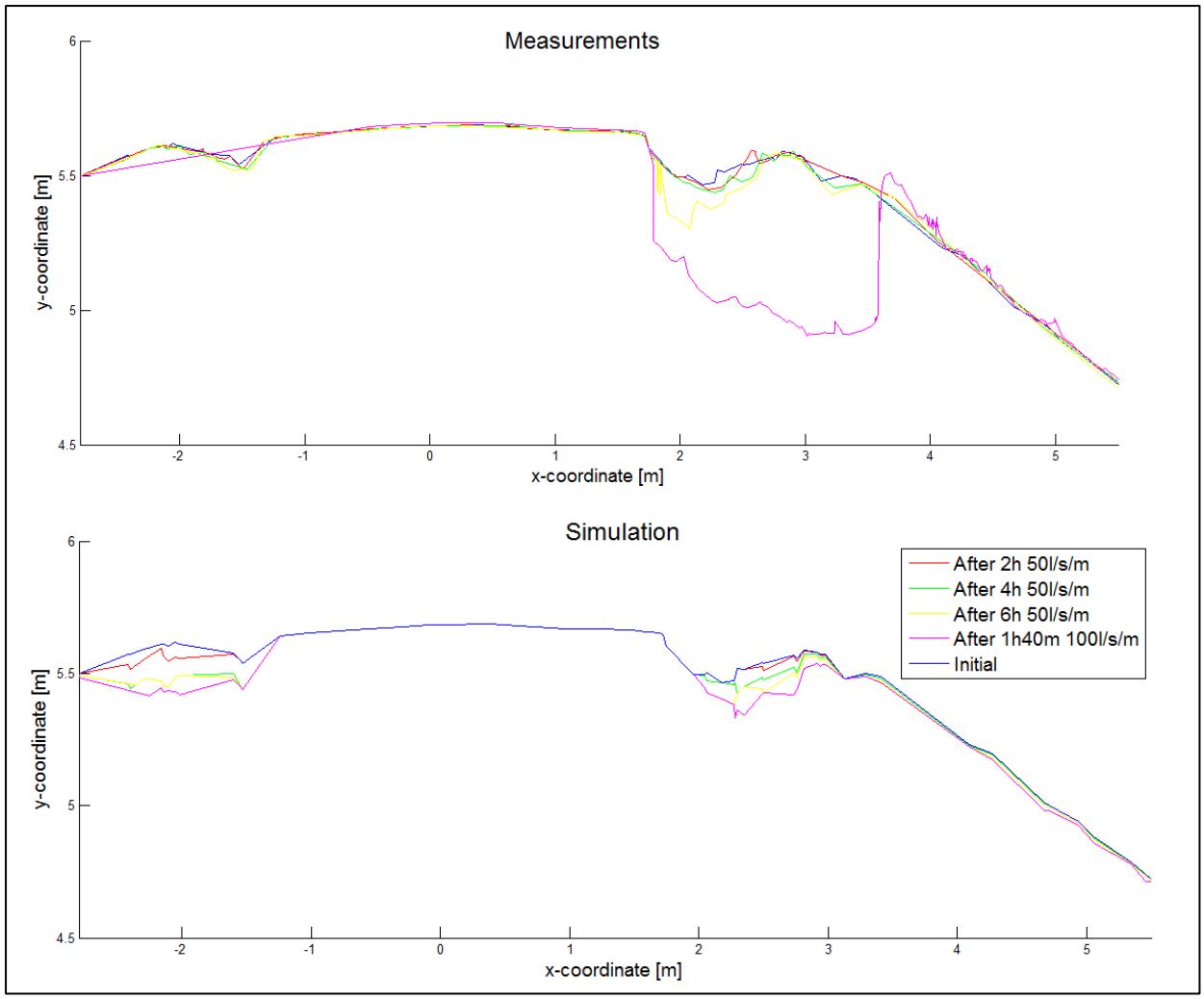

Figure 4.17. Overview of the measured and simulated erosion depths during the overtopping experiment

At several locations the measured profile after wave overtopping is higher than the initial profile. During wave overtopping the grass sod is folded before it is teared off. This leads to a temporarily increase of the dike profile. The model neglects this process. In addition, the model only takes erosion into account and neglects the processes of deposition. Both simplifications lead to discrepancies between the measured and simulated dike profiles.

Erosion is highly influenced by irregularities of the dike profile. The high sensitivity of the irregularities on the shear stresses makes updating of the dike profile during the simulations extremely important. By updating the profile the location and magnitude of irregularities are changed, leading to a change in maximum shear stresses and therefore amount of erosion. In the initial phase of the experiment the erosion rate of the left transition was more substantial than the right transition. Due to the irregularities the overtopping tongue was slowed down, leading to loss of energy and less erosion at the right transition. The bumps at the left side were flattened, leading to a smoother dike profile. As a consequence the flow is more capable to flow with high velocities along the dike crest, which leads to substantial scour of the right transition. Figure 4.18 presents the scour depths of the two berms as a function of overtopping time. At the end a more or less equilibrium depth is reached in which the erosion that evolves in the deepest points of the two transitions is more or less negligible. In this state the berms are broadened instead of deepened. This differs significant from the measurements. The measured scour depth

kept increasing gigantically. This discrepancy may be as a result of overestimation of the increase of the clay cohesion over depth and the assumption of a homogeneous clay core.

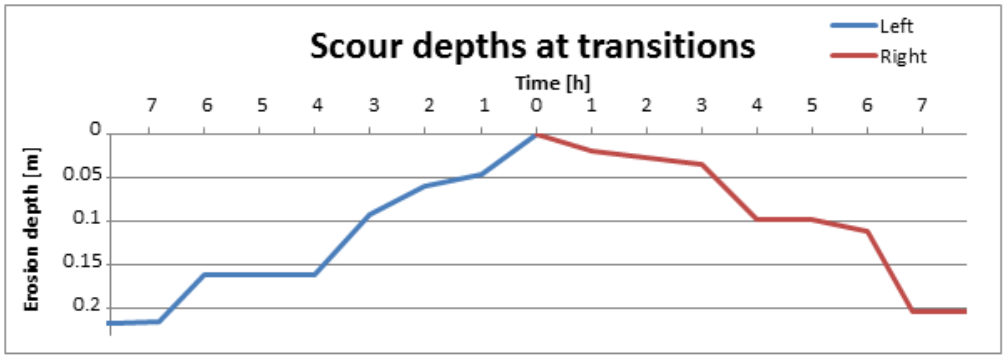

Figure 4.18. Erosion depths of the left and right transition as a function of overtopping duration

4.2. DIRECT IMPACT OF A ROAD

The asphalt has a smaller roughness coefficient than the grass sod. The changes in hydrodynamics that evolve due to the smoother asphalt section are the direct impact of a road. To investigate this direct impact, a simulation is performed in which the roughness of the road section is changed to grass, leaving the geometry intact. Erosion is computed as a consequence of 50 overtopping waves with a volume of 1500 l/m, where after the dike profile is updated. Due to the change in roughness, the hydrodynamics and therefore the erosion development at the right transition change. Figure 4.19 and 4.20 present the eroded dike profiles of the right transition for a grass covered dike and for a dike with a road on top, respectively. Figure 4.21 shows corresponding erosion depths.

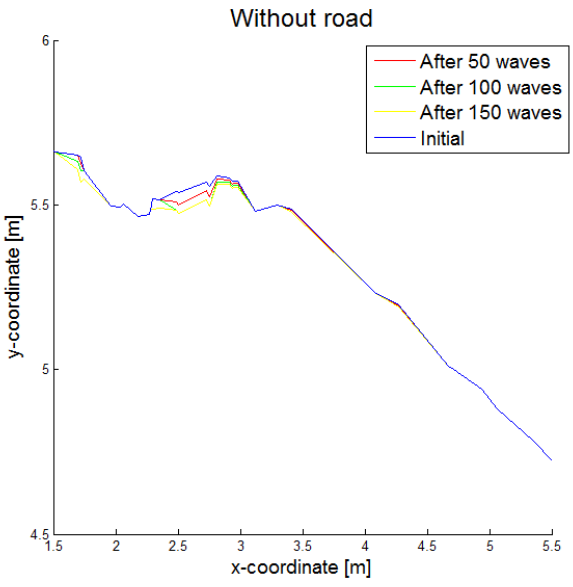

Figure 4.19. Erosion of right transition for a dike profile without a road on top

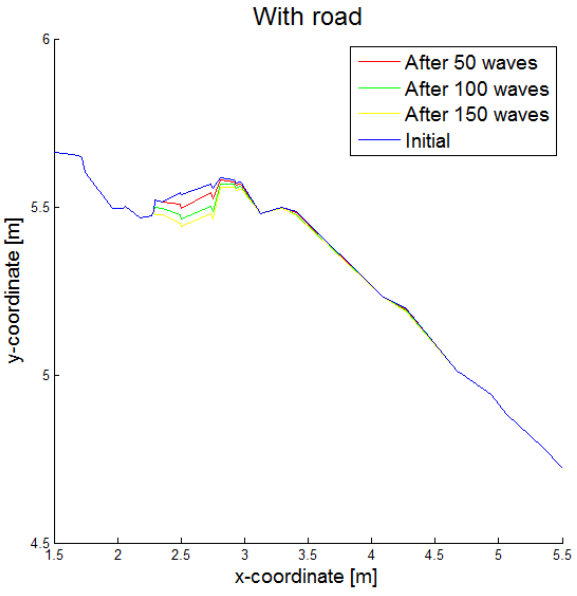

Figure 4.20. Erosion of right transition for a dike profile with a road on top

The figures show that the amount of scour of the right transition increases due to the road. The asphalt layer has a lower roughness coefficient compared to a grass sod. Therefore the overtopping tongue is more capable of conserving his energy and is less slowed down. This leads to an increase of the forces acting on the bed and as a consequence to an increase of erosion development. In addition, the turbulence of the flow increases due to a sudden increase of the bed roughness which leads to higher bed shear stresses. The amount of scour of the right transition after 150 waves increases with 51.1% due to the change in roughness. However, a scour pit of approximately 76 millimetres in front of the right transition evolves for the grass covered dike. This section is covered by the asphalt layer for the profile with a road located at the crest and therefore no erosion is able to develop.

It can be concluded that the roughness of the road section leads to higher erosion development of the right transition. Contrarily, no erosion in front of the right transition evolves due to the asphalt layer.

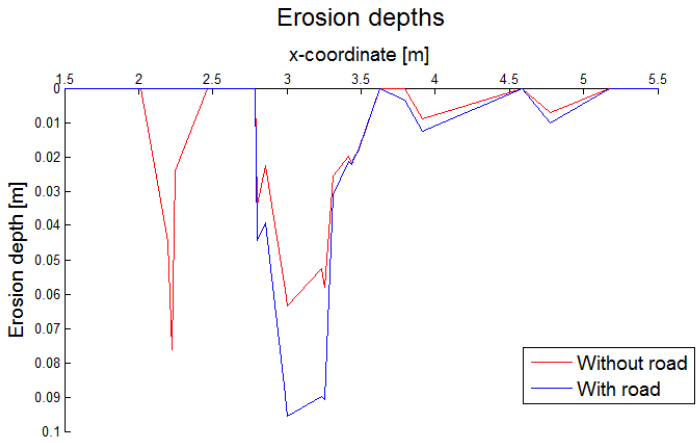

Figure 4.21. Erosion depths right transition

4.3. INDIRECT IMPACT OF A ROAD

Due to traffic the berms next to the road section are damaged and pits are present. These pits have an indirect impact on the hydrodynamics and erosion development during wave overtopping. To investigate these indirect impacts a model is simulated in which the large pits at the transitions are removed and the complete dike profile has a roughness corresponding with grass. Figure 4.22 shows the smooth dike profile. This section is divided in two parts. First the effects a road on the overtopping volume along the dike profile are investigated, where after the change in erosion development is provided.

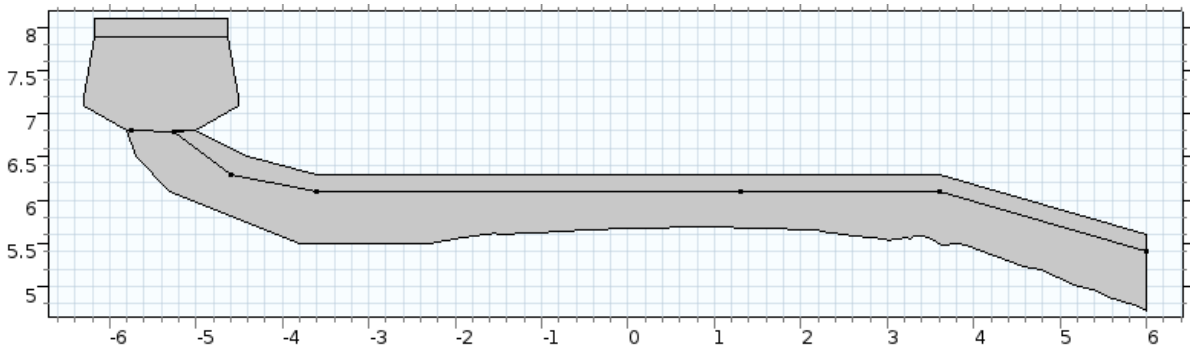

Figure 4.22. Smooth dike profile

4.3.1. CHANGE IN OVERTOPPING VOLUME

The overtopping volume can be calculated by multiplying the flow velocities and water depths over time. The overtopping volume is determined at two locations to investigate the change. These locations as well as the initial profile with a road and a smooth profile without a road are given in Figure 4.23.

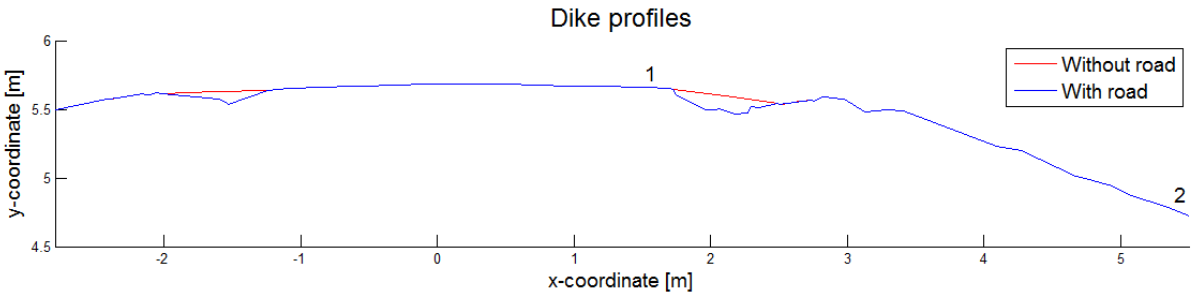

Figure 4.23. Differences dike profiles and locations of determination overtopping volumes

Figure 4.24 and 4.25 present the flow velocities and water depths, respectively, at location 1 for the grass covered dike. These figures show that the flow velocity is largest in front of the overtopping tongue and decreases gradually. Appendix G.6 provides the graphs of the other locations and the graphs of the dike profile with a road on top.

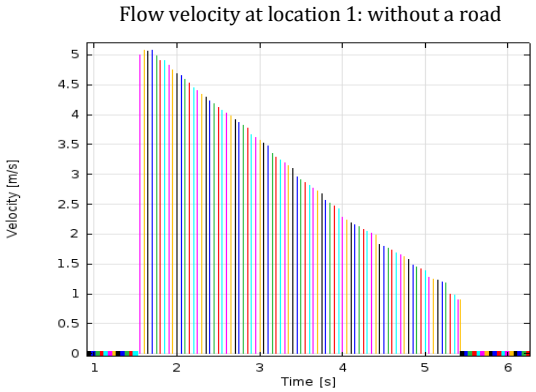

Figure 4.24. Flow velocity at location 1 for a smooth dike profile

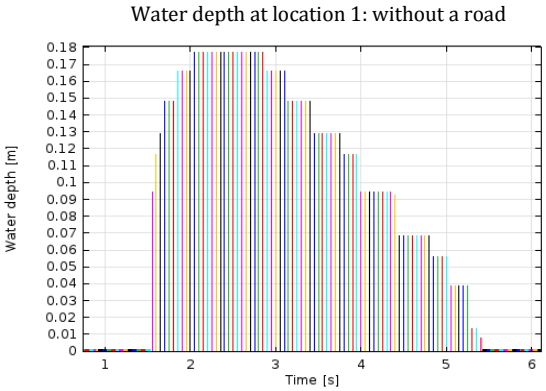

Figure H4.25. Flow depth at location 1 for a smooth dike profile

Figure 4.26 and 4.27 show the overtopping discharges in m^3/s. The surface area of the graphs give the total overtopping volumes. Several differences between the geometries are present before the overtopping tongue reaches location 1 (Figure 4.23). The dike profile with a road has a relatively large pit at the left transition between the grass sod and the road section. As a consequence a part of the water retains in this pit, leading to a lower overtopping volume at location 1. In addition, the roughness of the crest changes due to the road section. The afsphalt has a lower friction coefficient and therefore the flow is less slowed down. The maximum velocity at location 1 is higher for the profile with a road compared to the bare grass covered profile. The overtopping time for both profiles increases along the dike crest. The friction of the bed leads to restriction to flow and larger overtopping times.

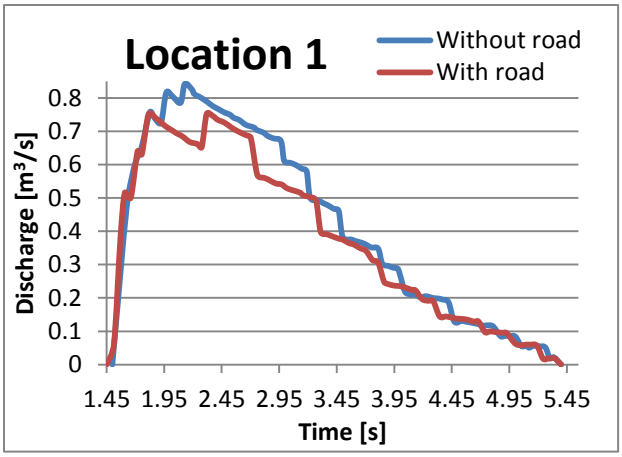

Figure 4.26. Overtopping volumes at location 1

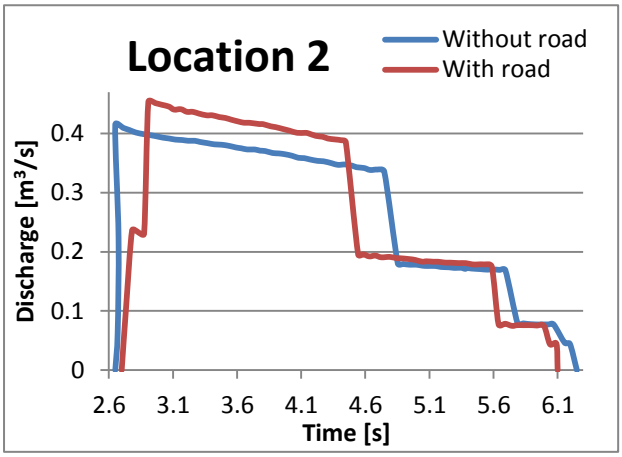

Figure 4.27. Overtopping volumes at location 2

Location 2 is situated at the dike slope (Figure 4.22). Two large pits are present in the dike profile with a road structure, leading to a lower overtopping volume at location 2 compared to the grass covered dike (Figure 4.27). Furthermore, the maximum discharge at location 2 increases due to a road and the pits. This is caused by a slightly larger water depth between t = 3s and t = 4.5s for the road profile compared to the smooth profile. The shear stresses that evolve along the dike slope are significant smaller than at the crest. The increase of the overtopping discharge has therefore almost no effect on the increase of the erosion development along this slope.

The overtopping times at location 2 of both profiles are smaller compared to the overtopping times at the crest. Due to the steep slope the flow velocities increase resulting in smaller overtopping time. Moreover, the water depths are significant smaller along the slope compared to the crest.

It can be concluded that the transitions between the grass sod and road section leads to a decrease of the overtopping discharge along the dike profile. During overtopping water retains in the large pits. When a new wave overtops, this results in lower shear stresses at these pits due to the damping effect of the retaining water. This process is not considered during the CFD simulation. A dry dike profile is assumed for each overtopping wave, which may lead to an overestimation of the maximum bed shear stresses. For a really smooth dike profile, the decrease of the water volume is negligble.

4.3.2. CHANGE IN EROSION

The erosion as a result of 50 waves of 1500 l/m is computed. Thereafter the dike profile is updated and the process is repeated three times. Figure 4.28 provides the maximum shear stresses for both the smooth profile with no road on top and the profile with a road. The maximum shear stresses for the irregular profile are slightly higher compared to the maximum shear stresses that evolve at the smooth profile. The second peak in Figure 4.28 increases with approximately 46 N/m² due to the irregular profile. In addition, the maximum shear stresses decreases at the road section as a result of the lower friction of the asphalt compared to the grass sod.

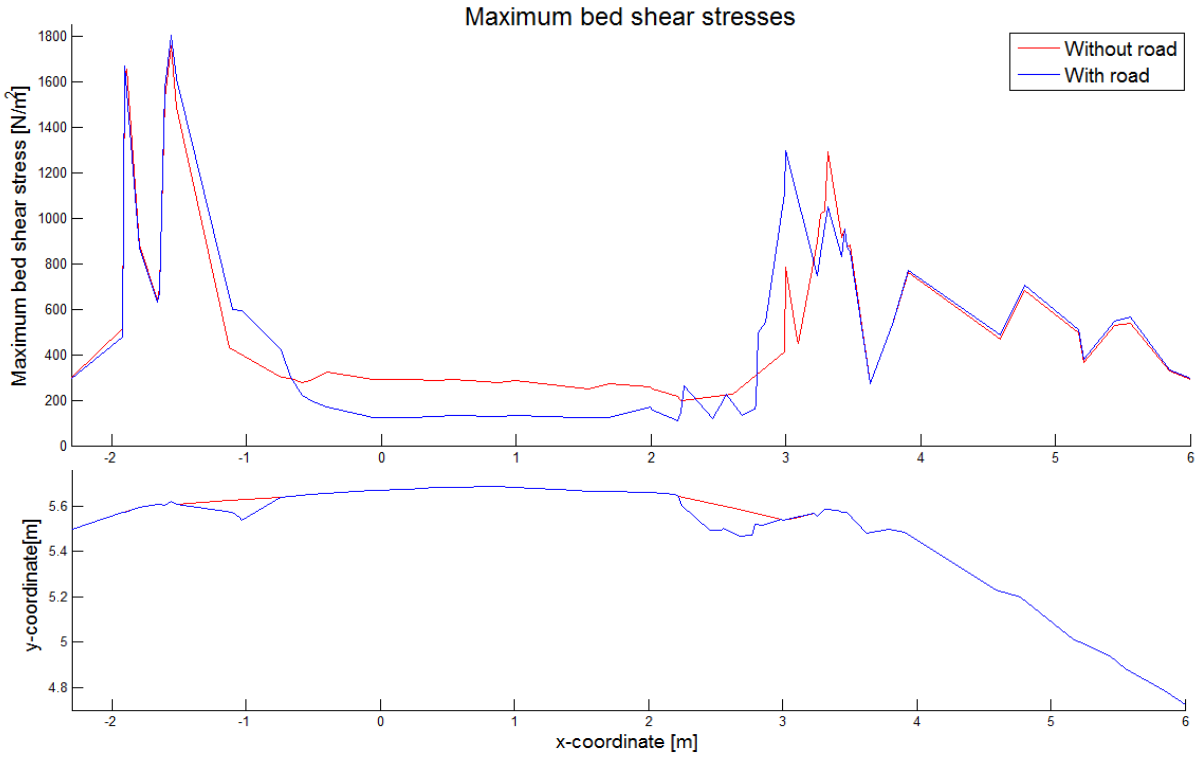

Figure 4.28. Maximum bed shear stresses for a smooth dike profile and a profile with a road on top

Figure 4.29 shows the erosion development caused by the maximum bed shear stresses. During wave overtopping less erosion evolves for the smooth dike profile without a road located at the crest. A more precise overview of the eroded depths along the dike profiles is presented in Figure 4.30. The increase of scour due to a road equals 41.9%. It can be stated that the increase of scour of the left transition is mainly caused by the irregularities of the dike profile. An irregularity, with an upward slope, leads to energy loss and a sudden increase of the shear stresses which are substantial larger than the critical bed shear stress. Section 4.2 showed that the change in roughness due to the asphalt section leads to more erosion development at the right transition. Therefore the scour development of the right transition is caused by the combination of the lower roughness of the road structure and the irregularities of the dike profile.

This leads to the finding that a road with damaged transitions is more vulnerable for erosion development at the crest of the dike. However, due to the irregularities of the dike profile the flow velocities decrease significant leading to lower wave impact at the toe of the dike. During experiments performed with the wave overtopping simulator it was found that for a bare grass covered dike most erosion evolves at the toe of the dike (Van der Meer et al., 2010). To investigate the change of wave impact at the toe of the dike as a consequence of the road and the damaged berms, the complete dike profile is simulated in the next section.

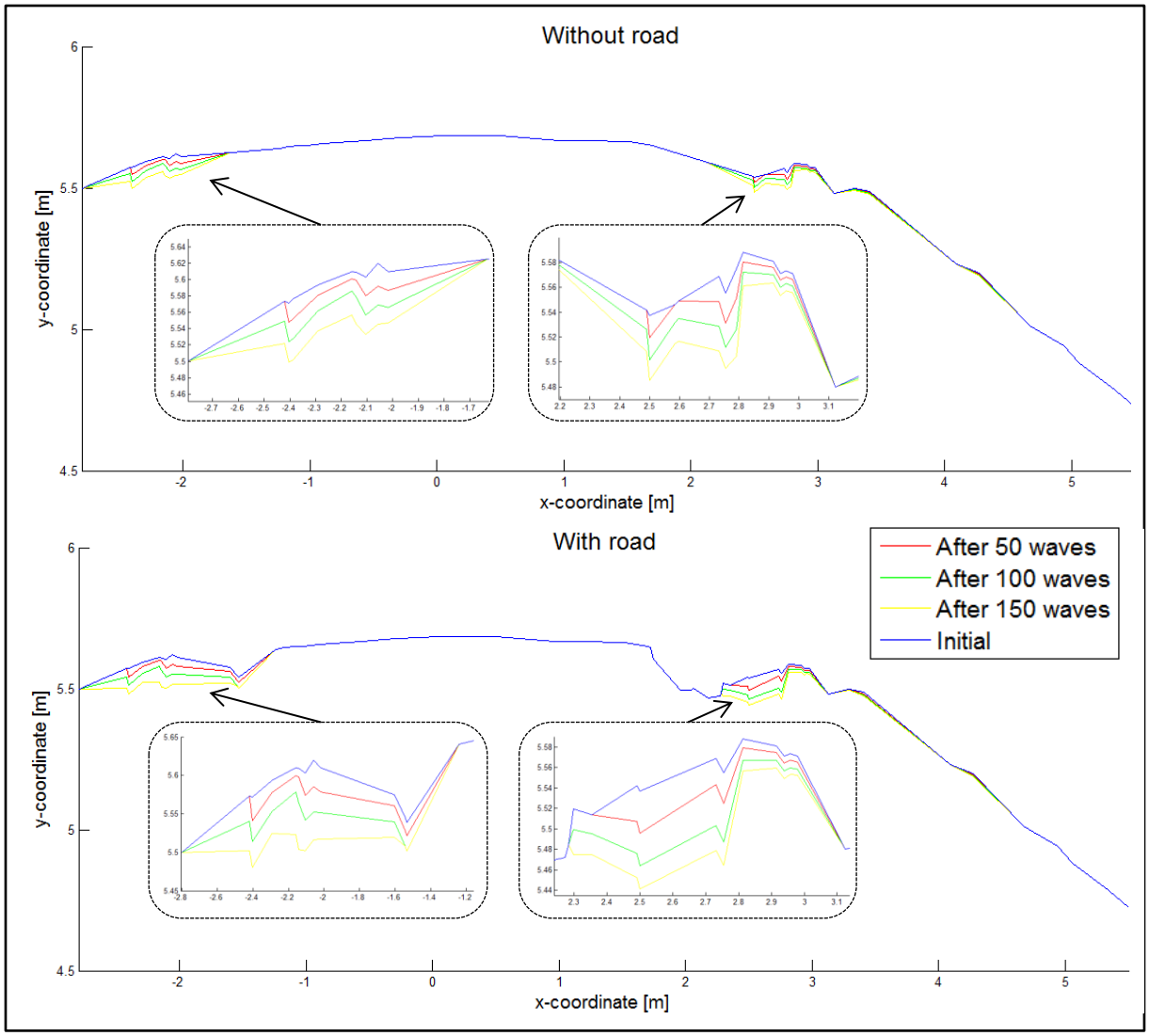

Figure 4.29. Erosion depths for a smooth dike profile and a profile with a road on top

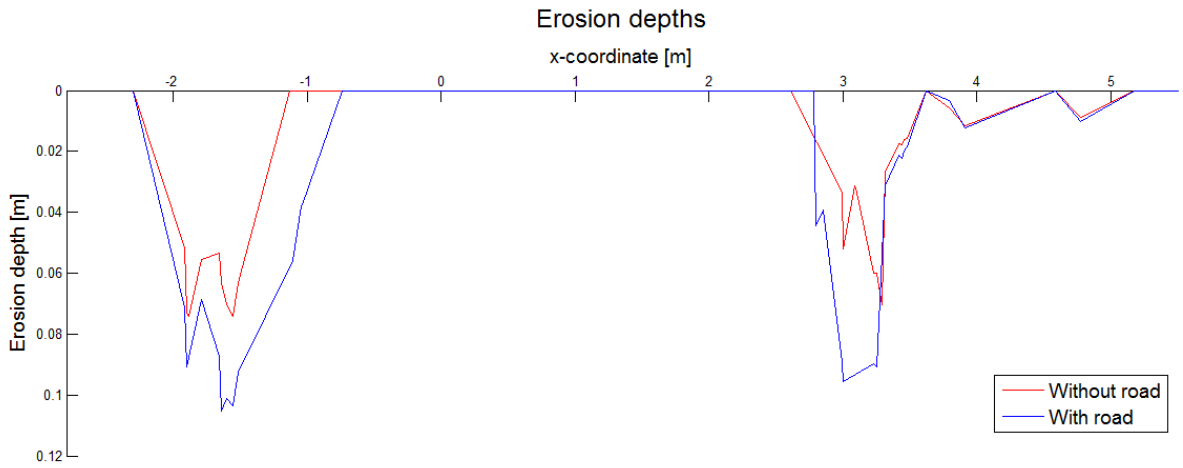

Figure 4.30. Erosion depths for a smooth dike profile and a profile with a road on top after 120 waves with a volume of 1500 l/m

4.4. EFFECTS OF A ROAD ALONG THE DIKE PROFILE

To investigate the changes of erosion development at the toe of the dike the complete dike profile is simulated with a wave overtopping volume of 2500 l/m. Figure 4.31 presents the maximum shear stresses. In front of the road section, the shear stresses for the situation with a road are larger compared to no road (before x-coordinate 2.5). Contrarily, after the road section the opposite accounts. The flow is slowed down due to the pits at the transition of the road section with the grass sod, leading to loss of energy and lower shear stresses. The two high peaks along the dike slopes develop due to irregularities in the geometry.

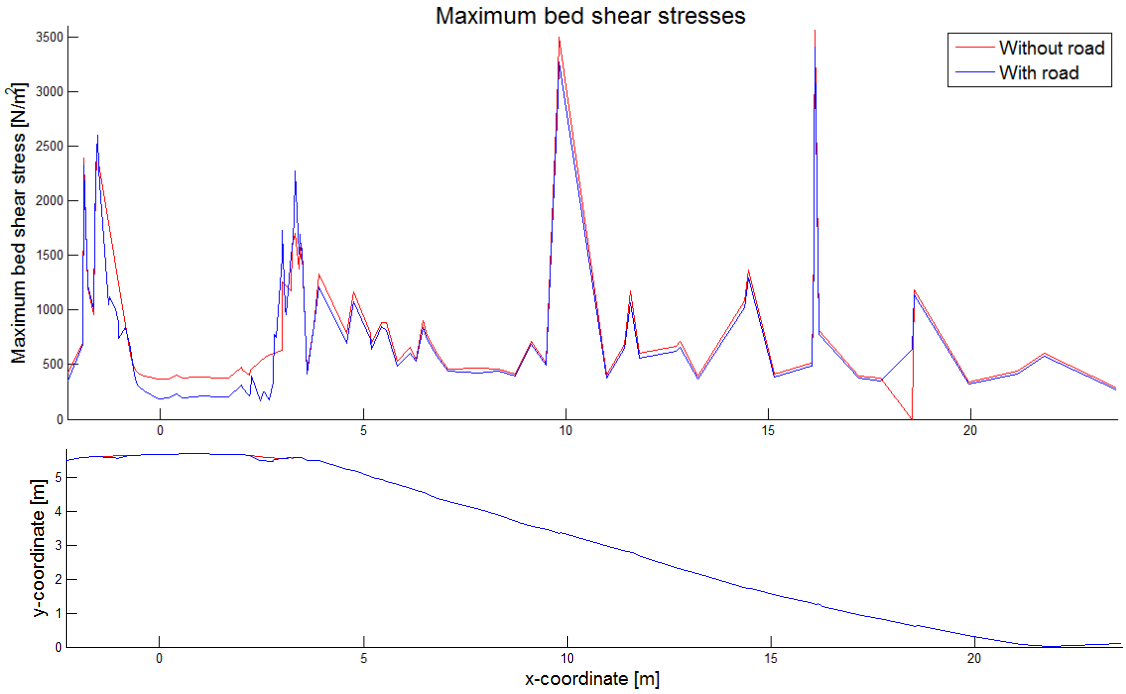

Figure 4.31. Maximum shear stresses for a smooth dike profile and a profile with a road on top due to an overtopping wave volume of 2500 l/m

The erosion is computed as a result of 150 overtopping waves with a volume of 2500 l/m. Note that this is a very extreme condition and most probably will not occur in reality. Figure 4.32 shows the erosion depths for a dike with and without a road and Table 4.3 summarizes the maximum depths at the left and right transition, slope and toe of the dike. Appendix G provides the eroded dike profiles. Erosion at the crest for a dike with a road is larger than for a dike without a road, as was already concluded in previous section. The maximum erosion at the crest increases with 44.4% as a consequence of the right berm. The erosion along the dike slope and the toe of the dike is slightly larger for the bare grass covered dike. The dike profile is smoother and therefore the flow is less slowed down leading to more erosion. However, the maximum change of scour is only 5.4% along the slope and 9.5% at the toe of the dike. The increase in scour at the crest of the dike due to a road structure is substantial greater than the decrease of scour along the dike profile and toe. It should be investigated which erosion location is more vulnerable to dike failure. However, it is most likely that the total safety of the dike reduces as a consequence of the road structure due to the large increase of scour depths at the crest.

Table 4.3. Erosion depths transition for a dike profile with and without a road on top

Location	Erosion depth [mm]	Erosion depth [mm]	Difference [%]
	No road	***Road***	
left transition	207	212	+2.2
right transition	176	255	+44.4
slope	90	85	-5.4
toe	14	12	-9.5

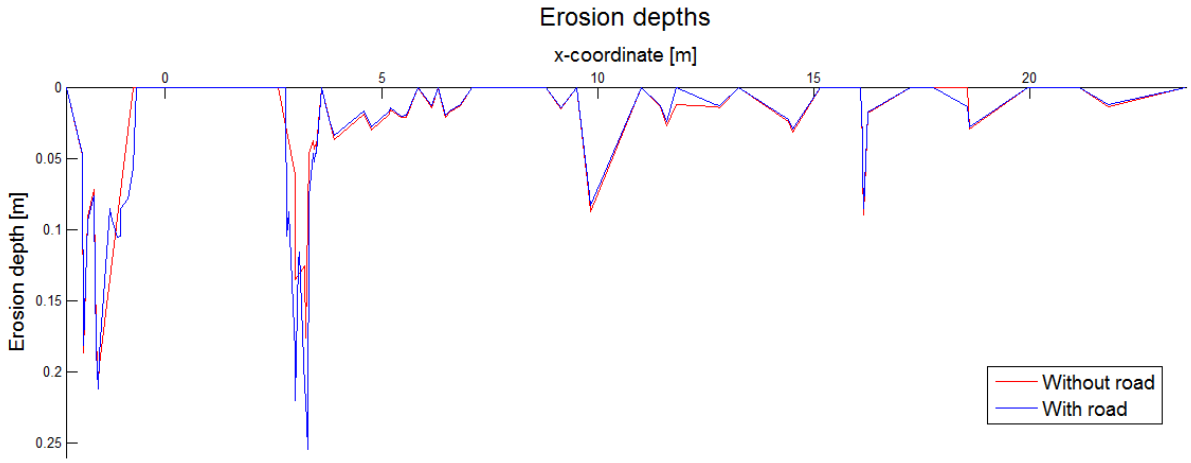

Figure 4.32. Erosion depths for a smooth dike profile and a dike profile with a road on top after 150 waves with a volume of 2500 l/m

The safety assessment in the Netherlands is based on a bare grass covered dike. A road located at the crest is not considered during the assessment at the moment. However, it can be concluded that a road structure on top of the dike has a high influence on the erosion development along the dike profile and therefore on the safety level. Due to a road section the amount of scour at the crest increases significantly, which is caused by the irregularities of the damaged berms and the change in roughness. For this reason it is important that a road structure will be incorporated in the safety assessment for a more reliable analysis.

5. SENSITIVITY ANALYSIS

A sensitivity analysis of the coupled hydrodynamic-bed model is executed. This analysis gives insight in the influence of different parameters on the erosion development during wave overtopping. The sensitivity is determined by decreasing or/and increasing the parameters and investigating the changes in the amount of erosion. The change in the amount of scour is computed for the initial state, where the grass cover is still intact, as a consequence of 100 overtopping waves with a volume of 1500 l/m.

5.1. SENSITIVITY CFD SIMULATION

In this section the sensitivity of the parameters included in the CFD simulation are investigated.

5.1.1. VOLUME FRACTION COEFFICIENT (VF)

The volume fraction was used for calibration of the hydrodynamics. Table 5.1 and Figure 5.1 show the maximum erosions as a function of the different volume fractions. The table also gives the change with respect to a volume fraction of 0.6. A small volume fraction leads to high bed shear stresses and large overtopping times compared to large volume fractions. This is most probably due to the inclusion of air volumes in the smaller volume fractions. The erosion development is both a function of overtopping time and bed shear stresses and therefore an increase of these parameters leads to an increase of the amount of scour, leading to conclusion that the erosion development is sensitive to the volume fraction coefficient.

Table 5.1. Erosion for different volume fraction coefficients

Volume fraction [-]	Erosion [mm]	Change [%]
0.30	130	+57.7
0.40	107	+30.2
0.50	98	+19.3
0.60	***83***	**--**
0.70	67	-18.5

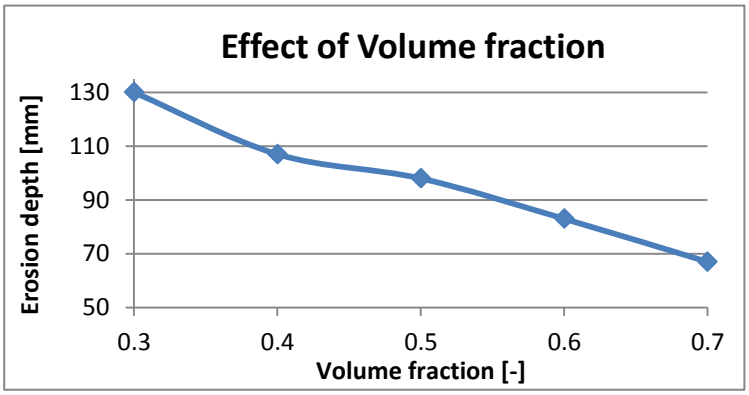

Figure 5.1. Dependency volume fraction coefficient on erosion development

5.1.2. INITIAL INTERFACE THICKNESS (ϵ_{PF})

To investigate the influence of the initial interface thickness different values are simulated. Figure 5.2 presents the pattern of the flow for a thickness of 0.05, 0.075 and 0.1 meters. The red color indicates that only air is present, while the blue color represents water. The colors in between indicate the transition zone.

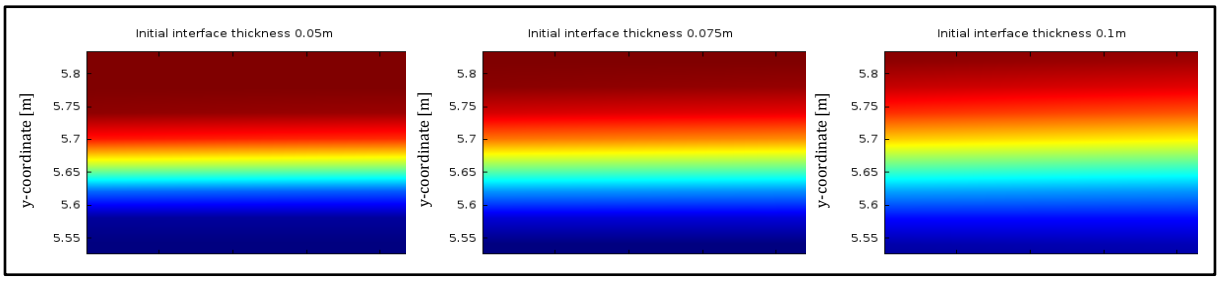

Figure 5.2. Initial interface thickness of 0.05, 0.075 and 0.1 meters

Table 5.2 provides the amount of erosion due to the different initial interface thicknesses. It is notable that a smaller thickness leads to higher erosion development. This increase is mainly due to a significant increase of the overtopping time for smaller initial interface thicknesses. It was found that a thickness of 0.1 meters leads to an overtopping time of 2.1 seconds, while a thickness of 0.05 meters leads to an overtopping time of 2.6 seconds. This leads to the conclusion that the erosion development is sensitive to the initial interface thickness.

Table 5.2. Erosion for initial interface of 0.05, 0.075 and 0.1

Initial interface thickness [m]	Erosion [mm]	Change [%]
0.05	78	--
0.075	59	-25.1
0.1	53	-31.9

5.1.3. MOBILITY TUNING PARAMETER (X)

The mobility tuning parameter has influence on the front and end edges of the overtopping tongue. For a smaller mobility tuning parameter the flow is more spread out, while for a larger value the edges are sharper. Figure 5.3 shows this pattern.

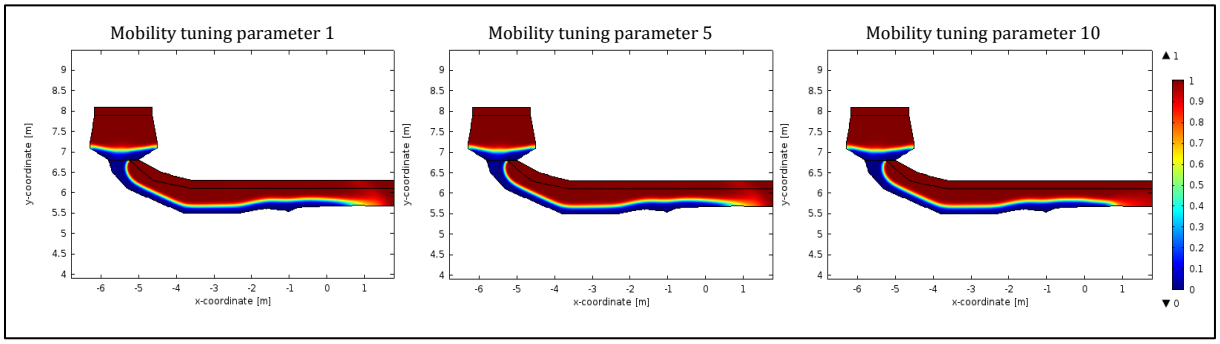

Figure 5.3. Overtopping tongues for mobility tuning parameter of 1, 5 and 10

Table 5.3 gives the maximum erosion and change in erosion for the different mobility tuning parameters. It shows that the erosion development decreases with increasing mobility parameter. An increase of the parameter with a factor 10 results in a decrease of 10.4%. It can therefore be concluded that the amount of scour is sensitive to the mobility tuning parameter.

Table 5.3. Hydrodynamics for mobility tuning parameter of 1, 5 and 10

Mobility tuning parameter [-]	Erosion [mm]	Change [%]
1	77	--
5	70	-8.1
10	69	-10.4

5.1.4. SURFACE TENSION

Table 5.4 presents the erosion development when surface tension is included and neglected. This shows that neglecting surface tension leads to more erosion. However, this increase in erosion development is relatively small. It can be concluded that the results of the model has low sensitivity to the surface tension.

Table 5.4. Outcomes test model with and without surface tension

	Erosion [mm]
Surface tension included	77
Surface tension neglected	80
Change [%]	+3.7

5.1.5. NIKURADSE ROUGHNESS HEIGHT (K_{ES})

The roughness of the steel of the wave overtopping simulator is unknown. To see the effect of the roughness of the steel on the erosion development the minimum and maximum values based on the work of Chow (1959) are modelled. Table 5.5 shows the maximum amount of scour that evolves along the dike profile due to the different steel roughnesses. This shows that for a larger roughness coefficient, the erosion development is higher. The turbulent character of the overtopping tongue increases as a consequence of a higher steel roughness. This leads to an increase of the bed shear stresses and therefore to more scour. However, the amount of scour decreases only 3.8% for the minimum roughness value compared to the maximum value and therefore it can be concluded that the erosion development has low sensitivity to the roughness of the steel.

Table 5.5. Hydrodynamics for minimum and maximum roughness of steel

	Nikuradse roughness height [m]	Erosion [mm]
Maximum roughness steel	6.7×10^{-3}	83
Minimum roughness steel	8.4×10^{-4}	80
Change [%]	-87.5	-3.8

5.1.6. VELOCITY SCALE (U_{SCALE}) AND LENGTH SCALE (L_{FACT})

The velocity and length scale are two turbulent characteristics of the flow. The velocity scale represents the friction velocity, which characterises the shear strength at the boundary (Zagarola & Smits, 1998). The length scale describes the size of the large-energy containing eddies (CFD Online, 2012). The velocity scale and length scale are as default set to 1 meter per second and 0.035 meters respectively. These values are changed to investigate the effects of the parameters on the outcomes of the model. Table 5.6 shows that the length and velocity scale

have almost no influence on the erosion development, which leads to the conclusion that the model output has low sensitivity to the velocity and length scale.

Table 5.6. Outcomes test model with different velocity and length scale values

	Erosion [mm]	Change [%]
u_{scale} = 1 m/s and l_{scale} = 0.035 m/s	56	--
u_{scale} = 5 m/s and l_{scale} = 0.035 m/s	55	-1.8
u_{scale} = 1 m/s and l_{scale} = 0.070 m/s	55	-1.8

5.1.7. TIME STEP (T)

A time step had to be determined for which the results are computed. This time step has a significant influence on the computation time. Choosing a larger time step leads to more convergence problems in the beginning of the solution, however the total computation time decreases. Two models with time steps of 0.005 and 0.05 seconds are simulated. Table 5.7 provides the results. This shows that an increase of the time step with a factor 10 leads to almost no changes in erosion development. This leads to the conclusion that the model has low sensitivity to the time step chosen.

Table 5.7. Hydrodynamics for time step 0.05 and 0.005 seconds

Time step [s]	Erosion [mm]
0.05	76
0.005	75
Change [%]	-0.7

5.2. SENSITIVITY BED MODEL

In this section the sensitivity of the parameters included in the bed model are provided. The results are presented in Table 5.8 and are discussed sequentially.

Table 5.8. Sensitivity erosion model

Parameter	Changed value	Erosion [mm]	Change with respect to reference [%]
	Reference	**83**	**--**
Bed shear stress [kN/m²]	Reference + 10% τ_{max}	91	+9.6
	Reference + 50% τ_{max}	100	+52.5
	Reference + 100% τ_{max}	172	+107.2
Turbulence [-]	0.20	131	+57.8
Reference r_0 = 0.17	0.15	58	-43.1
Grass strength [kN/m²]	10.0	67	-19.3
Reference $\boldsymbol{\sigma_{roots,0}}$ = 7.76	5.0	115	+38.6
Soil density [kg/m³]	3000	73	0
Reference $\boldsymbol{\rho_s}$ = 2000 kg/m³	1000	74	+1.4
Clay cohesion [kN/m²]	14.9	59	-19.2
Reference $\boldsymbol{\tau_{clay,0}}$ = 11.9	8.9	96	+31.5

The bed shear stresses are computed during the CFD simulation. The maximum values are used to compute the amount of scour. These values are increased and resulting erosion is computed. Table 5.8 shows that the increase of bed shear stress is more or less equal to the changes in erosion. It has a linear relationship.

This leads to the conclusion that the model output is sensitive to the shear stresses and therefore shear stress accuracy is very important for correct erosion estimation.

The turbulence in the flow is determined by the depth-averaged relative turbulence intensity. The model output is highly sensitive to the turbulence of the flow. Only an increase of the turbulence intensity of smaller than 20% leads to an increase in the amount of scour of 57.8%. Accurate measurements of this intensity are necessary to be able to compute the amount of scour during overtopping.

Table 5.8 shows that a significant increase and decrease of the soil density leads to almost no changes in the amount of scour. This leads to the conclusion that erosion development has low sensitivity to the density of the soil.

Figure 5.4 provides an overview of the sensitivities. This shows that the erosion model is most sensitive to the turbulence of the flow, having the steepest slope. However, for values smaller than 0.1 the model is insensitive to the turbulence. The flow is uniform under this condition and the effects due to turbulence are negligible.

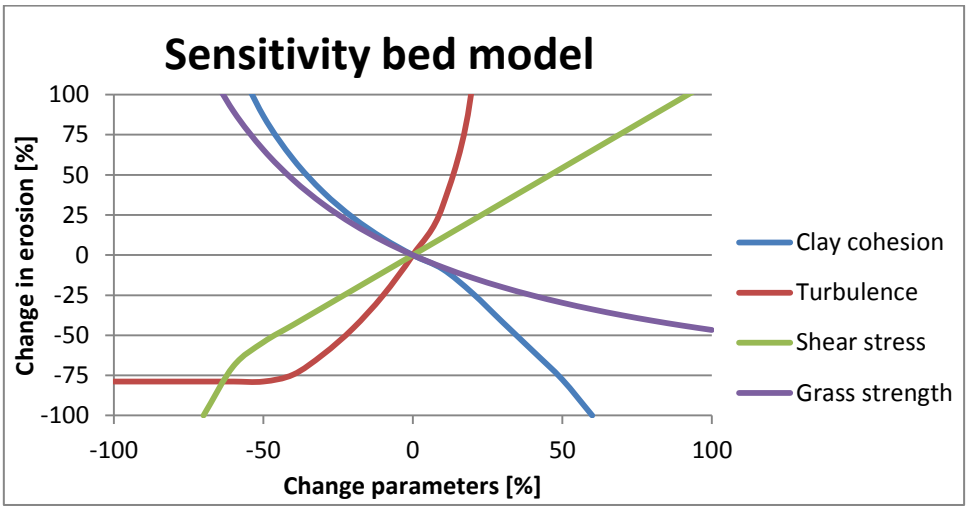

Figure 5.4. Sensitivity of the erosion model for different input parameters

The figure shows furthermore that the model is less sensitive to an increase of the grass strength compared to a decrease. This means that the reduction in scour due to better grass conditions are smaller compared to the increase of the scour as a result of worse grass conditions.

The model is equally sensitive to the shear stress, clay cohesion and grass strength up to a decrease of 20% and an increase of 10%. After this the model becomes more sensitive to changes of the clay cohesion compared to the other two parameters. However, sensitivity of the clay cohesion is determined at a depth of 0.1 meters, assuming that the grass is eroded as a consequence of earlier overtopping waves. The strength of the clay is negligible at the surface compared to the strength of the grass.

Moreover, an increase of the turbulence and shear stress lead to an increase of the erosion development. Contrarily, an increase of the grass strength and clay cohesion leads to a decrease of the erosion development. This corresponds with the fact that the first two parameters represent the load terms in the model, while the grass strength and clay cohesion represent the strength terms.

6. Discussion

The CFD simulation includes many assumptions. The hydrodynamics were computed with the use of the Reynolds-Averaged Navier-Stokes equations combined with a k-ε turbulence model. With this method all of the unsteadiness due to turbulence is averaged out. It leads to only slightly over- and underestimation of the flow velocities. The validation of the CFD simulation showed that the modelled hydrodynamics and erosion development were in the same order of magnitude as was measured during the experiment in Millingen aan de Rijn and therefore the simplifications of the turbulence model are justified.

The initial interface thickness was set to a value of 5 centimetres. A smaller value leads to a higher accuracy and is therefore desirable. However a smaller initial interface needs a smaller maximum mesh element size, because the initial interface may not be smaller than this maximum element size. The focus of this research was to investigate the influences of a road section on the erosion development. The simulated amount of scour was of the same order of magnitude as was measured during the experiment in Millingen aan de Rijn. Therefore an initial interface thickness of 5 centimetres is adequate. However, when the objective is to compute the hydrodynamics more precise a smaller interface thickness is desirable.

During the CFD simulation it was assumed that the characteristics inside a mesh element correspond with the hydrodynamics for a volume fraction of water larger than 0.6. The turbulent character of the flow has a high influence on the bed shear stresses and therefore on the erosion development of the dike profile. The effect of the turbulence on the bed shear stresses may be underestimated for a volume fraction of 0.6. However, the flow velocities and layer thicknesses of the overtopping tongue were most precise simulated for a volume fraction of 0.6 and therefore it was assumed that this value leads to accurate prediction of the bed shear stresses.

The overtopping tongue flows over the crest and some water remains in pits of the dike profile. When a new wave overtops, the shear stresses at these pits are lower caused by the damping effect of the water layer that is present in the pits. This process is not considered in the CFD simulation as every overtopping wave is modelled on a dry slope. This may lead to an overestimation of the shear stresses during the overtopping process. During the CFD simulation it was found that only a thin layer of water retains in these pits and therefore the damping effect is most probably negligible.

The flow conditions inside the wave overtopping simulator are extremely uncertain. Many factors, such as roughness of the steel and geometry of the opening valve, determine the hydrodynamic character at the outlet of the simulator. These factors are based on assumptions, bringing uncertainty in the model. During the validation it was found that the hydrodynamics are accurate simulated at the outlet of the wave overtopping simulator. In addition, the erosion development has low sensitivity to the roughness of the steel. Therefore the influence on the computed amount of scour is little.

The bed shear stresses are highly sensitive to irregularities of the dike profile. Upward slopes with an angle larger than 25° leads to a significant increase of the maximum shear stress.

Updating the dike profile is therefore extremely important. During the simulation the profile was updated every 60 and 50 minutes for the 50 and 100 l/s per meter test respectively. However, updating this profile more frequently leads most probably to results with a higher accuracy. For defining the influence of a road structure this was not necessary. Dike profiles with and without a road on top were updated simultaneously and therefore it was possible to define the impact of the road on the erosion development. However, when the objective is to simulate the erosion process with a higher accuracy, updating with a higher frequency is desirable.

In this research an erosion model of Valk (2009) was used. This erosion model was developed during a master thesis and has not been reviewed. Although this model is based on the erosion model of Hoffmans et al. (2008) uncertainties remain about the reliability of the model. During the validation it was found that the model was capable of simulating the correct locations of erosion development and also the amount of scour was of the same order of magnitude. Although the erosion model of Valk (2009) has not been reviewed it was applicable for the objective of this research.

The complexity of the grass sod and clay layer was extremely simplified. It was assumed that the grass strength is the same along the dike profile and that all roots break simultaneously. In reality the transition of the road and grass sod were damaged due to traffic. This assumption may lead to an overestimation of the grass strength, leading to too high critical bed shear stresses. In addition, the model does not simulate the folding process of the grass sod. It was assumed that it is teared off immediately without being folded. Finally, some minor erosion was already developed as a consequence of the 1 and 10 l/s per meter tests. To investigate the influence of a road on the erosion development during wave overtopping it is not necessary to model the complexity of the grass sod exactly as it is only important to know to what extend erosion increases as a result of a road structure.

An assumption was made about the increase of the clay cohesion over depth. This increase has a high influence on the erosion resistance. The amount of scour at the right transition was underestimated and therefore it may be that the increase of the clay cohesion was overestimated. Furthermore, it was assumed that the soil only consists of grass and clay. In reality the soil is much more complex. Underneath the road a foundation layer was present, which was easily to erode. In addition, debris and sand was present at the berms and most dikes in the Netherlands consist of a sand core. Sand is much easier to erode than the cohesive clay, which leads to discrepancies between the measured and simulated erosion depths. However to investigate the influences of a road, which is the objective of this research, this complex composition of the dike is not relevant. With the use of these assumptions it was possible to simulate erosion depths for a dike profile with and without a road on top and to observe the differences.

During this research only the influence of a road on the erosion development during wave overtopping was investigated. However, the stability of a dike is based on much more factors such as macro stability. The road has not only an effect on the erosion development, but also on the soil properties of the dike core. The load of the road as a result of the asphalt layer and traffic may lead to compaction of the soil underneath. The influence of this compaction and other failure characteristics are not investigated. To evaluate the safety level of the dike all these failure mechanisms must be considered, which is not part of this research.

7. CONCLUSIONS

The conclusions are drawn by answering the research questions. Answering these questions leads to the objective of this research.

1. How can erosion of the dike profile be modelled for a dike with a road on top?

The hydrodynamics of wave overtopping can be determined with the use of a CFD simulation. This simulation uses the Reynolds-Averaged Navier-Stokes equations, combined with a k-ε turbulence model. The two phase flow method is able to solve the set of equations for the air and water phase. The finite element method subdivides the domain into elements and for each element the hydrodynamic characteristics can be computed.

The CFD simulation models the bed shear stresses along the dike profile. The erosion model of Valk (2009) computes the erosion that evolves as a consequence of the maximum bed shear stresses and is applicable for a grass covered dike with a clay layer underneath. The model parameters were set to the conditions of the experiment performed in Millingen aan de Rijn.

Erosion of multiple overtopping waves can be computed by accumulating the erosion developments caused by the single waves. After an overtopping duration of 1 hour and 50 minutes for a discharge of 50 and 100 l/s per meter respectively, the CFD simulation must be performed with the eroded dike profile. This leads to the coupled hydrodynamic-bed model.

2. How does a road structure at the crest of a dike influence the erosion process of the dike profile during wave overtopping?

A road located at the crest of the dike leads to higher erosion development at the crest during wave overtopping. In front of the road section, this increase is caused by the damaged berm at the transition of the grass sod with the road section. Irregularities with an upward slope larger than 25% leads to a significant increase of the maximum bed shear stress, which is the indicator of erosion development. The increase of scour after the road section is a combination of the smoother asphalt section and the damaged berm at the transition. The asphalt layer has a lower roughness coefficient than the grass sod and therefore the overtopping tongue loses less energy when it flows over the crest of the dike. In addition, the turbulence of the flow increases due to a sudden increase of the bed roughness at the transition of the asphalt layer with the grass sod. This leads to higher bed shear stresses and more erosion development.

Due to the large pits at the two transitions of the road section with the grass sod, the overtopping tongue is slowed down leading to a decrease of the bed shear stresses at the slope and the toe of the dike. As a consequence, the amount of scour along the slope and toe of the dike decreases compared to a smooth grass covered dike profile. However, this decrease of amount of scour is relatively small compared to the increase of erosion development at the crest.

It can be concluded that a dike profile with a road structure on top is more vulnerable to erosion development at the crest during wave overtopping compared to a smooth grass covered dike profile. The substantial increase of the amount of scour at the crest may lead to earlier dike failure. Therefore a road structure must be incorporated in the safety assessment of a dike.

3. What is the sensitivity of the parameters with respect to the model output?

The coupled hydrodynamic-bed model is highly sensitive to the depth-averaged relative turbulence intensity. The turbulent character of the flow is an important indicator of the amount of scour that evolves. Accurate measurements of the turbulence intensity are necessary to be able to compute erosion development during wave overtopping accurately.

The output of the CFD simulation is sensitive to the volume fraction coefficient, initial interface thickness and mobility tuning parameter chosen. A volume fraction needs to be determined for which is considered that the characteristics inside the element are caused by water and not by the air motion. The initial interface thickness and mobility tuning parameter influences the hydrodynamics of the overtopping tongue.

Furthermore, the erosion development is sensitive to the strength terms of the grass sod and clay layer. Overestimation of the clay cohesion and grass strength leads to too little erosion development, while underestimation leads to substantial increase of the amount of scour.

The model output has low sensitivity to the Nikuradse roughness height of steel, surface tension, velocity and length scale, time step and soil density.

8. RECOMMENDATIONS

In order to guide further research on the influence of a road structure at the crest of a dike on the erosion development during wave overtopping, the following recommendations are given:

During the CFD simulation a volume fraction of water of 0.60 was used to compute the maximum bed shear stresses. It was found that the hydrodynamics of the 700 till 1500 l/m wave volumes were simulated accurately. However, the flow velocities at the crest were too low and too high for the smaller and larger wave overtopping volumes respectively. For this reason it is recommended to use different volume fractions for the different overtopping wave volumes.

The CFD simulation includes the geometry of the wave overtopping simulator. However, the hydrodynamics inside this simulator are dependent on many factors, bringing uncertainties in the model. It is advised to use the hydrodynamics at the outlet of the simulator as boundary condition and to exclude the wave overtopping simulator from the geometry. This leads to less uncertainty and to a significant reduction of the computation time.

The coupled hydrodynamic-bed model does not consider local variations of the grass strength. However, the berms were damaged and some bare spots were present over a length of 0.5 meters at both sides of the road. This has a high influence on the erosion resistance and it is therefore advised to investigate the grass strength along the dike profile in more detail in order to be able to incorporate this in the CFD simulation.

The cohesion of the clay was based on the qualification of Hoffmans et al. (2008) and the increase of this cohesion on the suggestions of Valk (2009). Both parameters have a high influence on the amount of scour. During future experiments the quality of the clay cohesion should be defined at several depths in order to be able to define the increase of clay cohesion over depth.

The influence of a road located at the crest was only determined based on the change of erosion development during wave overtopping. However, a road has more consequences such as compaction of the soil underneath the road. Dike failure may evolve due to many failure mechanisms, while here only wave overtopping was investigated. In order to compute the exact change of safety level of the dike due to a road located at the crest also the other influences of this road must be investigated.

The computation time of the CFD simulation of a single wave is relatively large. In order to compute the safety level of a dike many simulations with different boundary conditions must be performed. In order to decrease the computation time significantly it is advised to investigate if the maximum bed shear stress can be expressed as a function of the wave overtopping volume, slope and bed roughness. With this expression it is possible to compute the maximum bed shear stresses without performing the CFD simulation.

9. REFERENCES

Anderson, J. D., Degrez, G., J.Degroote, E.Dick, Grundmann, R., & Vierendeels, J. (2009). *Computational Fluid Dynamic*. (J. F. Wendt, Ed.). Springer.

Badalassi, V. E., Ceniceros, H. D., & Banerjee, S. (2003). Computation of multiphase systems with phase field models. *Journal of Computational Physics*, *190*(2), 371–397. Retrieved from http://www.sciencedirect.com/science/article/B6WHY-49324BB-2/2/cc4a57b033af5ebee588edc0d730eeb8

Bakker, J., Melis, R., & Mom, R. (2013). *FACTUAL REPORT : Overslagproeven Rivierenland*.

Carrica, P. M., Wilson, R. V, & Stern, F. (2005). an Unsteady Single-Phase Level Set Method for, (444).

CFD Online. (2012). Turbulence length scale. Retrieved April 15, 2015, from http://www.cfd-online.com/Wiki/Turbulence_length_scale

Chinnarasri, C., Tingsanchali, T., Weesakul, S., & Wongwises, S. (2003). Flow patterns and damage of dike overtopping. *International Journal of Sediment Research*, *18*(4), 301–309.

Chow, V. Te. (1959). *Open-Channel Hydraulics*. New York: McGraw-Hill Book Company, Inc.

Ciria. (2013). *The International Levee Handbook*. London: CIRIA, Griffin Court.

ComCoast. (2007). *Design, construction, calibration and the use of the wave overtopping simulator*.

COMSOL bv. (2008). *COMSOL Multiphysics MODELING GUIDE*.

COMSOL bv. (2012). *Comsol Multiphysics User's Guide version 4.3*.

COMSOL bv. (2015). Which Turbulence Model Should I Choose for my CFD Application? Retrieved March 15, 2015, from https://www.comsol.nl/blogs/which-turbulence-model-should-choose-cfd-application/

Cormont, H. (1995). De dijk tussen Kesteren en Opheusden tijdens extreem hoogwater van de Neder Rijn ID312770. Retrieved April 30, 2015, from https://beeldbank.rws.nl/MediaObject/Details/312770

EurOtop. (2007). *Wave overtopping of sea defences and related structures: Assessment manual*. *Kuste*. Boyens Offset.

Ferziger, J. H., & Peric, M. (2002). *Computational Methods for Fluid Dynamics*. *Vasa* (third). Springer.

Frei, W. (2013a). Meshing your Geometry: When to Use the Various Element Types. Retrieved March 23, 2015, from https://www.comsol.nl/blogs/meshing-your-geometry-various-element-types/

Frei, W. (2013b). Which Turbulence Model Should I Choose for my CFD Application? Retrieved March 10, 2015, from https://www.comsol.nl/blogs/which-turbulence-model-should-choose-cfd-application/

Gonzalez, J. A., Melching, C. S., & Oberg, K. A. (1996). Analysis of Open-Channel Velocity Measurements Collected With an Acoustic Doppler Current Profiler. *New /Emerging Concepts of Rivers*, 1–8.

Hoffmans, G., Akkerman, G. J., Verheij, H., Hoven, A. Van, & Van der Meer, J. (2008). The erodibility of grassed inner dike slopes against wave overtopping. *ASCE, Proc. ICCE 2008, Hamburg.*, 3224–3236. Retrieved from http://www.vandermeerconsulting.com/downloads/stability_a/2008_hoffmans.pdf

Jervis, M., & Peregrine, D. H. (1996). Overtopping of waves at a wall: a theoretical approach. In *Coastal Engineering* (pp. 2192–2205).

Kok, M., & Vrijling, J. K. (2013). Towards an integrated evaluation framework for Multi-Functional Flood Defences. *Comprehensive Flood Risk Management*, 921–926.

Kuiken, M. (2012). Creatieve oplossingen voor een dijkweg. Retrieved March 2, 2015, from http://www.rovgmakelaar.nl/creatieve-oplossingen-voor-dijkweg/

Launder, B., Morse, A., Rodi, W., & Spalding, D. (1972). The prediction of free shear flows - A comparison of the performance of six turbulent models. In *Proceedings of NASA Conference on Free Shear Flows*.

Morris, M. (2012). *WP 3 : Reliability of Urban Flood Defences - D.3.1 Guidance on improved performance of urban flood defences*. Retrieved from http://www.floodprobe.eu/project-documents.asp

Novak, P., Moffat, A. I. B., Nalluri, C., & Narayanan, R. (2007). *Hydraulic structures* (Fourth edi). Abingdon: Taylor & Francis.

Schlegel, F. (2015). Which Multiphase Flow Interface Should I Use? Retrieved April 30, 2015, from http://www.comsol.com/blogs/which-multiphase-flow-interface-should-i-use/

Senocak, I., & Iaccarino, G. (2005). Progress towards RANS simulation of free-surface flow around modern ships, 151–156.

Spalding, D. B., & Launder, B. E. (1973). The Numerical Computation of Turbulent Flows. *Computer Methods in Applied Mechanics and Engineering*, (3), 269–289.

Steendam, G. J., De Vries, W., Van der Meer, J. W., Van Hoven, A., De Raat, G., & Frissel, J. Y. (2009). Influence of management and maintenance on erosive impact of wave overtopping on grass covered slopes of dikes ; Tests, (Smith 1994), 95–96.

Steendam, G. J., Van Hoven, A., Van der Meer, J. W., & Hoffmans, G. (2013). WAVE OVERTOPPING SIMULATOR TESTS ON TRANSITIONS AND OBSTACLES AT GRASS COVERED SLOPES OF DIKES, 1–14.

Technische Adviescommissie voor de Waterkeringen. (1997). *TECHNICAL REPORT EROSION RESISTANCE OF GRASSLAND AS DIKE COVERING TECHNICAL REPORT*. Delft.

Technische Adviescommissie voor de Waterkeringen. (1998). *Fundamentals on Water Defences*. Retrieved from http://repository.tudelft.nl/view/hydro/uuid:fe16f99c-6ddc-49bd-b7f7-18223e9b73b4/

Troch, P., Van Gent, M. R. A., Schüttrumpf, H., Lemos, C., & De Rouck, J. (2002). Numerical simulation of wave overtopping over a smooth impermeable sea dike, 3–4.

Valk, A. (2009). *Wave overtopping impact of water jets on grassed inner slope transitions*. TU Delft. Retrieved from http://repository.tudelft.nl/view/ir/uuid:5ca03ac7-0296-4ccd-b7b0-e9485cfc934f/

Van Adrichem, M., & Paulissen, M. (2013). D . Vegetatieonderzoek Dike grassland vegetation research at wave overtopping test sites Rivierenland, 1–32.

Van der Meer, J. W. (2002). *Technical report wave run-up and wave overtopping at dikes*. *Technical Advisory Committee on Flood Defence, Delft, The Netherlands*.

Van der Meer, J. W., Bernardini, P., Snijders, W., & Regeling, W. (2007). THE WAVE OVERTOPPING SIMULATOR, 1–13. doi:10.1142/9789812709554_0390

Van der Meer, J. W., Hardeman, B., Steendam, G. J., Schüttrumpf, H., & Verheij, H. (2010). FLOW DEPTH AND FLOW VELOCITY Distribution of Overtopping Wave Volumes, (2007).

Van der Meer, J. W., Schrijver, R., Hardeman, B., Hoven, A. Van, Verheij, H., & Steendam, G. J. (2009). Guidance on erosion resistance of inner slopes of dikes from three years of testing with the Wave Overtopping Simulator. *Proc. ICE*, (1994), 1–14. Retrieved from http://www.vandermeerconsulting.nl/downloads/2009_vandermeer_schrijver.pdf

Van Hoven, A., Hardeman, B., Van der Meer, J. W., & Steendam, G. J. (2010). SLIDING STABILITY OF LANDWARD SLOPE CLAY COVER LAYERS OF SEA DIKES SUBJECT TO WAVE OVERTOPPING. In *ASCE, Proc. ICCE* (p. 12). Shanghai.

Van Hoven, A., Verheij, H., Hoffmans, G., & Van der Meer, J. W. (2013). *Evaluation and Model Development: Grass Erosion Test at the Rhine dike*. Delft.

Vavrina, D. L. (2006). Report Erosion Processes on Dike Slopes (Draft from July 2006), (July), 0–80.

Wu, T. H., McKinnel, W. P., & Swanston, D. N. (1979). Strength of tree roots and landslides on Prince of Wales. *Canadian Journal of Geotechnical Research*, *16*(1), 19–33.

Yuan, S., Li, L., Amini, F., & Tang, H. (2014). Numerical Study of Turbulence and Erosion of an HPTRM-Strengthened Levee under Combined Storm Surge Overflow and Wave Overtopping. *Journal of Coastal Research*, *293*, 142–157. doi:10.2112/JCOASTRES-D-12-00250.1

Zagarola, M. V, & Smits, A. J. (1998). A new mean velocity scaling for turbulent boundary layers. In *Fluids Engineering Division Summer Meeting* (pp. 1–6). Washington DC.

LIST OF SYMBOLS

$\frac{A_r}{A}$	= root area ratio (RAR)	[-]
a_{cs}	= coefficient of increase clay cohesion over depth	[-]
$C_{\epsilon 1}$	= dimensionless constant	[-]
$C_{\epsilon 2}$	= dimensionless constant	[-]
C_{μ}	= dimensionless constant	[-]
C_E	= overall strength parameter	[$m^{-1}s^{-1}$]
c_0	= a coefficient (1.21)	[-]
c'	= effective cohesion	[N/m^2]
c_r	= artificial root cohesion	[N/m^2]
c_s	= clay cohesion	[N/m^2]
D	= average grain size	[m]
d	= erosion depth caused by earlier overtopping waves	[m]
d_a	= aggregate diameter	[m]
dy	= change of dike profile in vertical direction	[m]
dt	= time step	[s]
E_{soil}	= soil parameter	[-]
F	= volume force field	[N/m^3]
f	= a factor for the clay cohesion	[-]
g	= gravitational acceleration	[m/s^2]
H_{m0}	= significant wave height at toe of dike	[m]
k	= turbulence kinetic energy	[m^2/s^2]
k_s	= Nikuradse roughness height	[-]
L_{fact}	= length scale	[m]
n	= Manning's coefficient	[-]
P_0	= pressure at t = 0	[Pa]
P_{ov}	= probability of overtopping per wave	[-]
P_V	= probability that wave overtopping volume per wave V is greater than or same as $\underline{V}$	[-]
p	= pressure	[Pa]
q	= average wave overtopping discharge	[m^3/s per m]
R	= hydraulic radius	[m]
R_c	= free crest height above still water line	[m]
r_0	= depth-averaged relative turbulence intensity	[-]
S	= slope of energy line	[-]
T	= overtopping time	[s]
T_m	= average wave period	[s]
T_r	= parallel component of the root tensile stress	[N/m^2]
t_r	= root tensile stress	[N/m^2]
$\tan \propto$	= slope	[-]
U	= depth-averaged flow velocity	[m/s]
U_c	= critical bed shear stress	[m/s]
U_{scale}	= velocity scale	[m/s]
u	= velocity field	[m/s]
u_*	= friction velocity	[m/s]
V	= wave overtopping volume per wave	[m^3/m]
Vf	= volume fraction coefficient	[-]
v	= mean velocity	[m/s]
Y	= amount of scour	[m]
y	= y-location	[m]

α_0	= a coefficient (0.29)	[-]
α_E	= a coefficient (10^{-10})	[-]
α_τ	= pressure fluctuation coefficient (1/18)	[-]
β	= coefficient of root decrease over depth	[-]
γ	= influence factors of berm, roughness elements, angle of wave attack, and vertical wall on slope	[-]
Δ	= relative density	[-]
ϵ	= rate of dissipation of turbulence energy	[m^2/s^3]
ϵ_{pf}	= initial interface thickness	[m]
η	= dynamic viscosity	[Pa*s]
η_a	= air content	[-]
Θ	= angle of shear deformation	[°]
θ	= Shields number	[-]
ϑ	= angle of the slope	[°]
μ	= shear rate viscosity	[Pa*s]
μ_T	= turbulent viscosity	[Pa*s]
μ_t	= eddy viscosity	[m^2/s]
ν	= kinematic viscosity of water	[m^2/s]
ξ_0	= breaker parameter	[-]
ρ_s	= density of soil	[kg/m^3]
ρ_w	= density of water	[kg/m^3]
σ	= soil normal stress	[N/m^2]
σ	= effective turbulent Prandtl number	[-]
σ_g	= normal grass tensile stress	[N/m^2]
σ_r	= perpendicular component of the root tensile stress	[N/m^2]
σ_{roots}	= grass strength	[N/m^2]
τ	= shear stress	[N/m^2]
τ_b	= bed shear stress	[N/m^2]
$\tau_{b,max}$	= maximum bed shear stress	[N/m^2]
τ_c	= critical bed shear stress	[N/m^2]
τ_{clay}	= clay cohesion	[N/m^2]
χ	= mobility tuning parameter	[-]
ω	= turbulence coefficient	[-]
$\emptyset'$	= effective internal friction angle	[°]
∇	= nabla operator	$[\frac{\partial}{\partial x} + \frac{\partial}{\partial y}]$
$\equiv$	= identical to	[-]

Appendixes

A. Steering list 67
B. Theoretical background CFD 68
B.1. Navier-Stokes 68
B.2. Turbulence model 69
B.3. Finite element method 70
B.4. COMSOL Multiphysics 70
C. Mesh properties 71
D. Bed model 72
D.1. Derivation critical bed shear stress and critical flow velocity 72
D.2. Quality grass and clay 74
E. MATLAB-scripts 75
E.1. Construction dike slope 75
E.2. Bed model 76
F. Influence volume fraction 78
G. Results 79
G.1. Eroded dike profiles after 1 hour of testing: 50 l/s per meter test 79
G.2. Eroded dike profiles after 2 hours of testing: 50 l/s per meter test 80
G.3. Eroded dike profiles after 4 hours of testing: 50 l/s per meter test 80
G.4. Eroded dike profile after 5 hours of testing: 50 l/s per meter test 81
G.5. Eroded dike profile after 50 minutes of testing: 100 l/s per meter test 82
G.6. Flow velocities and water depths along dike slope 83
G.7. Erosion development along complete dike profile with and without a road 84

A. STEERING LIST

Table A.1 gives the first part of the steering list of the 50 l/s per meter test. This shows that the volumes released by the wave overtopping simulator are very diverse and randomly in size and time.

Table A.1. First part of the 50 l/s per meter test

Nr	l/m	hh:mm:ss		Nr	l/m	hh:mm:ss		Nr	l/m	hh:mm:ss
1	248	0:00:04		**51**	212	0:07:01		**101**	200	0:13:13
2	576	0:00:15		**52**	417	0:07:09		**102**	200	0:13:17
3	848	0:00:32		**53**	727	0:07:23		**103**	274	0:13:23
4	655	0:00:45		**54**	532	0:07:34		**104**	200	0:13:27
5	258	0:00:50		**55**	200	0:07:39		**105**	252	0:13:32
6	200	0:00:54		**56**	293	0:07:44		**106**	288	0:13:37
7	200	0:00:58		**57**	200	0:07:48		**107**	236	0:13:42
8	340	0:01:05		**58**	526	0:07:59		**108**	200	0:13:46
9	630	0:01:17		**59**	329	0:08:05		**109**	200	0:13:50
10	445	0:01:27		**60**	241	0:08:10		**110**	377	0:13:58
11	200	0:01:31		**61**	290	0:08:16		**111**	200	0:14:02
12	447	0:01:39		**62**	457	0:08:25		**112**	717	0:14:16
13	462	0:01:49		**63**	1029	0:08:45		**113**	250	0:14:21
14	200	0:01:53		**64**	200	0:08:50		**114**	351	0:14:28
15	212	0:01:57		**65**	431	0:08:58		**115**	342	0:14:35
16	423	0:02:05		**66**	200	0:09:03		**116**	609	0:14:47
17	762	0:02:20		**67**	599	0:09:14		**117**	200	0:14:51
18	227	0:02:25		**68**	317	0:09:21		**118**	379	0:14:59
19	200	0:02:29		**69**	200	0:09:25		**119**	837	0:15:15
20	1538	0:02:59		**70**	293	0:09:31		**120**	235	0:15:20
21	450	0:03:09		**71**	219	0:09:35		**121**	625	0:15:32
22	200	0:03:13		**72**	822	0:09:51		**122**	200	0:15:37
23	200	0:03:17		**73**	247	0:09:56		**123**	808	0:15:52
24	200	0:03:21		**74**	346	0:10:03		**124**	219	0:15:57
25	482	0:03:31		**75**	579	0:10:15		**125**	200	0:16:01
26	200	0:03:35		**76**	234	0:10:20		**126**	200	0:16:05
27	451	0:03:44		**77**	383	0:10:27		**127**	558	0:16:16
28	799	0:03:59		**78**	200	0:10:31		**128**	200	0:16:20
29	354	0:04:07		**79**	265	0:10:37		**129**	200	0:16:24
30	1099	0:04:28		**80**	249	0:10:41		**130**	494	0:16:34
31	200	0:04:33		**81**	200	0:10:46		**131**	368	0:16:41
32	200	0:04:37		**82**	553	0:10:56		**132**	200	0:16:46
33	282	0:04:42		**83**	200	0:11:01		**133**	211	0:16:50
34	210	0:04:47		**84**	200	0:11:05		**134**	200	0:16:54
35	518	0:04:57		**85**	200	0:11:09		**135**	284	0:16:59
36	302	0:05:03		**86**	437	0:11:17		**136**	200	0:17:03
37	398	0:05:11		**87**	232	0:11:22		**137**	200	0:17:07
38	305	0:05:17		**88**	298	0:11:28		**138**	262	0:17:13
39	295	0:05:23		**89**	225	0:11:32		**139**	200	0:17:17
40	744	0:05:37		**90**	338	0:11:39		**140**	200	0:17:21
41	418	0:05:46		**91**	200	0:11:43		**141**	200	0:17:25
42	200	0:05:50		**92**	388	0:11:51		**142**	387	0:17:32
43	200	0:05:54		**93**	200	0:11:55		**143**	200	0:17:36
44	213	0:05:59		**94**	374	0:12:02		**144**	871	0:17:53
45	245	0:06:03		**95**	432	0:12:11		**145**	200	0:17:58
46	488	0:06:13		**96**	525	0:12:21		**146**	313	0:18:04
47	243	0:06:18		**97**	200	0:12:26		**147**	219	0:18:09
48	583	0:06:29		**98**	918	0:12:43		**148**	607	0:18:20
49	1007	0:06:49		**99**	643	0:12:56		**149**	200	0:18:25
50	346	0:06:57		**100**	621	0:13:09		**150**	601	0:18:36

B. Theoretical background CFD

In this Appendix theoretical background of the Navier-Stokes equations are provided, which forms the basis of the CFD simulation. Thereafter information of the k ~ ε turbulence model is given and the finite element method is explained. The Appendix ends with a description of COMSOL Multiphysics.

B.1. NAVIER-STOKES

The CFD simulation uses the two dimensional Navies-Stokes equations for the conservation of momentum and a continuity equation for the conservation of mass. These equations are given with (COMSOL bv, 2008):

$$\rho\frac{\partial u}{\partial t} - \nabla \times [\eta(\nabla u + (\nabla u)^T)] + \rho(u \times \nabla)u + \nabla p = F \tag{18}$$

And

$$\nabla \times u = 0 \tag{19}$$

Where:

∇	= nabla operator	$[\frac{\partial}{\partial x} + \frac{\partial}{\partial y}]$
ρ	= density	[kg/m^3]
u	= velocity field	[m/s]
η	= dynamic viscosity	[Pa*s]
p	= pressure	[Pa]
F	= volume force field	[N/m^3]

Equation (18) is the momentum transport equation and Equation (19) represents the equation of continuity for incompressible fluids. These formulas are general enough to account for all types of incompressible flow. However, when the Reynolds number increases small eddies develop and the timescales of the oscillations become so short that it is computationally unfeasible to solve the Navier-Stokes equations (COMSOL bv, 2015). For this reason COMSOL Multiphysics uses the Reynolds-Averaged Navier-Stokes (RANS) equation and this modified Navier-Stokes equation is as follow:

$$\rho\frac{\partial u}{\partial t} - [(\mu + \mu_T)(\nabla u + (\nabla u)^T)] + \rho(u \times \nabla)u + \nabla p = F \tag{20}$$

Where:

μ	= shear rate viscosity	[Pa*s]
μ_T	= turbulent viscosity	[Pa*s]

With this equation all of the unsteadiness due to turbulence is averaged out. The equation is obtained by averaging the equations of motion over an ensemble of realizations. This means averaging over an imagined set of flows in which all controllable factors are kept fixed (Ferziger & Peric, 2002). Figure B.1 gives the result of ensemble averaging. This figure shows that ensemble averaging leads to slightly over- and underestimation of the real velocities.

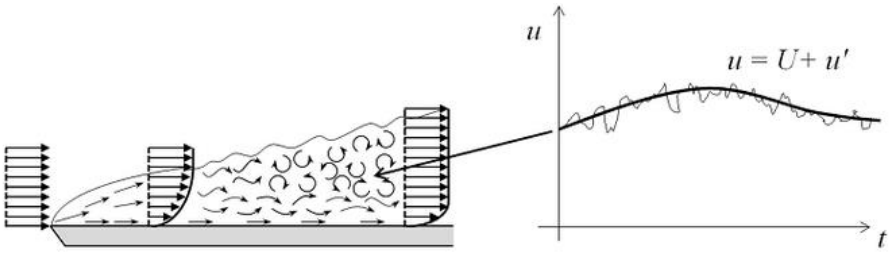

Figure B.1. From turbulent flow towards RANS method (Frei, 2013b)

The RANS method takes much less processing time and memory to solve the set of equations than the DNS and LES methods. However, it should be kept in mind that the RANS equations are slightly less accurate in the simulation of the turbulent flow.

In order to solve for two phase flow, the phase field application is used. The phase field application utilizes the Cahn-Hilliard equation. This equation describes the process of phase separation. COMSOL Multiphysics uses ϕ to describe the concentration of a fluid inside the domain. A value of -1 indicates that only fluid A is present, while a value of 1 represents that only fluid B is present (Badalassi, Ceniceros, & Banerjee, 2003). With this the Cahn-Hilliard equation can be given with:

$$\frac{\partial \phi}{\partial t} + u \times \nabla \phi = \nabla \times \left(\frac{\gamma \lambda}{{\epsilon_{pf}}^2}\right) \nabla \psi \quad \text{with} \quad \gamma = \chi {\epsilon_{pf}}^2 \quad \text{and} \quad \lambda = \frac{3 \epsilon_{pf} \sigma}{\sqrt{8}} \tag{21}$$

And

$$\psi = -\nabla \times {\epsilon_{pf}}^2 \nabla \phi + (\phi^2 - 1) + \frac{{\epsilon_{pf}}^2}{\lambda} \frac{\partial f}{\partial \phi} \tag{22}$$

Where:

ϕ	= concentration of the fluid	[-]
ϵ_{pf}	= initial interface thickness	[m]
χ	= mobility tuning parameter	[-]

B.2. TURBULENCE MODEL

To solve the complex behaviour of wave overtopping a turbulence model is implemented. A good turbulence model has extensive universality and is not too complex to develop or use. This means that a single set of empirical constants or functions provides close simulation of a large variety of types of flow. Complexity is measured by the number of differential equations which the model contains, and the number of the empirical constants and functions which are required to complete them (Spalding & Launder, 1973).

The k ~ ε turbulence model is very popular due to its good convergence rate and relatively low memory requirements. The model is a good trade-off between accuracy and complexity and for this reason COMSOL Multiphysics uses a k ~ ε turbulence model for the two-phase flow interface. In addition, the model performs well around complex geometries (Frei, 2013b). The k ~ ε turbulence model includes two parameters, namely the turbulent kinetic energy and the rate of dissipation of kinetic energy. The general differential equations of the k ~ ε model are (Spalding & Launder, 1973):

$$\frac{\partial \epsilon}{\partial t} = \frac{1}{\rho}\frac{\partial}{\partial x_k}\left[\frac{\mu_t}{\sigma_\epsilon}\frac{\partial \epsilon}{\partial x_k}\right] + \frac{C_1 \mu_t}{\rho}\frac{\epsilon}{k}\left(\frac{\partial U_i}{\partial x_k} + \frac{\partial U_k}{\partial x_i}\right)\frac{\partial U_i}{\partial x_k} - C_2\frac{\epsilon^2}{k} \quad (23)$$

And

$$\frac{\partial k}{\partial t} = \frac{1}{\rho}\frac{\partial}{\partial x_k}\left[\frac{\mu_t}{\sigma_k}\frac{\partial k}{\partial x_k}\right] + \frac{\mu_t}{\rho}\left(\frac{\partial U_i}{\partial x_k} + \frac{\partial U_k}{\partial x_i}\right)\frac{\partial U_i}{\partial x_k} - \epsilon \quad (24)$$

And

$$\mu_t = \rho C_\mu \frac{k^2}{\epsilon} \quad (25)$$

Where:

μ_t	= eddy viscosity	[m²/s]
ϵ	= rate of dissipation of turbulence energy	[m²/s³]
k	= turbulence kinetic energy	[m²/s²]
σ	= effective turbulent Prandtl number	[-]
U	= mean velocity component	[m/s]
C	= dimensionless coefficients	[-]

B.3. FINITE ELEMENT METHOD

The finite element method (FEM) is a numerical technique for solving partial differential equations. The continuum field or domain is subdivided into cells or elements, which forms a grid. These two dimensional elements have a triangular or a quadrilateral form (Ferziger & Peric, 2002). Another characteristic of the FEM is that it does not look for the solution of the partial differential equation (PDE) itself, but looks for a solution of an integral form of the PDE. The most general integral form is obtained from a weighted residual formulation (Anderson et al., 2009). Due to this formulation, FEM allows easily the construction of higher order accurate methods and incorporation of differential type boundary conditions, which is a second advantage of FEM compared to FVM. In the FVM, the higher order accurate formulations are quite complicated (Anderson et al., 2009). Besides this, FEM permits a rapidly change in element size. This may be relevant in this research, because the air can be modelled less accurate than the water flow. It is therefore useful when a larger element size can be used for the part where only air is located and almost no physical changes occur in order to reduce the computation time.

B.4. COMSOL MULTIPHYSICS

The CFD simulation is performed with the use of COMSOL Multiphysics. COMSOL Multiphysics is a platform for physics-based modelling and simulation. It can be used as simulation tool for a wide range of applications, such as electrical, mechanical, fluid flow and chemical applications. The software provides a powerful integrated desktop environment with a Model Builder (COMSOL bv, 2012). COMSOL Multiphysics is used in this research for several reasons. First of all it is a very user-friendly software. The interface needed can be selected, and all the equations that needs to be solved are added automatically. The software shows which parameters need to be implemented and which boundary and initial conditions can be used. Besides this, the geometry of the domains can easily be implemented and adapted. In addition, COMSOL Multiphysics makes it possible to plot the results in figures and graphs in order to be able to evaluate the results.

C. MESH PROPERTIES

Table C.1 provides the properties of the mesh for the different overtopping wave volumes. Figure C.1 shows where mesh 1 and 2 are located and where boundary layers are applied. This figure corresponds with the geometry of an overtopping volume of 2500 l/m.

Table C.1. Mesh properties

Mesh 1	Maximum element size	0.05
	Minimum element size	0.002
	Maximum element growth rate	1.2
	Curvature factor	0.8
Mesh 2	Maximum element size	1.0
	Minimum element size	0.05
	Maximum element growth rate	1.3
	Curvature factor	0.3
Boundary layers	Number of boundary layers	3
	Boundary layer stretching factor	1.2
	Thickness adjustment factor	2
150 litres per meter	Domain elements	11234
	Boundary elements	874
400 litres per meter	Domain elements	11870
	Boundary elements	942
700 litres per meter	Domain elements	12040
	Boundary elements	907
1000 litres per meter	Domain elements	12515
	Boundary elements	917
1500 litres per meter	Domain elements	13391
	Boundary elements	930
2500 litres per meter	Domain elements	14675
	Boundary elements	965

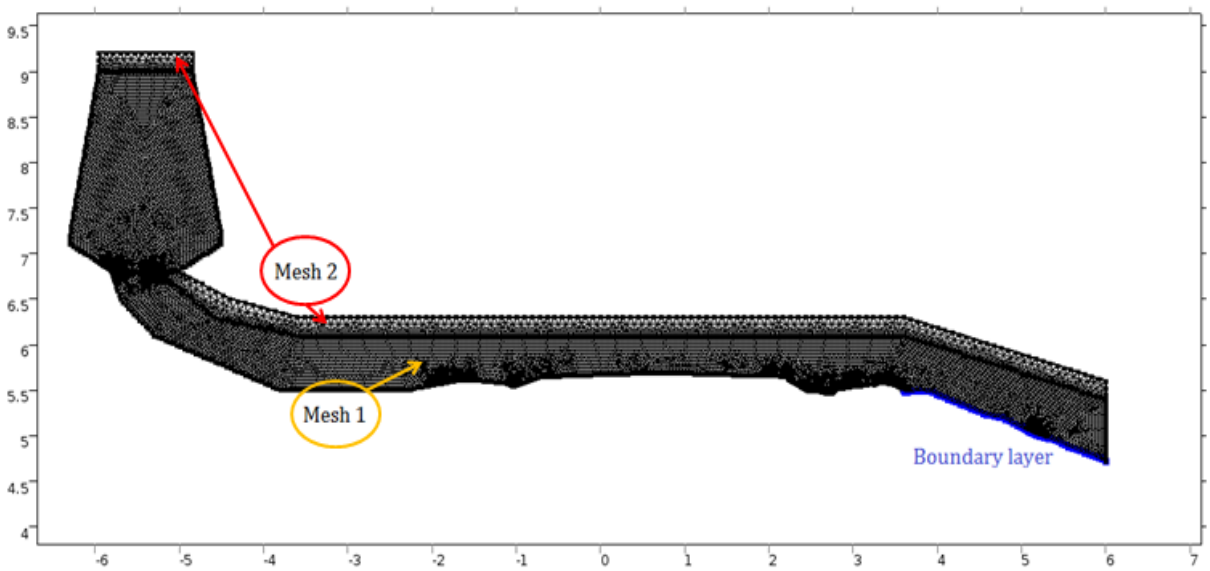

Figure C.1. Mesh properties of the geometry

D. EROSION MODEL

This Appendix describes the derivation of the critical bed shear stress and the critical flow velocity. Thereafter an explanation is provided of how the qualities of the grass sod and clay layer are determined.

D.1. DERIVATION CRITICAL BED SHEAR STRESS AND CRITICAL FLOW VELOCITY

The erosion model of Valk (2009) is based on the turf-element model. The turf-element model uses the Mohr Coulomb criterion instead of the Shields parameter. This criterion describes soil failure in terms of shear stress and effective normal stress along an sliding plane (Hoffmans et al., 2008). The shear stress is given with:

$$\tau = c' + c_r + (\sigma - \rho_w) \tan \emptyset' \tag{26}$$

Where:

τ	= shear stress	[N/m²]
c'	= effective cohesion	[N/m²]
c_r	= artificial root cohesion	[N/m²]
σ	= soil normal stress	[N/m²]
$\emptyset'$	= effective internal friction angle	[°]

The shear strength in this formula is obtained from the shear stress that can be mobilised between soil particles. The effective normal stress is caused by the pore water pressure and the weight of the soil, whereas the effective internal friction angle represents the frictional interaction of soil particles and the interlocking of these particles (Hoffmans et al., 2008).

The turf-element model calculates the cohesion caused by the root system with the use of the root equation of Wu, McKinnel, & Swanston (1979). This equation requires the root tensile stress, the root diameter and the angle of shear deformation and is often used to determine the effects of root reinforcement. The strength of the roots can be resolved into parallel and perpendicular components when a root crosses a shear zone. The components are given in Figure E.1 and leads to the following equations for the artificial root cohesion and normal grass strength (Hoffmans et al., 2008):

$$c_r = t_r \frac{A_r}{A} (\cos \Theta \tan \Theta + \sin \Theta) \qquad \text{with} \quad T_r = t_r \sin \Theta \quad \text{and} \quad \sigma_r = t_r \cos \Theta \tag{27}$$

And

$$\sigma_g = t_r \frac{A_r}{A} \cos \Theta \tag{28}$$

Where:

t_r	= root tensile stress	[N/m²]
$\frac{A_r}{A}$	= root area ratio (RAR)	[-]
Θ	= angle of shear deformation	[°]
T_r	= parallel component of the root tensile stress	[N/m²]

σ_r = perpendicular component of the root tensile stress [N/m²]
σ_g = normal grass strength [N/m²]

The term ($\cos\Theta \tan\Theta + \sin\Theta$) is insensitive to changes in Θ and is close to 1.2 for a wide range of Θ values. Therefore the formula of the artificial root cohesion can be simplified to (Hoffmans et al., 2008):

$$c_r = 1.2 t_r \frac{A_r}{A} \tag{29}$$

These equations assume that all roots in the grass sod break at the same time. However, in reality some roots are stronger than others and therefore do not break simultaneously. This may lead to an overestimation of the artificial root tensile strength and the normal grass strength.

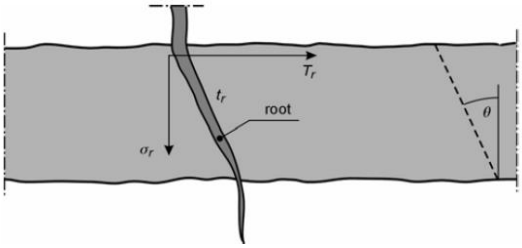

Figure D.1. Strength components of a root (Hoffmans et al., 2008)

The main focus of the turf-element model is that it investigates the forces that act on a clay aggregate, assuming this particle has the form of a cube. The forces acting on a cubic aggregate are the vertical force (F_p) caused by pressure fluctuations above and underneath the particle, the weight (F_w) and the forces caused by shear (F_s), cohesion (F_c) and the roots of the grass (F_g) (Hoffmans et al., 2008). Figure D.2 present these forces.

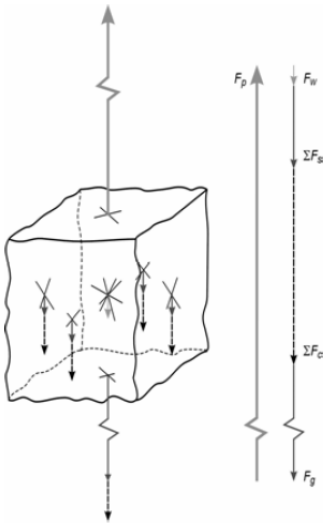

Figure D.2. Forces acting upon a turf-element (Hoffmans et al., 2008)

Incipient of motion occurs if the load on an aggregate is larger than the strength, and is defined as (Hoffmans et al., 2008):

$$F_p \geq F_w + \sum F_s + \sum F_c + F_g \tag{30}$$

With this information the critical bed shear stress and critical depth-averaged velocity are defined, assuming the flow is hydraulically rough. They are given with (Hoffmans et al., 2008):

$$\tau_c = \alpha_\tau((\rho_s - \rho_w)gd + c_s + \sigma_g) \qquad \text{with} \qquad \alpha_\tau = 1/18 \tag{31}$$

And

$$U_c = \frac{\alpha_0}{r_0}\sqrt{\Delta g d + \frac{c_s}{\rho} + \frac{\sigma_g}{\rho}} \qquad \text{with} \qquad \alpha_0 = \sqrt{\alpha_\tau {c_0}^2} \tag{32}$$

Where:

τ_c	= critical bed shear stress	[N/m²]
α_τ	= pressure fluctuation coefficient	[-]
d	= depth	[m]
α_0	= coefficient	[-]
c_0	= coefficient	[-]
Δ	= relative density	[-]
c_s	= clay cohesion	[N/m²]
σ_g	= normal grass tensile stress	[N/m²]

D.2. QUALITY GRASS AND CLAY

The quality of the grass sod is determined based on the root density rate. This method is based on the number of roots and is defined by counting the number of roots within a soil sample obtained with a ground drill with a diameter of 3 centimetres. By counting the number of roots every 2.5 centimetres, the root density as a function of the depth can be determined (Valk, 2009). This leads to a relationship as given in Figure D.3. This figure represents one of the measurements performed on the dike slope in Millingen aan de Rijn. Hoffmans et. al (2008) specified the qualification as given in Table D.1.

Table D.1. Qualification grass covers (Hoffmans et al., 2008)

Category	σ_g [kN/m²]
Very poor	2.8
Poor	5.6
Averaged	8.4
Good	11.2

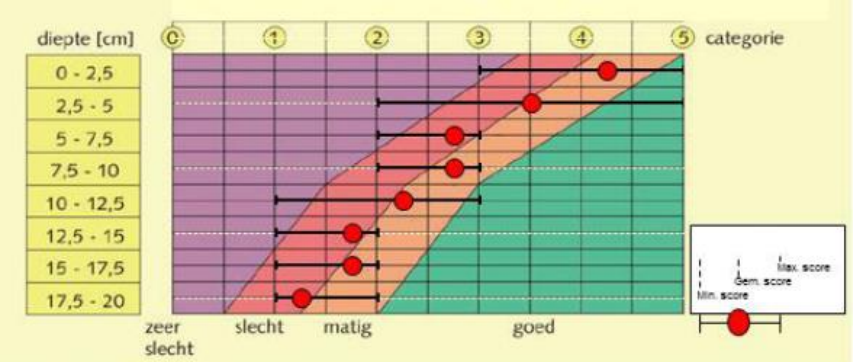

Figure D.3. Quality of grass cover (Van Adrichem & Paulissen, 2013)

The quality of the clay layer can be divided into five classes. With the use of the turf-element model Hoffmans et. al (2008) determined the clay cohesion for each class. These values are presented in Table D.2.

Table D.2. Qualification grass layer (Hoffmans et al., 2008)

Quality of the clay	c_s [kN/m²]
Sand	-
Poor	0
Structured	0.11
Good	0.25
Very good	0.50

E. MATLAB-SCRIPTS

This Appendix gives the MATLAB-scripts used during the research.

E.1. CONSTRUCTION DIKE SLOPE

```
% Construction reference slope
clear,clc
slope = load('M1_10_E.asc');        % Load data points of 3D laser scan
      x = slope(:,1);
      y = slope(:,2);
      z = slope(:,3);

teller = 0;
matrix = [-2300,5500];              % Starting point of slope
Midden = 431.5;

figure(1)
hold on

% Plot data points that are within a section of 3 mms
for i = 1:length(x);
    if (y(i) >= -2500 & y(i) <= -1000) & (x(i) > (Midden - 1.5) & x(i) <
(Midden + 1.5));
         teller = teller + 1;
         plot(y(i)./1000,z(i)./1000,'*r');
         matrix = [matrix;y(i),z(i)];
    elseif (y(i) >= 1500 & y(i) <= 3000) & (x(i) > (Midden - 1.5) & x(i) <
(Midden + 1.5));
         teller = teller + 1;
         plot(y(i)./1000,z(i)./1000,'*r');
         matrix = [matrix;y(i),z(i)];
    elseif ((y(i) >= -2800 & y(i) < -2500) | y(i) > 3000) & (x(i) > (Midden
- 0.15) & x(i) < (Midden + 0.15));          % Less data points along the
slope
         teller = teller + 1;
         plot(y(i)./1000,z(i)./1000,'*r');
         matrix = [matrix;y(i),z(i)];
    elseif (y(i) > -1000 & y(i) < 1500) & (x(i) > (Midden - 0.75) & x(i) <
(Midden + 0.75));                          % Less data points at road section
         teller = teller + 1;
         plot(y(i)./1000,z(i)./1000,'*r');
         matrix = [matrix;y(i),z(i)];
              title('Data points 3D scanner')
              xlabel('Position along the dike slope [m]')
              ylabel('Elevation [m]')
    end
end

%% Plot interpolated dike profile
slope_10L_E = sortrows(matrix)./1000;
plot(slope_10L_E(:,1),slope_10L_E(:,2),'*r')
plot(slope_10L_E(:,1),slope_10L_E(:,2))
        title('Interpolated dike profile','FontSize',18)
        xlabel('Position along the dike slope [m]','FontSize',14)
        ylabel('Elevation [m]','FontSize',14)
```

E.2. BED MODEL

```
%% Erosion Model

clear,clc

%% Setting parameters
a0 = 2;
a_tau = 1/18;
a_cs = 20;            % increase clay cohesion [1/m]
o_r0 = 7760;          % root strength [N/m2]
tau_c0 = 11900;       % strength clay layer [N/m2]
beta = 22.32;         % decrease root density
a_soil = 1;
a_e = 1e-10;
visc = 1e-6;          % viscosity [m2/s]
da = 0.004;           % [m]
phro_s = 2000;        % [kg/m3]
phro_w = 1000;        % [kg/m3]
g = 9.81;             % gravitational acceleration
f = 0.21;             % factor in formula for total shear stress [-]
t = 0.05;             % timestep [s]
delta = (phro_s - phro_w) ./ phro_w;

%% Calculation strength terms
datapoints = load('xy locations.txt');
input = load('shear stress.txt');              % Output data of COMSOL
      x = datapoints(:,1);
      y = datapoints(:,2);
      x_t = input(:,1);

% different turbulence for crest and slope
r0 = zeros(length(x),1);
for i = 1:length(r0)
    if x(i) < 3.3
        r0(i) = 0.17;
    else r0(i) = 0.1;
    end
end
      w = 1.5 + 5 .* r0;

% calculation d at t = 0
d = zeros(length(x),1);

% Calculation critical shear stress
tau_tot = f .* (tau_c0 .* (1 + a_cs * d)) + (o_r0 .* exp(-beta*d));
tau_c = a_tau .* ((phro_s - phro_w) .* g .* da + tau_tot);

% Calculation Esoil
Uc = (a0 ./ r0) .* sqrt(delta .* g .* da +(tau_tot ./ phro_w));
% calculation critical flow velocity
Ce = a_e .* ((g^2 .* da) ./ (visc .* Uc .^2));
% calculation Ce
Esoil = a_soil ./ Ce;

%% Calculation erosion as a result of wave volume
tau0 = input(:,2);                  % Bed shear stress at output data points

% Select maximum bed shear stress for each location
```

```
tau_max = zeros(length(x),1);

for i = 1:length(x)
    for j = 1:length(x_t)
    if x(i) == x_t(j) & tau0 (j)> tau_max (i)
        tau_max (i) = tau0 (j);
    end
    end
end

% Calculation Overtopping times at each location
teller = zeros(length(x),1);
erosion = [];

for i = 1:length(x)
    for j = 1:length(x_t)
        if x(i) == x_t(j) & tau0 (j) > 0
            teller(i) = teller(i) + 1;
        end
    end
end
      Tovt = teller .* t;

% Replace Tovt at road transition (bump)
for i = 1:length(Tovt)
    if x(i) > 2.25 & x(i) < 3.2
       Tovt(i) = (Tovt(31) + Tovt(42)) ./ 2;
    end
end

% Calculation erosion depth
for i = 1:length(tau_max);
    if tau_max_400(i) >= tau_c(i)
        scour(i) = ((w(i) .^2 .* tau_max (i) - tau_c(i)) ./ Esoil(i)) .*
Tovt(i);      % change in depth [m]
        erosion= [erosion;scour(i)];
    else scour(i) = 0;
        erosion_ = [erosion;scour(i)];
    end
end

%% Total erosion and calculation new y-locations
total_erosion = X .* erosion              % where X is amount of waves
y_after = y - total_erosion;
Slope = [x,y_50L_01u];

% Plot reference and new profile
figure(1)
hold on
      plot(x,y)
      plot(x,y_50L_01u,'r')
```

F. INFLUENCE VOLUME FRACTION

Table F.1 shows the maximum flow velocities, overtopping times and velocities at test location SM1 for different volume fractions.

Table F.1. Results volume fraction

	Volume fraction [-]	u_{max} [m/s]	T_{ovt} [s]	u_{sm1} [m/s]	Difference [%]
150L	0.30	3.36	0.6	2.39	--
	0.40	3.16	0.4	0.00	--
	0.50	0.00	0.0	0.00	--
	0.60	**0.00**	**0.0**	**0.00**	**--**
	0.65	0.00	0.0	0.00	--
	0.70	0.00	0.0	0.00	--
	0.75	0.00	0.0	0.00	--
400L	0.30	4.27	1.3	3.46	-0.8
	0.40	4.27	1.2	3.19	-11.1
	0.50	3.97	1.0	3.06	-14.8
	0.60	**3.76**	**0.9**	**2.83**	**-21.1**
	0.65	3.76	0.8	2.69	-25.1
	0.70	3.60	0.7	2.44	-32.0
	0.75	3.60	0.7	2.05	-42.9
700L	0.30	4.75	1.9	4.18	--
	0.40	4.75	1.8	4.05	--
	0.50	4.75	1.7	3.95	--
	0.60	**4.45**	**1.4**	**3.78**	--
	0.65	4.45	1.4	3.78	--
	0.70	4.22	1.3	3.69	--
	0.75	4.22	1.2	3.61	--
1000L	0.30	5.61	2.3	4.79	+15.6
	0.40	5.61	2.1	4.66	+12.4
	0.50	5.06	2.1	4.63	+11.7
	0.60	**5.06**	**2.0**	**4.49**	**+8.3**
	0.65	5.06	1.9	4.37	+5.4
	0.70	4.71	1.8	4.37	+5.4
	0.75	4.71	1.8	4.26	+2.8
1500L	0.30	5.75	2.9	5.61	+22.0
	0.40	5.75	2.8	5.36	+16.5
	0.50	5.75	2.7	5.31	+15.4
	0.60	**5.75**	**2.6**	**5.24**	**+13.9**
	0.65	5.30	2.5	5.14	+11.7
	0.70	5.30	2.4	5.11	+11.1
	0.75	5.30	2.4	5.05	+9.8
2500L	0.30	7.00	3.9	7.60	+50.0
	0.40	7.00	3.9	7.12	+40.7
	0.50	7.00	3.7	7.12	+40.7
	0.60	**6.31**	**3.6**	**6.91**	**+36.5**
	0.65	6.31	3.5	6.91	+36.5
	0.70	6.31	3.5	6.86	+35.6
	0.75	6.31	3.4	6.82	+34.8

G. RESULTS

This Appendix gives the results of the coupled hydrodynamic-bed model

G.1. ERODED DIKE PROFILES AFTER 1 HOUR OF TESTING: 50 L/S PER METER TEST

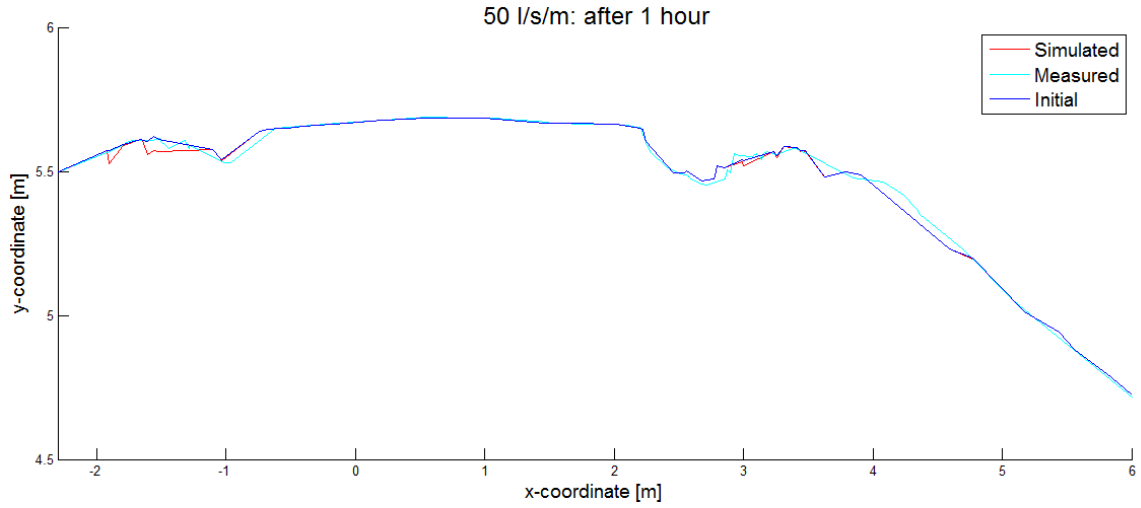

Figure G.1. Dike profiles after 1 hour of testing with a discharge of 50 l/s per meter

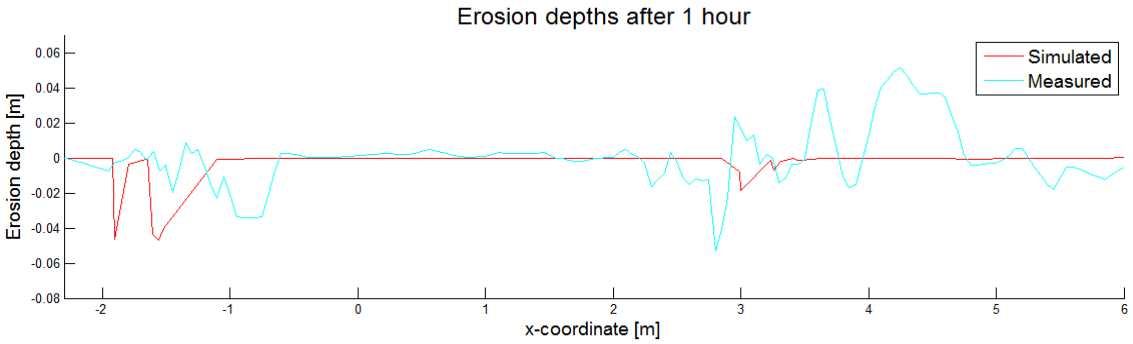

Figure G.2. Erosion depths after 1 hour of testing with a discharge of 50 l/s per meter

G.2. ERODED DIKE PROFILES AFTER 2 HOURS OF TESTING: 50 L/S PER METER TEST

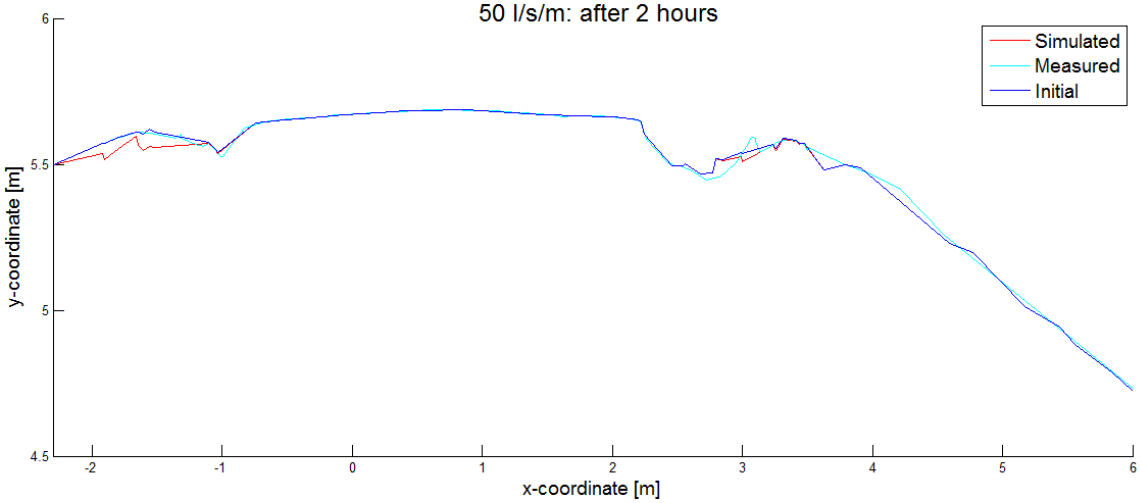

Figure G.3. Dike profiles after 2 hours of testing with a discharge of 50 l/s per meter

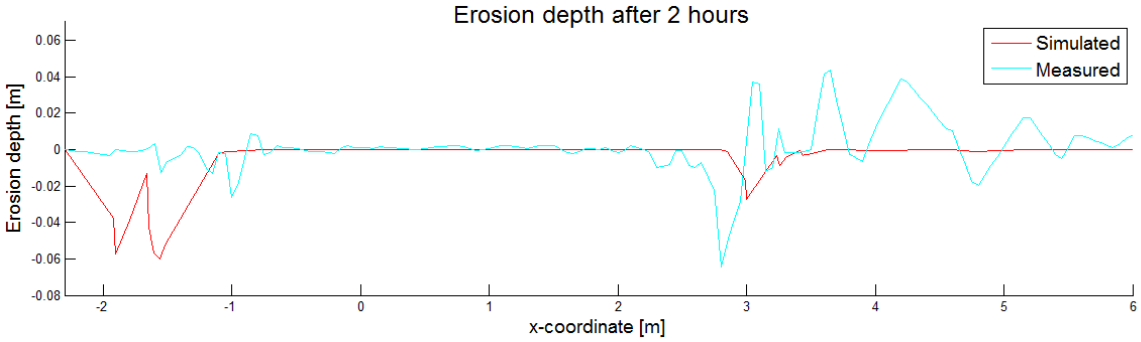

Figure G.4. Erosion depths after 2 hours of testing with a discharge of 50 l/s per meter

G.3. ERODED DIKE PROFILES AFTER 4 HOURS OF TESTING: 50 L/S PER METER TEST

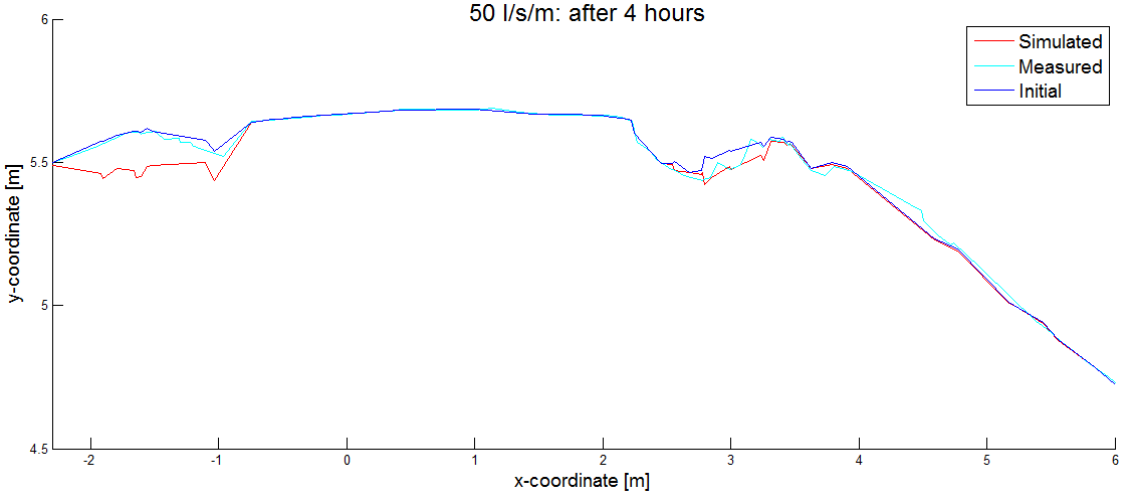

Figure G.5. Dike profiles after 4 hours of testing with a discharge of 50 l/s per meter

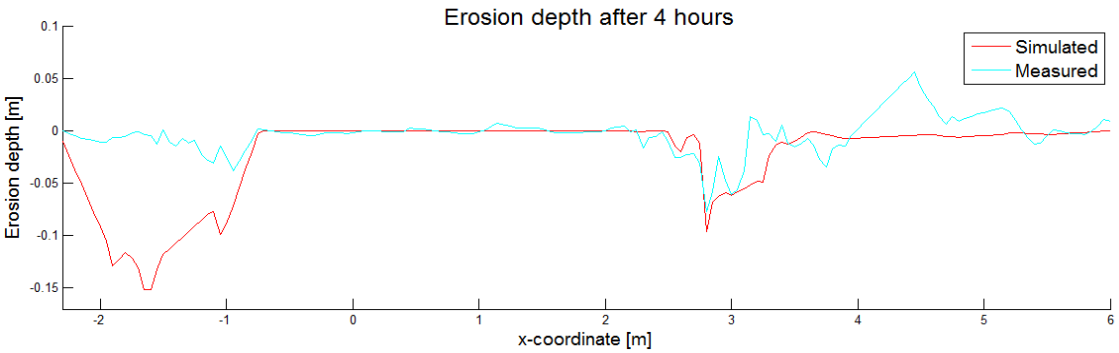

Figure G.6. Erosion depths after 4 hours of testing with a discharge of 50 l/s per meter

G.4. ERODED DIKE PROFILE AFTER 5 HOURS OF TESTING: 50 L/S PER METER TEST

No measured data is available after five hours of testing and for this reason only the simulated eroded profile is presented.

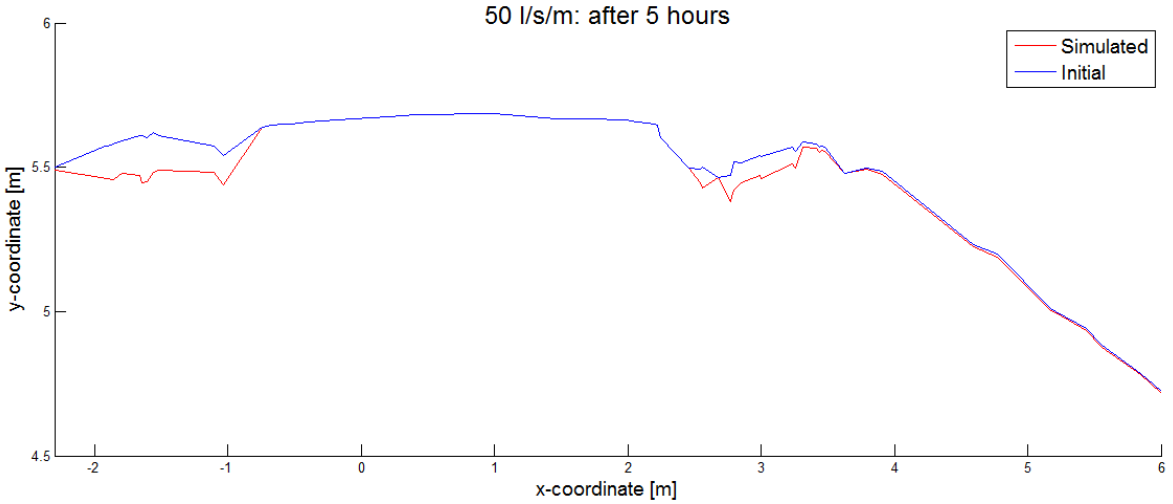

Figure G.7. Dike profile after 5 hours of testing with a discharge of 50 l/s per meter

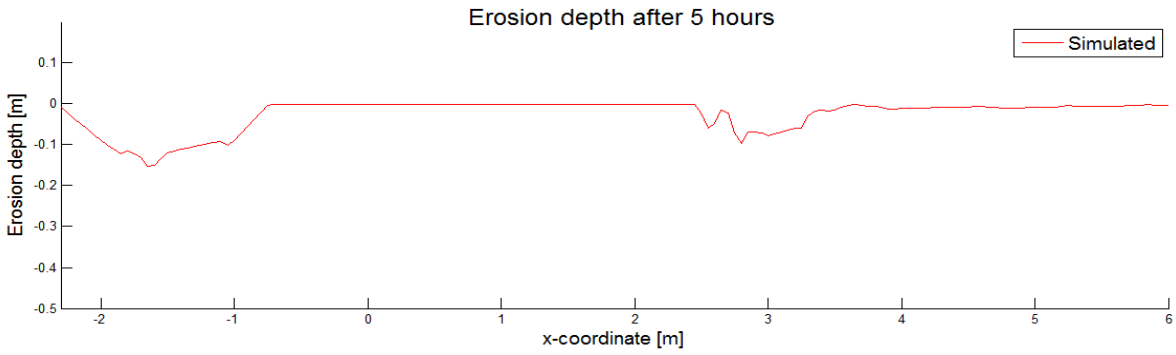

Figure G.8. Erosion depth after 5 hours of testing with a discharge of 50 l/s per meter

G.5. ERODED DIKE PROFILE AFTER 50 MINUTES OF TESTING: 100 L/S PER METER TEST

No measured data is available after 50 minutes of testing with a discharge of 100 l/s per meter and for this reason only the simulated eroded profile is presented.

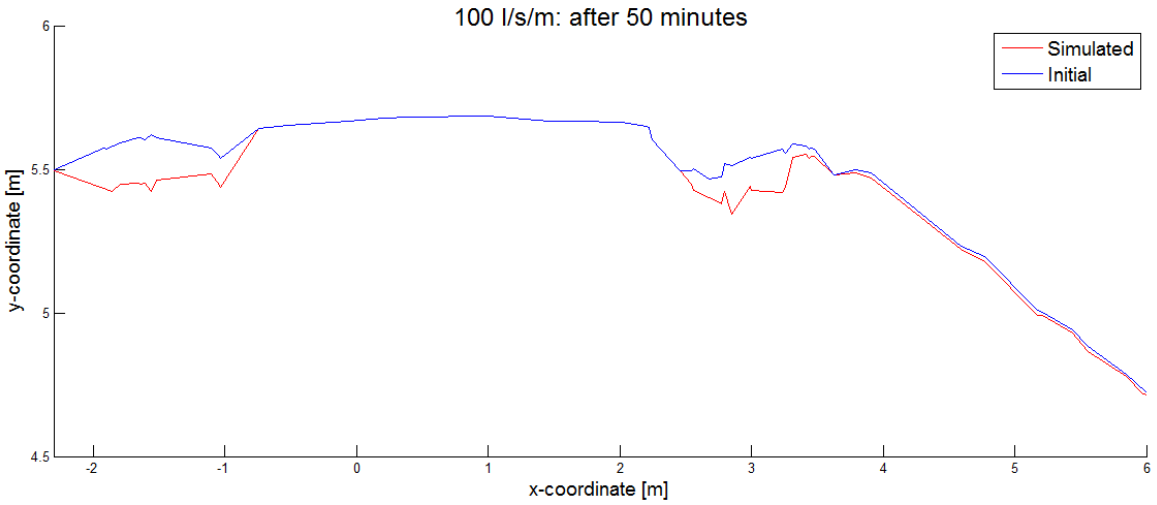

Figure G.9. Dike profile after 50 minutes with a discharge of 100 l/s per meter

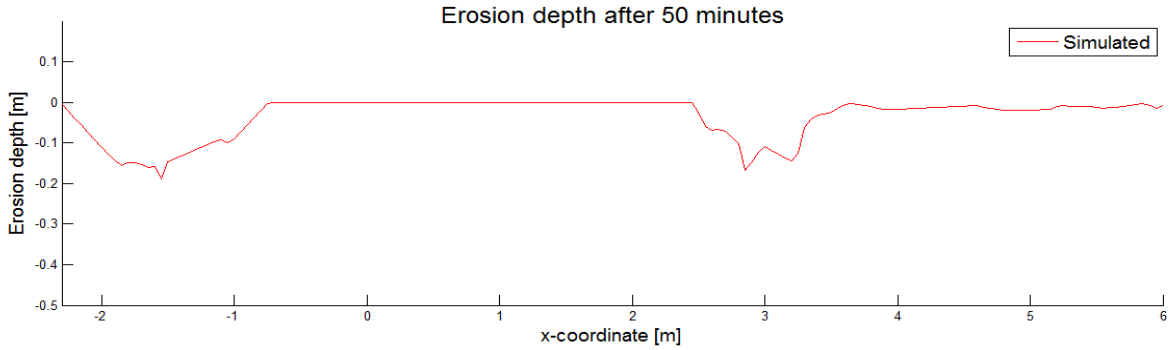

Figure G.10. Erosion depth after 50 minutes of testing with a discharge of 100 l/s per meter

G.6. FLOW VELOCITIES AND WATER DEPTHS ALONG DIKE SLOPE

In Figure G.11 and G.12 the flow velocities and water depths over time at location 2 are presented for a smooth grass covered dike profile.

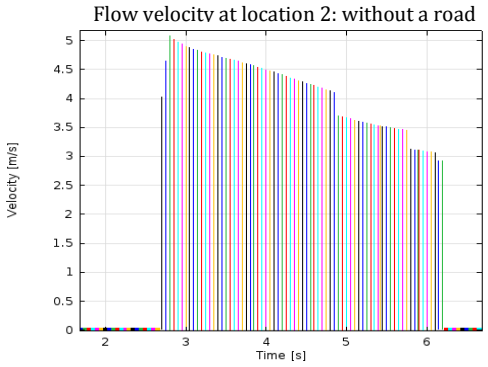

Figure G.11. Flow velocity at location 2 for a smooth dike profile

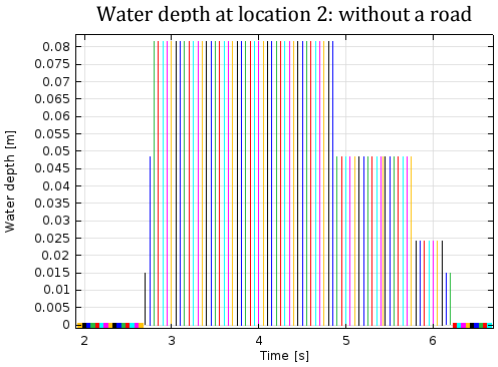

Figure G.12. Flow depth at location 2 for a smooth dike profile

In Figure G.13 till G.16 the flow velocities and water depths over time at location 1 and 2 are presented for a dike profile with a road located at the crest.

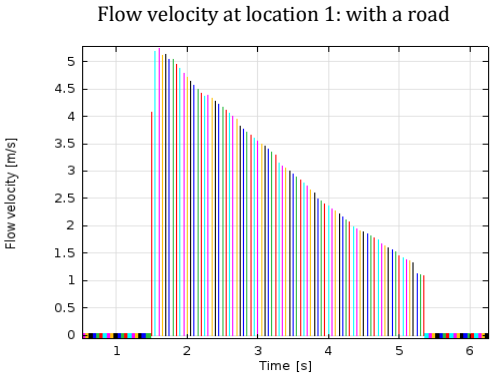

Figure G.13. Flow velocity at location 1 for a dike profile with a road on top

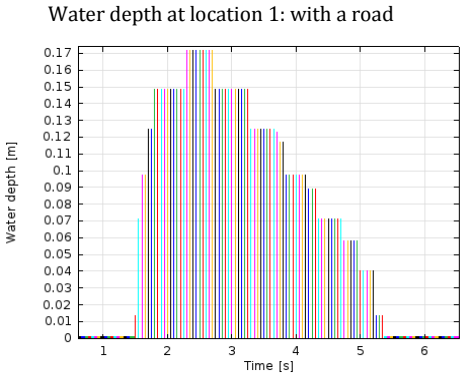

Figure G.14. Flow depth at location 1 for a dike profile with a road on top

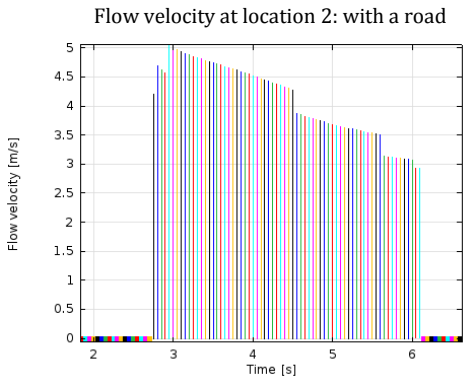

Figure G.15. Flow velocity at location 2 for a dike profile with a road on top

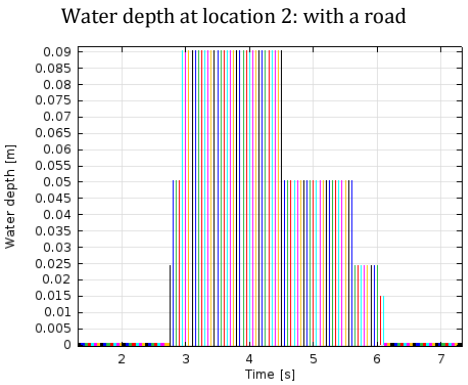

Figure G.16. Flow depth at location 2 for a dike profile with a road on top

G.7. EROSION DEVELOPMENT ALONG COMPLETE DIKE PROFILE WITH AND WITHOUT A ROAD

Figures G.17 and G.18 give the reference slope and eroded slope due to wave overtopping of 150 waves with a volume of 2500 l/m for a dike profile with and without a road on top respectively.

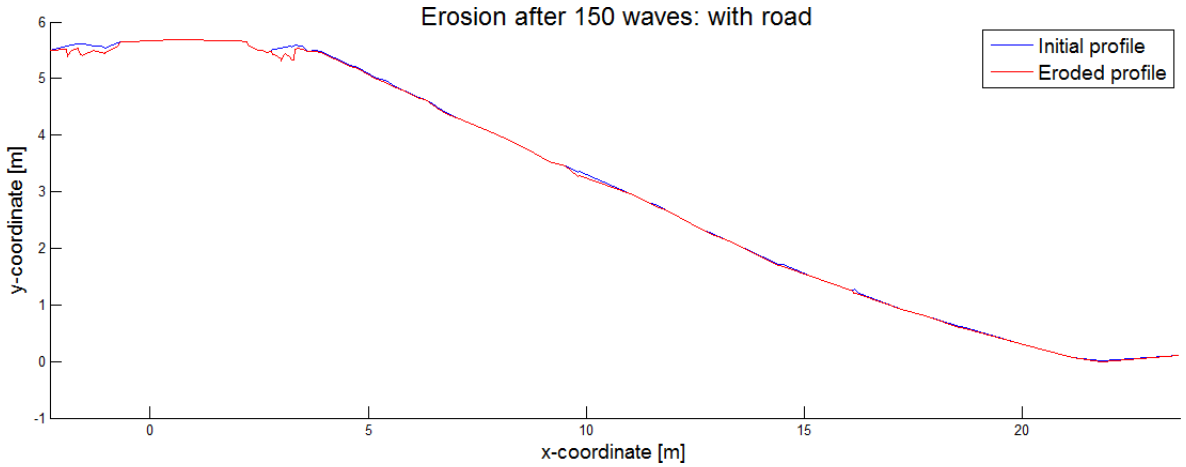

Figure G.17. Erosion for a dike profile with a road on top after 150 waves with a volume of 2500 l/m

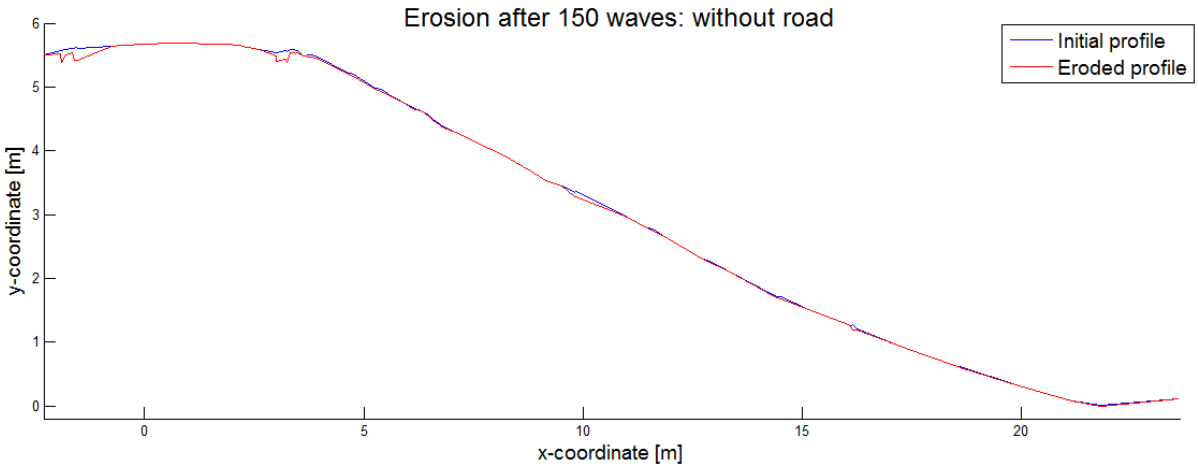

Figure G.18. Erosion for a smooth dike profile after 150 waves with a volume of 2500 l/m